Three-gluon vertex and quark-gluon vertex functions in the Landau gauge

Dissertation

zur Erlangung des akademischen Grades Doktor der Naturwissenschaften (Dr.rer.nat.)

verfasst am Institut für Physik, Fachbereich Theoretische Physik der Karl-Franzens-Universität Graz

vorgelegt von
Adrian Lorenz Blum

Graz, August 2017

Abstract

This work aims at investigating the coupled system of quark-gluon vertex, quark propagator and three-gluon vertex in Landau gauge. For this purpose we proceed in several steps. As a first step the coupled system of quark-gluon vertex and quark propagator will be calculated separately using a model for the three-gluon vertex. In a second step, the results of this computation will be used to unquench the three-gluon vertex. Finally, the coupled system of quark-gluon vertex, quark propagator and three-gluon vertex will be considered. Due to this calculation we are capable of drawing conclusions about the interplay between quarks and gluons. We are especially interested in two aspects:
Firstly, we will study how a dynamic three-gluon vertex affects dynamical chiral symmetry breaking. With respect to this we will show that a small change in the Yang-Mills sector has a big impact on dynamical chiral symmetry breaking.
Moreover, it was found in earlier investigations that the dressing function of the tree-level tensor structure of the three-gluon vertex exhibits a zero crossing. Although this feature of the three-gluon vertex has attracted much attention since then, the exact position of the zero crossing is still unknown. In this work we will investigate how the unquenching of the three-gluon vertex affects the position of the zero crossing. The calculations will be performed using Dyson-Schwinger equations and the nPI formalism.

Zusammenfassung

Ziel dieser Arbeit ist die Berechnung des gekoppelten Systems aus Quark-Gluon-Vertex, Quark-Propagator und Drei-Gluon-Vertex in Landau Eichung. Hierzu gehen wir in mehreren Schritten vor. In einem ersten Schritt betrachten wir das System aus Quark-Gluon-Vertex und Quark-Propagator gesondert unter Verwendung eines Modells für den Drei-Gluon-Vertex. In einem zweiten Schritt verwenden wir das Ergebnis dieser Berechnung dazu, den Drei-Gluon-Vertex „unzuquenchen“. Schließlich betrachten wir das gekoppelte System aus Quark-Gluon-Vertex, Quark-Propagator und Drei-Gluon-Vertex. Diese Berechnung versetzt uns in die Lage, Rückschlüsse über das Wechselspiel zwischen Quarks und Gluonen zu ziehen. Hierbei stehen vor allem zwei Aspekte im Fokus unseres Interesses. Zunächst werden wir untersuchen, wie sich ein dynamischer Drei-Gluon-Vertex auf dynamische chirale Symmetriebrechung auswirkt. Diesbezüglich werden wir zeigen, dass bereits kleine Änderungen im Yang-Mills Bereich große Auswirkungen auf die dynamische chirale Symmetriebrechung haben. In früheren Untersuchungen konnte darüber hinaus gezeigt werden, dass die Dressingfunktion der Tree-Level-Tensorstruktur des Drei-Gluon-Vertex einen Nulldurchgang besitzt. Obwohl diese Eigenschaft des Drei-Gluon-Vertex große Aufmerksamkeit auf sich gezogen hat, ist die genaue Position des Nulldurchganges bislang noch unbekannt. In dieser Arbeit werden wir untersuchen, wie sich die Position des Nulldurchgangs des Drei-Gluon-Vertex unter Einbeziehung von Quarks ändert. Für die Berechnungen verwenden wir Dyson-Schwinger-Gleichungen und den nPI-Formalismus.

Contents

1. Introduction

Quantum Chromodynamics (QCD), the theory of the strong interaction, has been an active research area for decades now and especially at the beginning much insight could be gained by means of Perturbation Theory. In doing so one exploits the fact that QCD is an asymptotically free theory, that is, the running coupling tends to zero at large momenta and allows in this way for a systematic expansion in the coupling constant. However, due to its restriction to high energies/small coupling constants two of the most striking effects of QCD lie outside of the range of application of Perturbation Theory: **confinement** and **dynamical chiral symmetry breaking (DχSB)**. We will understand the former as the impossibility to detect quantities that carry a color charge. This behaviour seems to be a consequence of the non-Abelian nature of QCD and thus is linked to gluodynamics. One consequence of DχSB is the dynamical generation of mass which is (besides the Higgs mechanism) responsible for most of the mass of visible matter. In this work it will be emphasized that it has even more consequences.
Both features require a non-perturbative treatment and to this end a multitude of methods is available. In this work we will mainly employ Dyson-Schwinger equations and the nPI formalism. Both methods aim at the calculation of n-point functions which contain all the information about the theory and can be used to calculate hadron properties. However, n-point functions are no gauge independent quantities and thus a gauge choice is required. In this thesis we will work in Landau gauge.
Two n-point functions are of particular interest: the **quark-gluon vertex** and the **three-gluon vertex**.
The quark-gluon vertex links the gauge and the matter sector and has been at the center of intensive research for many years. The methods applied to study the quark-gluon vertex range from Perturbation Theory [1, 2, 3, 4, 5] to Lattice calculations [6, 7, 8, 9] to continuum methods [10, 11, 12, 13, 14, 15, 16, 17, 18, 19, 20]. One of the reasons why the quark-gluon vertex has attracted so much attention is due to the role it plays in DχSB. It was found that the quark-gluon vertex needs to have a certain strength in order to enable chiral symmetry breaking. A profound knowledge of the quark-gluon vertex therefore seems to be a good starting point for a better insight into DχSB. Since the quark-gluon vertex mediates the interaction between quarks and gluons, it is moreover elementary for bound state calculations and for this purpose several models for the quark-gluon vertex have been developed. However, over the last years there has been growing interest in studying the effects that a fully dressed quark-gluon vertex has on hadrons [21, 22, 13].
The three-gluon vertex on the other hand directly reflects the non-Abelian nature of QCD. The three-gluon vertex of pure Yang-Mills theory, i.e., disregarding the contribution of the quark sector, has been the object of different calculations [23, 24, 25, 26, 27, 28, 29, 30, 31, 32, 33, 34, 35, 36, 37, 38]. A striking observation is that the dressing function of the tree-level tensor structure of the three-gluon vertex – in contrast to earlier believes – does not increase in the infrared but rather declines

until it crosses zero and finally becomes negative [1]. Although there is large evidence for the existence of this zero crossing, its definite position still remains unsettled. A deeper meaning can be given to the zero crossing in the sense that its position may serve as a guideline for the strength of the three-gluon vertex at the scale relevant for hadrons.
Most of the research so far aimed at studying the quark-gluon vertex and the three-gluon vertex separately, but less is known about the interplay between both quantities in a non-perturbative treatment [13, 9]. Our goal is therefore to examine the mutual dependence of quark-gluon vertex and three-gluon vertex on each other. To this effect we will finally consider the coupled system of quark propagator, quark-gluon vertex and three-gluon vertex. In doing so we are especially interested in the question how sensitive the quark-gluon vertex and with it DχSB is to a dynamical three-gluon vertex. Furthermore, we are able to research how the unquenching of the three-gluon vertex affects the position of the zero crossing. Putting this work into a broader context we hope to shed some new light on the notion that quarks are screening and gluons are anti-screening.
Having this in mind the structure of this thesis can be best understood from its aim, the calculation of the coupled system of quark propagator, quark-gluon vertex and three-gluon vertex. In order to accomplish this we will take small steps starting with laying down the basics of QCD in chapter 2, where we will focus on those aspects of QCD that will play an important role in the subsequent chapters. In chapter 3 we will give an overview of the Functional Methods that we will employ in this work, namely Dyson-Schwinger equations, the nPI formalism and the Functional Renormalization Group. In doing so we will highlight the characteristics of each method. In the subsequent chapter 4 we will tackle the calculation of the quark-gluon vertex and the quark propagator. We will find an appropriate parametrization of the quark-gluon vertex and comment on the basis systems that can be found in the literature. Moreover, we will perform the calculation of the quark-gluon vertex two times, one time using the 3PI formalism and another time employing its Dyson-Schwinger equation, and compare the results of both methods with each other. In the calculation the three-gluon vertex is described by a model and we will analyze the impact that a variation of the model parameters has on the quark-gluon vertex. We will turn to the three-gluon vertex in chapter 5 beginning with a calculation of the three-gluon vertex in Yang-Mills theory. This calculation will then be augmented by the quark sector and a calculation of the unquenched three-gluon vertex will be performed. At first, a static quark-gluon vertex will be employed, that is, back coupling effects of the three-gluon vertex on the quark sector will be ignored. Finally, we will calculate the coupled system of quark-gluon vertex, quark propagator and three-gluon vertex. Our investigation will be concluded in chapter 6 and we will give an outlook of possible future work.
Chapter 7 stands apart from the previous investigations. Instead of QCD we will deal with a scalar ϕ^4-theory using the Functional Renormalization Group. Interesting about ϕ^4-theory is that it shares the same universality class with the Ising model. We will study the system in the symmetric and symmetry broken phase and finally present a calculation of the pressure in the symmetry broken phase at finite temperature. This chapter may be viewed as a supplement to the main work.

[1] In future we will refer to this feature as the zero crossing of the three-gluon vertex.

2. Aspects of QCD

In this chapter we will introduce some fundamental concepts of Quantum Chromodynamics (QCD). This chapter hence lays the foundations for all further chapters. To begin with we introduce the generating functional of the correlation functions of QCD and perform a gauge fixing procedure. The gauge fixed generating functional is then used to derive the effective action. Next, we will have a closer look at the symmetries of our gauge fixed theory with the focus on chiral symmetry and BRST symmetry. The latter will lead us then to the formulation of the Slavnov-Taylor identities (STIs). We will conclude this chapter by a discussion of dynamical chiral symmetry breaking and present order parameters by means of which it can be detected.

2.1. The gauge fixing procedure

QCD is a gauge theory based on the group (color) $SU(3)$. Demanding invariance under local gauge transformations

$$\Omega(x) = \exp\left[-ig\theta^a(x)T^a\right] \tag{2.1}$$

we can write down the matter part of the QCD action[1]:

$$\begin{aligned} S_M &= \int d^4x\, \mathcal{L}_M \ , \\ &= \int d^4x \sum_{i=1}^{N_f} \overline{q}_i(-D_\mu\gamma_\mu + m_i)q_i \ . \end{aligned} \tag{2.2}$$

Here, we have introduced the covariant derivative in the fundamental representation

$$D_\mu = \partial_\mu + igA_\mu \ , \tag{2.3}$$

and used the abbreviation $A_\mu = A^a_\mu T^a$ with T^a being the generators of $SU(3)$. q, $\overline{q}$ and A^a_μ denote the quark, antiquark and gluon fields. In (2.2) the flavour index i has been written out explicitly, but will be suppressed henceforth.
The dynamics of the gluon is described by the term

$$\begin{aligned} S_{YM} &= \int d^4x\, \mathcal{L}_{YM} \ , \\ &= \int d^4x\, \frac{1}{4} F^a_{\mu\nu} F^a_{\mu\nu} \ , \end{aligned} \tag{2.4}$$

[1] We work entirely in Euclidean space-time.

which constitutes the Yang-Mills part of the QCD action. $F^a_{\mu\nu}$ is the field strength tensor given by

$$F^a_{\mu\nu} = \partial_\mu A^a_\nu - \partial_\nu A^a_\mu - g f^{abc} A^b_\mu A^c_\nu \,. \tag{2.5}$$

The last term reflects the non-Abelian nature of $SU(3)$ and is responsible for the self-interaction of the gluon as can be seen by inserting (2.5) into $\mathcal{L}_{YM}$.
Putting both terms together the full action of QCD reads

$$\begin{aligned} S_{QCD} &= \int d^4x \, \mathcal{L}_{QCD} \;, \\ &= \int d^4x \, \mathcal{L}_M + \mathcal{L}_{YM} \;, \\ &= \int d^4x \, \overline{q}(-D_\mu \gamma_\mu + m)q + \frac{1}{4} F^a_{\mu\nu} F^a_{\mu\nu} \;. \end{aligned} \tag{2.6}$$

We can now naively define a generating functional by

$$Z[J, \eta, \overline{\eta}] = \int \mathcal{D}[A\overline{q}q] \exp\left[-S_{QCD} + \int d^4x \left(A^a_\mu J^a_\mu + \overline{\eta} q + \overline{q} \eta \right) \right] \;. \tag{2.7}$$

Here, we have introduced the source for the gluon field J^a_μ and the Grassmann valued sources for the quark and anti-quark $\overline{\eta}$ and η. The measure is assumed to be gauge invariant.
However, a more careful treatment reveals that the generating functional (2.7) is plagued by two problems:
All gauge fields that are connected through a gauge transformation form a so-called gauge orbit, which we will denote by $[A^\Omega]$. The members of a gauge orbit are called gauge copies. Due to the invariance of the action and the measure all fields that belong to the same gauge orbit give the same value for the integrand. Carrying out the path integral would thus lead to an infinite constant which can be identified with the volume of the gauge group.
A further consequence of the gauge freedom [39] refers to the part of (2.4) that is quadratic in the gluon fields. This part can be identified with the inverse of the gluon propagator. However, in the form given above it is not free of zero modes and consequently a definition of the gluon propagator is prevented.
A solution to both problems is given in form of gauge fixing. From the first problem it is evident that because of gauge invariance it suffices to take only one element per gauge orbit into account. The idea is thus to impose a further constraint onto the system that singles out exactly one representative of each gauge orbit. In a generic form this condition can be written as

$$f^a(A^\Omega) = d^a(x) \;. \tag{2.8}$$

There are different ways how this can be specified. A suitable covariant condition is given by

$$\partial_\mu A^a_\mu = 0 \;. \tag{2.9}$$

This condition has somehow to be included into the generating functional. For this purpose the method of Faddeev and Popov proved to be successful [40]. The central

idea is to write the identity as

$$1 = \int \mathcal{D}\Omega \Delta[A] \delta(f^a(A^\Omega) - d^a(x)) \; . \tag{2.10}$$

Here the delta distribution implements the condition (2.8) and $\Delta[A]$ is the so-called Faddeev-Popov determinant

$$\Delta[A] = \det \left[\frac{\delta f^a(A^\Omega(x))}{\delta \theta^b(y)} \right] \Bigg|_{\theta=0} \; . \tag{2.11}$$

A distinctive feature of this equation is that the integration is performed over a group with the measure being a Haar measure [41]. A special property of the Haar measure is that it is invariant under the transformations of the group. With this one can show that the Faddeev-Popov determinant is invariant as well [42].
Setting for now the sources in (2.7) to zero we can introduce the identity (2.10) into our generating functional

$$Z[0] = \int \mathcal{D}[A\bar{q}q] \int \mathcal{D}\Omega \Delta[A] \delta(f^a(A^\Omega) - d^a(x)) \exp\left[-S_{QCD}\right] \; . \tag{2.12}$$

In order to circumvent the problems outlined above we would like to absorb the volume of the gauge group $\int \mathcal{D}\Omega$ in the normalization. Yet, this is at the moment prevented by the appearance of $f^a(A^\Omega)$ in the integrand. We can, however, take advantage of the gauge invariance of both measures, the Faddeev-Popov determinant and the action. On account of this a gauge transformation from A^Ω to A does not alter the result of the integration and we can pull $\int \mathcal{D}\Omega$ out of the integrand. This finally yields

$$Z[J, \eta, \overline{\eta}] = \int \mathcal{D}[A\bar{q}q] \Delta[A] \delta(f^a(A) - d^a(x)) \exp\left[-S_{QCD} + \int d^4x \left(A^a_\mu J^a_\mu + \overline{\eta} q + \bar{q} \eta \right) \right] \; . \tag{2.13}$$

For practical purposes it is common to rearrange the integrand such that all terms appear in the exponent. This is done for the Faddeev-Popov determinant by introducing two Grassmann valued auxiliary fields $\overline{c}^a$ and c^a. We find

$$\Delta[A] = \det\left[-\partial_\mu D^{ab}_\mu\right] = \int \mathcal{D}\left[c\overline{c}\right] \exp\left[-\int d^4x \overline{c}^a \partial_\mu D^{ab}_\mu c^b\right] \tag{2.14}$$

with the covariant derivative in the adjoint representation

$$D^{ab}_\mu = \partial_\mu \delta^{ab} + g f^{abc} A^c_\mu \; . \tag{2.15}$$

Altough they anticommute, the fields $\overline{c}^a$ and c^a exhibit a spin of zero in contradiction to the spin-statistic theorem. It is therefore evident that they have been introduced solely as a method of calculation and cannot form observable quantities. As a consequence of this c^a and $\overline{c}^a$ are given the names ghost and anti-ghost field, respectively. We would like to make a comment on this.
In spite of their unphysical nature the ghost and anti-ghost field are of high importance for the theory. For example, they cancel the unphysical polarizations of the gluon and thus help to render the S-Matrix unitary [43, 44].
We can use the Gaussian integral a second time to deal with the delta distribution

in (2.13). We can split off the normalization a constant of the form

$$\int \mathcal{D}[d] \exp\left[-\frac{1}{2\alpha}\int d^4x (d^a(x))^2\right] . \tag{2.16}$$

Inserting this expression into (2.13) the delta distribution can be integrated out and the generating functional takes its final form:

$$\begin{aligned} Z[J,\eta,\overline{\eta},\sigma,\overline{\sigma}] &= \int \mathcal{D}\left[A\overline{q}q\overline{c}c\right] \exp\left[-S_{eff} + \int d^4x \left(A^a_\mu J^a_\mu + \overline{\eta}q + \overline{q}\eta + \overline{\sigma}^a c^a + \overline{c}^a \sigma^a\right)\right] , \\ &= \int \mathcal{D}\left[A\overline{q}q\overline{c}c\right] \exp\Big[- (S_{QCD} + S_{GF} + S_{FP}) + \\ &\qquad \int d^4x \left(A^a_\mu J^a_\mu + \overline{\eta}q + \overline{q}\eta + \overline{\sigma}^a c^a + \overline{c}^a \sigma^a\right)\Big] , \end{aligned} \tag{2.17}$$

where we have introduced the Grassmann valued sources $\overline{\sigma}^a$ and σ^a for the ghost and anti-ghost field.
The two new terms in the action that are created in the Faddeev-Popov procedure are given by

$$S_{GF} = \int d^4x \mathcal{L}_{GF} = \int d^4x \frac{1}{2\alpha}(\partial_\mu A^a_\mu)^2 , \tag{2.18}$$

$$S_{FP} = \int d^4x \mathcal{L}_{FP} = \int d^4x \overline{c}^a \partial_\mu D^{ab}_\mu c^b . \tag{2.19}$$

α is the gauge parameter which has no physical meaning and therefore may be set to a fixed value. Of particular interest for this work is the limit $\alpha \to 0$ which corresponds to Landau gauge. The expression S_{FP} introduces the ghost propagator and the ghost-gluon vertex to our theory.
For later on when we discuss BRST symmetry it will be convenient to linearize the gauge fixing term by introducing the Nakanishi-Lautrup auxiliar field $B^a(x)$. For this purpose one employs the relation

$$\exp\left[\frac{1}{2\alpha}(\partial_\mu A^a_\mu)^2\right] = \text{const} \times \int \mathcal{D}[B] \exp\left[iB^a\partial_\mu A^a_\mu + \frac{\alpha}{2}B^a B^a\right] . \tag{2.20}$$

That both sides are indeed equal apart from a global constant can be checked explicitly by completing the square on the right-hand side and performing the Gaussian integral. The generating functional can then be rewritten as

$$\begin{aligned} Z[J,\eta,\overline{\eta},\sigma,\overline{\sigma}] = \int \mathcal{D}\left[AB\overline{q}q\overline{c}c\right] \exp\Big[- (S_{QCD} + S_{FP} + \int d^4x (iB^a\partial_\mu A^a_\mu + \frac{\alpha}{2}B^a B^a)) + \\ \int d^4x \left(A^a_\mu J^a_\mu + \overline{\eta}q + \overline{q}\eta + \overline{\sigma}^a c^a + \overline{c}^a \sigma^a\right)\Big] \end{aligned} \tag{2.21}$$

As convincing as the above outlined procedure may appear there are yet some problems that remain. One of the most notable is the Gribov problem [45] which has been the subject of extensive research since its discovery (for reviews see e.g. [46, 47, 48]). In short, this problem originates from the fact that within the Faddeev-Popov procedure more than one gauge copy per gauge orbit is singled out. On account of this the problem of overcounting is still present in the theory. Despite diverse efforts this

problem has not yet been satisfactorily solved.

2.2. The effective action

Having gauge fixed the generating functional we are able to derive correlation functions by differentiating 2.17 with respect to the sources and setting all source terms to zero. Although correlation functions are gauge dependent and thus do not constitute physical quantities by themselves, they can be used in a further step for the computation of observables. This is for example the case in the LSZ reduction formula [49] that relates correlation functions and S-matrix elements or the calculation of bound states in the BSE formalism [50]. A full knowledge of correlation functions therefore implies a complete description of the theory.
In terms of Feynman diagrams the correlation functions that are obtained from the generating functional $Z[J,\eta,\overline{\eta},\sigma,\overline{\sigma}]$ correspond to disconnected as well as reducible diagrams. Since these diagrams are composed of smaller building blocks, some of the information that they contain is redundant. We thus restrict ourselves to the calculation of irreducible diagrams from which all other kind of diagrams can be constructed. For this purpose we at first get rid of the unconnected diagrams by reformulating the generating functional:

$$Z[J,\eta,\overline{\eta},\sigma,\overline{\sigma}] = \exp\left[W[J,\eta,\overline{\eta},\sigma,\overline{\sigma}]\right] . \tag{2.22}$$

$W[J,\eta,\overline{\eta},\sigma,\overline{\sigma}]$ is the generating functional of connected Green's functions. In order to arrive at the effective action Γ from which the 1PI irreducible Green's functions can be derived we have to perform a Legendre transformation with respect to all sources

$$\Gamma[\Phi_A,\Phi_q,\Phi_{\overline{q}},\Phi_c,\Phi_{\overline{c}}] = -W[J,\eta,\overline{\eta},\sigma,\overline{\sigma}] + \int d^4x \Big(J^a_\mu(x)\Phi^a_{A\mu}(x) + \overline{\eta}(x)\Phi_q(x) + \eta(x)\Phi_{\overline{q}}(x) + \overline{\sigma}^a(x)\Phi^a_c(x) + \sigma^a(x)\Phi^a_{\overline{\sigma}}(x)\Big) . \tag{2.23}$$

The Φs on which the effective action depends are the so-called classical fields that are related to the generating functional of connected Green's functions W and the sources. In a generic way we can write

$$\Phi_i = \frac{\delta W}{\delta J_i} , \qquad J_i = \frac{\delta \Gamma}{\delta \Phi_i} . \tag{2.24}$$

By differentiating the effective action with respect to the classical fields and setting the sources to zero we obtain the n-point functions which are the relevant quantities that we will study in this thesis.
The above effective action is dubbed the 1PI effective action. From this action we gain all diagrams that do not fall apart by cutting one line. As the formulation 1PI suggests a generalization to a nPI effective action is possible. How this is done in detail will be expounded in the next chapter.

2.3. BRST symmetry and Slavnov-Taylor identities

Because of the terms S_{GF} and S_{FP} that come about with the gauge fixing procedure the full action S_{eff} is not invariant under gauge transformations anymore. However, it is possible to find a symmetry that leaves the gauge fixed action invariant. This symmetry has been named after its discoverers BRST symmetry [51, 52]. We can think of BRST symmetry as a gauge symmetry (2.1) which is extended to the ghost and auxiliary fields and where the following replacement has been performed:

$$\theta^a(x) \to \xi c^a(x) \; . \tag{2.25}$$

$c^a(x)$ is the ghost field and ξ is a Grassmann valued constant. Under the BRST symmetry the fields transform as

$$\begin{aligned}
\delta_{BRST} A^a_\mu &= \xi D^{ab}_\mu c^b \; , \\
\delta_{BRST} q &= -i\xi g T^a c^a q \; , \\
\delta_{BRST} \overline{q} &= i\xi g c^a \overline{q} T^a \; , \\
\delta_{BRST} c^a &= -\xi \frac{g}{2} f^{abc} c^b c^c \; , \\
\delta_{BRST} \overline{c}^a &= i\xi B^a \; , \\
\delta_{BRST} B^a &= 0 \; .
\end{aligned} \tag{2.26}$$

If we undo the replacement (2.25) we see that the transformation of the quark and the gluon is exactly the same as under the gauge transformation which is natural since we have merely chosen a specific value for $\theta^a(x)$. This implicates that S_{QCD} is already invariant under BRST transformations.
An important feature of BRST symmetry is that the transformations (2.26) are nilpotent, that is,

$$\delta^2_{BRST} A^a_\mu = \delta^2_{BRST} q = \delta^2_{BRST} \overline{q} = \delta^2_{BRST} c^a = \delta^2_{BRST} \overline{c}^a = \delta^2_{BRST} B^a = 0 \; . \tag{2.27}$$

By using the above transformations and exploiting the nilpotency of the BRST symmetry one can show in an explicit calculation that $\delta_{BRST}(S_{FP} + S_{GF}) = 0$.
A further symmetry that occurs in the gauge fixed action is the ghost symmetry. This symmetry corresponds to a rescaling of the ghost fields

$$c^a \to e^\gamma c^a \; , \tag{2.28}$$

$$\overline{c}^a \to e^{-\gamma} \overline{c}^a \; , \tag{2.29}$$

where γ is a real number. For this symmetry one finds a conserved charge Q_{gh} which gives rise to a conserved quantum number denoted as ghost number n_{gh}. Every ghost exhibits a ghost number of $n_{gh} = 1$ and for every anti ghost we have a ghost number of $n_{gh} = -1$. Consequently, we have to assign to the BRST transformations a ghost number $n_{gh} = 1$.
As for the ghost symmetry there exists also for the BRST symmetry a conserved charge Q_{BRST}. Both charges play a crucial role in the definition of a physical subspace of the full state space. Such a definition becomes necessary because the full state space also contains states with a negative norm that impedes a probability

interpretation. One thus has to select the physical states $|\phi\rangle_{phys}$ via the condition

$$Q_{BRST}\,|\phi\rangle_{phys} = 0 \tag{2.30}$$

like it is done in QED by implementing the Gupta-Bleuler condition. Since in QCD the definition of physical states is closely entwined with the notion of confinement a thorough treatment finally leads to the Kugo-Ojima confinement scenario [53, 54, 55]. As we do not deal with this topic in this thesis we leave it at this brief mentioning which underlines the broader significance of the BRST symmetry. Instead we would like to add two comments about BRST symmetry.
Although in our case we first carried out the Faddeev-Popov procedure and then identified the BRST symmetry in the gauge fixed Lagrangian, one should bear in mind that the BRST symmetry is more general than the Faddeev-Popov method in the sense that one can add BRST invariant terms to the Lagrangian that cannot be constructed from a Faddeev-Popov procedure [43, 56].
It is up to now unsettled whether BRST symmetry is a manifest symmetry in a non-perturbative treatment.
A further consequence of BRST symmetry with a more direct implication for our work are the Slavnov-Taylor identities [57, 58] which can be regarded as the generalization of the Ward-Takahashi identities in QED to non-Abelian theories. If we have again a look at the generating functional (2.17), we recognize that because of the source terms the whole integrand is not invariant under BRST transformations. Inspite of this the generating functional itself is BRST invariant. This can be understood as follows: since the measure and the action are BRST invariant we can always perform a variable transformation to the BRST transformed fields A_{tr}, $\overline{q}_{tr}$, q_{tr}, $\overline{c}_{tr}$ and c_{tr} without changing the form of the generating functional, or explicitly,

$$\begin{aligned}
Z[J,\eta,\overline{\eta},\sigma,\overline{\sigma}] &= \int \mathcal{D}\,[A\overline{q}q\overline{c}c] \exp\Big[- S_{eff}[A,\overline{q},q,\overline{c},c] + \int d^4x \Big(A^a_\mu J^a_\mu + \overline{\eta} q \\
&\qquad + \overline{q}\eta + \overline{\sigma}^a c^a + \overline{c}^a \sigma^a \Big) \Big] \,, \\
&= \int \mathcal{D}\,[A_{tr}\,\overline{q}_{tr}\,q_{tr}\,\overline{c}_{tr}\,c_{tr}] \exp\Big[- S_{eff}[A_{tr}\,,\overline{q}_{tr}\,,q_{tr}\,,\overline{c}_{tr}\,,c_{tr}] + \int d^4x \Big(A^a_{\mu\,tr} J^a_\mu \\
&\qquad + \overline{\eta} q_{tr} + \overline{q}_{tr}\eta + \overline{\sigma}^a c^a_{tr} + \overline{c}^a_{tr} \sigma^a \Big) \Big] \,, \\
&= Z_{BRST}[J,\eta,\overline{\eta},\sigma,\overline{\sigma}] \,,
\end{aligned}$$

where we made the dependence of the action on the fields explicit. Since already the generating functionals for the transformed and untransformed fields coincide, the same has to be true for the Green's functions that are derived by differentiating with respect to the sources.

$$\frac{\delta^n Z[J,\eta,\overline{\eta},\sigma,\overline{\sigma}]}{\delta J^a_\mu(x)\ldots} = \frac{\delta^n Z_{BRST}[J,\eta,\overline{\eta},\sigma,\overline{\sigma}]}{\delta J^a_\mu(x)\ldots} \,. \tag{2.31}$$

We thus obtain the condition

$$\delta_{BRST} \frac{\delta^n Z[J,\eta,\overline{\eta},\sigma,\overline{\sigma}]}{\delta J^a_\mu(x)\ldots} = 0 \,, \tag{2.32}$$

which gives rise to the Slavnov-Taylor identities (STIs) of the Green's functions of the generating functional Z. Since we are mainly dealing with the effective action

we have to work out the corresponding expressions for the STIs. Starting from the generating functional (2.21) this can be done in an elegant way by introducing further sources $K^a_{\mu\,A}, K_q, K_{\overline{q}}, K^a_c$ and K^a_B for the terms $\delta_{BRST}A^a_\mu, \delta_{BRST}\overline{q}, \delta_{BRST}q, \delta_{BRST}c^a$ and B^a:

$$Z[J,\eta,\overline{\eta},\sigma,\overline{\sigma},K_A,K_q,K_{\overline{q}},K_c,K^a_B] = \int \mathcal{D}\left[AB\overline{q}q\overline{c}c\right]\exp\left[-S_{full}\right]$$

Here, we have absorbed the source terms into the action

$$\begin{aligned} S_{full} =& S_{QCD} + S_{FP} + \int d^4x (iB^a\partial_\mu A^a_\mu + \frac{\alpha}{2}B^aB^a) \\ &- \int d^4x \Big(A^a_\mu J^a_\mu + \overline{\eta}q + \overline{q}\eta + \overline{\sigma}^a c^a + \overline{c}^a\sigma^a + K^a_{\mu\,A}\delta_{BRST}A^a_\mu + K_q\delta_{BRST}q + \\ &\qquad \delta_{BRST}\overline{q}K_{\overline{q}} + K^a_c\delta_{BRST}c^a + K^a_B B^a \Big) . \end{aligned} \tag{2.33}$$

The invariance of the generating functional under BRST transformations translates in this approach to

$$\begin{aligned} 0 &= \delta_{BRST}Z[J,\eta,\overline{\eta},\sigma,\overline{\sigma},K_A,K_q,K_{\overline{q}},K_c,K^a_B] \\ &= \int \mathcal{D}\left[AB\overline{q}q\overline{c}c\right]\exp\left[-S_{full}\right]\int d^4x \Big(\delta_{BRST}A^a_\mu J^a_\mu - \overline{\eta}\delta_{BRST}q + \delta_{BRST}\overline{q}\eta - \\ &\qquad \overline{\sigma}^a\delta_{BRST}c^a + \delta_{BRST}\overline{c}^a\sigma^a \Big) \\ &= \int d^4x \left(J^a_\mu \frac{\delta}{\delta K^a_{\mu\,A}} - \overline{\eta}\frac{\delta}{\delta K_q} + \frac{\delta}{\delta K_{\overline{q}}}\eta - \overline{\sigma}^a\frac{\delta}{\delta K^a_c} + i\xi\frac{\delta}{\delta K^a_B}\sigma^a \right) \times \\ &\qquad Z[J,\eta,\overline{\eta},\sigma,\overline{\sigma},K_A,K_q,K_{\overline{q}},K_c,K^a_B] , \end{aligned} \tag{2.34}$$

where we have used once more the invariance of the measure and the action and exploited the nilpotency of the BRST transformations and that $\delta_{BRST}B^a = 0$. In the third line we have pulled the bracket with the BRST transformed fields out of the path integral which is possible, if we replace the fields by derivatives with respect to the new sources. From this equation we obtain the STIs of the Green's functions by differentiating with respect to the old sources. Carrying out the steps described in the previous section to get from the generating functional Z to the effective action we obtain the identity

$$0 = \int d^4x \left(-\frac{\delta\Gamma}{\delta\Phi^a_{A\,\mu}}\frac{\delta\Gamma}{\delta K^a_{\mu\,A}} + \frac{\delta\Gamma}{\delta\Phi_q}\frac{\delta\Gamma}{\delta K_q} - \frac{\delta\Gamma}{\delta K_{\overline{q}}}\frac{\delta\Gamma}{\delta\Phi_{\overline{q}}} + \frac{\delta\Gamma}{\delta\Phi^a_c}\frac{\delta\Gamma}{\delta K^a_c} - i\xi\frac{\delta\Gamma}{\delta K^a_B}\frac{\delta\Gamma}{\delta\Phi^a_{\overline{c}}} \right) . \tag{2.35}$$

For this we have used (2.24) to replace the sources. Moreover, Γ is an abbreviation for $\Gamma = \Gamma[\Phi_A,\Phi_q,\Phi_{\overline{q}},\Phi_c,\Phi_{\overline{c}},K_A,K_q,K_{\overline{q}},K_c,K^a_B]$, that is, the new sources are not Legendre transformed in the process of calculating the effective action from the generating functional of the connected Green's functions. From the above equation we get the STIs of the effective action which are also reffered to as Lee identities [59, 60, 61].

In a nutshell, the STIs reflect the BRST symmetry by relating different Green's

functions in a non-trivial way. To give an example we consider the STI of the quark-gluon vertex [62]:

$$k^\mu \Gamma^{a,(L)}_\mu(p,q;k) = G(k^2)\left[S^{(-1)}(p)H^a(p,q) - \overline{H}^a(p,q)S^{(-1)}(q)\right] \tag{2.36}$$

$\Gamma^{a,(L)}_\mu$ is the longitudinal part of the quark-gluon vertex, p, q are the momenta of the outgoing and incoming quark, respectively, and k is the gluon momentum. On the right-hand side, G denotes the ghost dressing function and S the quark propagator (for a definition of the non-perturbative propagators and vertices see appendix A.2). H^a and its conjugate $\overline{H}^a$ are the quark-ghost scattering kernels which contain a non tree-level two-quark-two-ghost vertex. Consequently, the STI of the quark-gluon vertex relates information about four Green's functions to each other.
From the above example we can see that the STIs allow us in principle to calculate a given Green's function in terms of other known Green's functions. In QED, for instance, the Ward-Takahashi identity of the quark-photon vertex, which can be viewed as the Abelian counterpart of the quark-gluon vertex STI, resembles equation (2.36) but without the contribution from the ghost part, i.e., without $G(k^2)$, $H^a(p,q)$ and $\overline{H}^a(p,q)$. It is therefore possible to express the longitudinal part of the quark-photon vertex in terms of the quark propagator.
Since a violation of the Slavnov-Taylor identities corresponds to a violation of gauge invariance, their fulfilment is of uttermost importance. The STIs can therefore be used to judge the quality of an ansatz, like e.g. a truncation, that is introduced into the theory.
Although these are clearly important features, the STIs in their direct form will be of minor relevance for our purposes. The reason is that the STIs only affect the longitudinal part of the Green's function. However, as we will argue in section 4.2 in Landau gauge the dynamics of the theory are carried entirely by the transverse part to which we will therefore restrict ourselves.
More relevant to us will be the implications that the STIs have on renormalization. Up to now we have left the renormalization constants unmentioned. If one displays them explicitly in the equations, one becomes aware that the STIs do not only relate Green's functions but also renormalization constants to each other [63, 64]. To be explicit one finds the following relations:

$$\frac{\widetilde{Z}_1}{\widetilde{Z}_3} = \frac{Z_1}{Z_3} = \frac{Z_{1F}}{Z_2} = \frac{Z_4}{Z_1} \tag{2.37}$$

with $\widetilde{Z}_3, Z_3, Z_2, Z_{1F}, Z_1, \widetilde{Z}_1$ and Z_4 being the renormalization constants of the ghost, gluon and quark field and of the quark-gluon, three-gluon, ghost-gluon and four-gluon vertices. These relations will be used frequently throughout this thesis. If we speak of STIs in the following we will therefore have these relations in mind rather than the equations above.

2.4. Chiral Symmetry and its dynamical breaking

One of the most intriguing effects of QCD besides confinement is the breaking of chiral symmetry. It is mainly this process that is responsible for the generation of the mass of the light quarks and that gives rise to the existence of the pions (or

more general of the light mesons) as Nambu-Goldstone bosons.
In order to identify the chiral symmetry we have again a look at the matter part of the QCD action (2.2), but this time we will set the mass to zero

$$\mathcal{L}_M = \overline{q}(-D_\mu \gamma_\mu)q \ . \tag{2.38}$$

Note that in this notation the summation over flavour indices is implied.
This Lagrangian is invariant under the global $SU(N_f) \times SU_A(N_f) \times U(1) \times U_A(1)$ symmetry, which has no impact on the gauge bosons and acts on the quark fields as follows [2]:

$$q \to \exp[i\theta]q \ , \qquad \overline{q} \to \overline{q}\exp[-i\theta] \qquad : U(1) \tag{2.39}$$
$$q \to \exp[i\theta^a T^a]q \ , \qquad \overline{q} \to \overline{q}\exp[-i\theta^a T^a] \qquad : SU(N_f) \tag{2.40}$$
$$q \to \exp[i\theta\gamma_5]q \ , \qquad \overline{q} \to \overline{q}\exp[i\theta\gamma_5] \qquad : U_A(1) \tag{2.41}$$
$$q \to \exp[i\theta^a\gamma_5 T^a]q \ , \qquad \overline{q} \to \overline{q}\exp[i\theta^a\gamma_5 T^a] \qquad : SU_A(N_f) \tag{2.42}$$

where T^a are the generators of the group $SU(N_f)$. If one checks the invariance of the Lagrangian (2.38) under the above transformations explicitly one recognizes that for the transformations (2.41) and (2.42) this is fulfilled because γ_μ anticommutes with γ_5. This observation can be generalized to further quantities Γ like e.g. the quark-gluon vertex or the quark propagator. A necessary condition for chiral symmetry is hence

$$\{\gamma_5, \Gamma\} = 0 \tag{2.43}$$

and we will call quantities that respect this condition chirally even and quantities that violate it chirally odd. This condition will help us later when we classify the basis tensors of the quark-gluon vertex.
The symmetry $U_A(1)$ is also called axial symmetry. This symmetry is broken by a quantum anomaly which can be traced back to the fact that the measure of the path integral is not invariant under $U_A(1)$ [65]. Adding a mass term with the same mass for each flavour breaks the above symmetry to $SU(N_f) \times SU_A(N_f) \times U(1) \to SU_V(N_f) \times U(1)$, where $SU_V(N_f)$ is a diagonal subgroup of $SU(N_f) \times SU_A(N_f)$. Assigning a non-degenerate mass to each flavour breaks the symmetry further to $U(1)^{N_f}$. This is the case that is realized in nature where every flavour has a distinct mass. As a consequence of this chiral symmetry is explicitly broken. However, since the masses of the lightest quarks are very small relative to the QCD scale one finds chiral symmetry to be a good approximate symmetry for up and down quarks and – though to less extent – for strange quarks. We will, however, restrict ourselves entirely to the case of massless quarks which is called the *chiral limit*.
The explicit breaking cannot be the only way chiral symmetry is broken. This can be illustrated by a phenomenological argument concerning the mass spectrum of hadrons. If chiral symmetry was (approximately) realized in nature as an unbroken symmetry, the masses of the hadrons would be parity degenerate, that is, the parity partner of a particle and the particle itself should have the same mass. This is however in contradiction to what is observed in experiments. Moreover, the explicit

[2] Strictly speaking $SU_A(N_f)$ does not form a group. To be mathematically precise one would have to consider the group $SU_L(N_f) \times SU_R(N_f)$ referring to left-handed and right-handed quarks.

breaking of chiral symmetry is due to the small masses of the light flavours not sufficient to account for the mass difference between parity partners. This all hints to the fact that chiral symmetry is spontaneously broken as well. Since this breaking is not triggered by an additional scalar field (like in the Higgs mechanism) but solely by the strong interaction it is referred to as dynamical symmetry breaking.
An order parameter that indicates the breaking of chiral symmetry is given by the chiral condensate

$$\langle \bar{q}q \rangle \begin{cases} = 0, \text{ chiral symmetry is unbroken }, \\ \neq 0, \text{ chiral symmetry is broken }. \end{cases} \tag{2.44}$$

The chiral condensate is related to the quark propagator $S(p^2)$ by

$$-\langle \bar{q}q \rangle_{\mu^2} = Z_2 Z_m N_c \mathrm{Tr} \int \frac{d^4p}{(2\pi)^4} S(p^2) \ . \tag{2.45}$$

Here, the index μ^2 indicates that the chiral condensate is still renormalization point dependent. However, it can be brought into a renormalization point independent form

$$\langle \bar{q}q \rangle_{\mu^2} = \left(\frac{1}{2} \ln(\frac{\mu^2}{\Lambda^2_{QCD}}) \right)^{\gamma_m} \langle \bar{q}q \rangle \ , \tag{2.46}$$

with γ_m being the quark anomalous dimension.
A further order parameter for the breaking of chiral symmetry is given by the renormalization group invariant $M(p^2)$ which is called the quark mass function and which can be identified as one of two dressing functions of the quark propagator. Also in this case a non-vanishing mass function signals chiral symmetry breaking. Furthermore, a relation between quark mass function and chiral condensate can be found analytically [66].
For our purposes the use of the quark mass function as order parameter for chiral symmetry breaking will be more convenient since it will be directly the object of our calculations. We will therefore delve into the details of the quark mass function in chapter 4 when we will calculate the quark propagator.
At the end of this section we would like to mention that dynamical chiral symmetry breaking has also an impact on the quark-gluon vertex and therefore on the way how quark and gluons interact. This will be a central aspect of the investigations in this work.

3. Functional Methods

Crucial properties of matter like e.g. the formation of bound states or dynamical chiral symmetry breaking can not be explained in a perturbative framework. Therefore other methods need to be employed that allow for a non-perturbative analysis. Two main methods in this field are *Lattice gauge theories* and *Functional Methods*. In Lattice gauge theories the action of the theory is discretized and calculations are performed on a finite grid using statistical methods like Monte Carlo algorithms. On the other hand Functional Methods provide a way for calculations in the continuum. Both methods can be viewed as complementary in the sense that shortcomings of one of both (e.g. finite volume effects regarding Lattice gauge theories and truncation effects regarding Functional Methods) are circumvented by the other one.
In this section three different types of Functional Methods will be presented. These are the ones that are used in this thesis and moreover they have also attracted much attention over the last years. However, one should be aware that they only form a part of Functional Methods and other methods are available (see e.g. [67, 68, 69, 70]).
For the sake of simplicity we will consider a theory of bosonic scalars ϕ. However, these may be viewed as superfields, i.e., a reducible multiplet that comprises all other fields of the theory. For example for QCD in Landau gauge the superfield would have the following form: $\phi = \{A^a_\mu, \overline{q}, q, \overline{c}^a, c^a\}$.
Moreover, to keep the expressions as short as possible arguments are often suppressed.

3.1. Dyson-Schwinger equations

The Dyson-Schwinger equations (DSEs) [71, 72, 73] are the equations of motion of Green's functions. The most direct access to their derivation is provided by the consideration that the integral over a total derivative vanishes [74, 75, 76].

$$\begin{aligned} 0 &= \int \mathcal{D}[\phi] \frac{\delta}{\delta \phi_j} e^{-S + \int \phi_i J_i} \,, \\ &= \int \mathcal{D}[\phi] \left(-\frac{\delta S}{\delta \phi_j} + J_j \right) e^{-S + \int \phi_i J_i} \,, \end{aligned} \tag{3.1}$$

where the index of ϕ and J subsumes all indices of the field. If we replace the field by a derivative with respect to the source, we are allowed to pull the term in brackets out of the integral and can identify the generating functional $Z[J]$ on the right-hand side

$$0 = \left(-\left. \frac{\delta S}{\delta \phi_j} \right|_{\phi_j = \delta / \delta J_j} + J_j \right) Z[J] \,. \tag{3.2}$$

This equation can be regarded as the master equation for the DSEs because by differentiating with respect to the source we obtain the corresponding equations for the full Green's functions. However, for the same reasons as outlined in section 2.2 we are more interested in an equivalent equation for the effective action $\Gamma[\Phi]$ rather than for the generating functional $Z[J]$. Performing the steps described in section 2.2 to derive the effective action we receive after several manipulations the following master equation for the effective action [76]:

$$\begin{aligned}\frac{\delta\Gamma[\Phi]}{\delta\Phi_j} = \int S_{js}\Phi_s - \frac{1}{2}\int\int S_{jst}\left(\Phi_s\Phi_t + D^J_{st}\right) \\ - \frac{1}{3!}\int\int\int S_{jstu}\left(\Phi_s\Phi_t\Phi_u + 3\Phi_s D^J_{tu} + \int\int\int D^J_{sv}D^J_{tw}D^J_{ux}\Gamma^J_{vwx}\right) .\end{aligned} \tag{3.3}$$

For this equation we rewrote the action in the following way

$$S[\phi] = \frac{1}{2}\int\int S_{ij}\phi_i\phi_j - \frac{1}{3!}\int\int\int S_{ijk}\phi_i\phi_j\phi_k - \frac{1}{4!}\int\int\int\int S_{ijkl}\phi_i\phi_j\phi_k\phi_l \,. \tag{3.4}$$

Amongst others the advantage of this reformulation is that we can identify the expressions S_{ij}, S_{ijk} and S_{ijkl} with the inverse of a bare propagator and bare vertices, respectively. Over which arguments the integration is performed is in this notation indicated by the indices that are summed, e.g.,

$$\int S_{js}\Phi_s = \int dz S_{js}(x,z)\Phi_s(z)\,. \tag{3.5}$$

D^J_{ij} corresponds to

$$D^J_{ij} = \frac{\delta^2 W[J]}{\delta J_i \delta J_j}\,. \tag{3.6}$$

One needs to be careful with this expression, since it differs from the one for the propagator in that the sources are not yet set to zero. This is indicated by the index J. From equation (3.3) we obtain the DSEs for the correlation functions studied in this work by differentiating with respect to Φ.

An example for a DSE is given in figure 3.1, which shows the DSE for a propagator in a scalar theory with three- and four-point interactions. Regarding the graphical representation of DSEs a common convention – which we will follow throughout – is to denote dressed quantities with a thick and bare quantities with a thin blob. Although the thick blobs have been omitted for the sake of clarity, the internal lines represent dressed propagators. As one can see from figure 3.1 and as one can understand from equation (3.3) a special feature of DSEs is that every loop diagram exhibits exactly one bare vertex. Furthermore, for QCD in Landau gauge the loop diagrams can be at most of two-loop order.

What the DSEs have in common with most of the other methods presented here is that they form an infinite tower of coupled equations. This is best seen from figure 3.1 where the dressed propagator depends on dressed three- and four-point functions whose DSEs in turn depend on higher n-point functions and so forth. One therefore has to find a way to decouple the different DSEs from each other. One way to do so is to introduce a truncation in form of neglecting higher orders of a

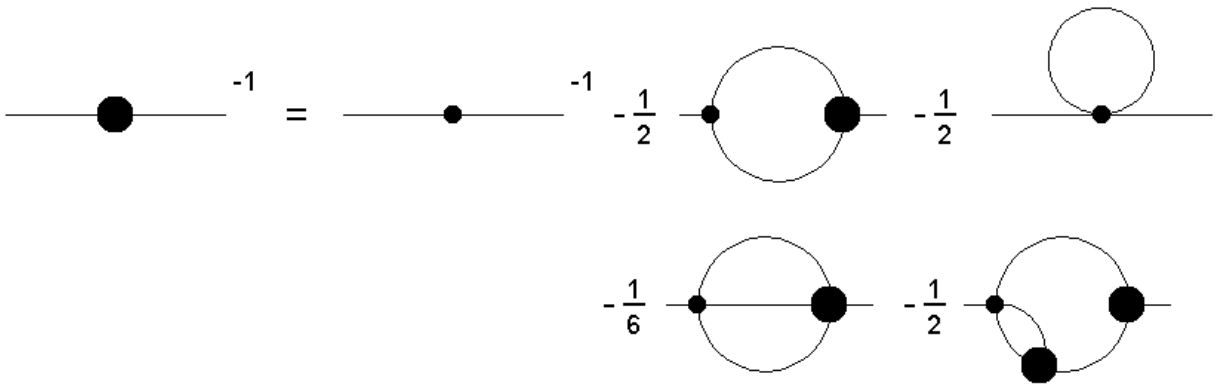

Figure 3.1.: As an example for the graphical depiction of a DSE the equation for the propagator in a scalar theory with three- and four-point interactions is shown. This and all following diagrams have been generated using *Jaxodraw* [77].

vertex expansion. For this one can formally expand the effective action as

$$\Gamma[\Phi] = \Gamma^{(0)} + \int \frac{\delta\Gamma}{\delta\Phi_i}\Phi_i + \frac{1}{2}\int\int \frac{\delta^2\Gamma}{\delta\Phi_i\delta\Phi_j}\Phi_i\Phi_j + \dots \ . \tag{3.7}$$

The idea is based on the assumption that higher n-point functions contribute very little and that the loss of information is negligible if these functions are left out. In practice one would just omit all diagrams that contain a given vertex (and of course also all diagrams with higher vertices) or employ a model for this vertex. Typically, in a first computation one neglects two-loop diagrams and diagrams with vertices that do not possess a tree-level counterpart.
This truncation scheme is the dominating scheme for almost all calculations using functional methods and has been very successful in the past. However, its downside is that one can not say in the first place whether the contribution of a vertex is negligible or not. One therefore relies on an enlargement of the truncation or on a comparison of the result of the own calculation with the result that is provided by using other methods or – if possible – on a direct comparison with measurements.

3.2. The nPI Formalism

The nPI formalism is a generalization of the 2PI formalism introduced by Cornwall, Jackiw and Tomboulis [78]. In a simplified view one may state that as much as the 1PI effective action leads to diagrams that do not fall apart into two diagrams by cutting a single line, the nPI effective action leads to diagrams that do not fall apart by cutting n lines[1].
A crucial difference between DSEs and the nPI formalism lies in the way the truncation is introduced. Regarding the DSEs the full effective action is used to derive a tower of infinitely many coupled equations and a truncation is needed to get a closed set of equations. In contrast in the nPI formalism a truncation is introduced

[1] Note, however, that this simplified picture is only true for $n \leq 4$. For n bigger than 4 irreducibility is lost [79].

by expanding the effective action itself up to a given order. From the expanded action one can then derive a closed set of equations.
One typically applies a loop expansion [80] to the effective action, however also every other expansion scheme is possible (see e.g. [81] and [82] for 2PI calculations employing a Large-N expansion).
In the loop expansion one exploits that with increasing loop order also the power of $\hbar$ increases. The effective action can then be expanded in powers of $\hbar$:

$$\Gamma[\Phi] = \sum_{L=0}^{\infty} \hbar^L \Gamma^{(L)}[\Phi] \, . \tag{3.8}$$

For example to one-loop order the effective action can be calculated to be

$$\Gamma[\Phi] = \mathcal{S}[\Phi] + \frac{\hbar}{2} \log \mathrm{Det} \left[\left(\frac{\delta^2 \mathcal{S}[\widetilde{\phi} + \Phi]}{\delta \widetilde{\phi}_i \delta \widetilde{\phi}_j} \right)_{\widetilde{\phi}=0} \right] + \mathcal{O}(\hbar^2) \, , \tag{3.9}$$

where the action $\mathcal{S}[\Phi]$ corresponds to the zeroth-loop order. By differentiating (3.9) with respect to the classical fields the equations for the n-point functions can be derived. Since we have already truncated the effective action itself these equations are closed (in contrast to DSEs).
The loop expansion so far only deals with bare quantities. To change this we have to introduce fully non-perturbative propagators and vertices to our effective action. This can be achieved by adding n non-local source terms to the generating functional [78, 83, 79]:

$$\begin{aligned} Z[J, R, R^{(3)}, \ldots] = \int \mathcal{D}\left[\phi\right] \exp\Big[-\frac{1}{\hbar}\mathcal{S} + \frac{1}{\hbar} \int J_i \phi_i + \frac{1}{2\hbar} \int\int R_{ij} \phi_i \phi_j \\ + \frac{1}{3!\hbar} \int\int\int R^{(3)}_{ijk} \phi_i \phi_j \phi_k + \ldots \Big] \, , \end{aligned} \tag{3.10}$$

where we have used again the abbreviation

$$\int\int R_{ij} \phi_i \phi_j = \int dx \int dy R_{ij}(x,y) \phi_i(x) \phi_j(y) \, , \tag{3.11}$$

and likewise for terms of higher order in ϕ. Consequently, the generating functional for connected Green's functions is given by

$$Z[J, R, R^{(3)}, \ldots] = \exp\left[\frac{1}{\hbar} W[J, R, R^{(3)}, \ldots] \right] . \tag{3.12}$$

To obtain the nPI-effective action from $W[J, R, R^{(3)}, \ldots]$ the Legendre transformation has to be performed with respect to all sources

$$\Gamma^{(nPI)}[\Phi, D, V^{(3)}, \ldots] = -W[J, R, R^{(3)}, \ldots] + \int \frac{\delta W}{\delta J_i} J_i + \int\int \frac{\delta W}{\delta R_{ij}} R_{ij} + \int\int\int \frac{\delta W}{\delta R^{(3)}_{ijk}} R^{(3)}_{ijk} + \ldots \, , \tag{3.13}$$

where

$$\frac{\delta W}{\delta J_i} = \frac{\delta W[J,R,R^{(3)},\ldots]}{\delta J_i(x)} = \Phi_i(x)\ , \tag{3.14}$$

$$\frac{\delta W}{\delta R_{ij}} = \frac{\delta W[J,R,R^{(3)},\ldots]}{\delta R_{ij}(x,y)} = \frac{1}{2}\left(\hbar D_{ij}(x,y) + \Phi_i(x)\Phi_j(y)\right)\ , \tag{3.15}$$

$$\frac{\delta W}{\delta R^{(3)}_{ijk}} = \frac{\delta W[J,R,R^{(3)},\ldots]}{\delta R^{(3)}_{ijk}(x,y,z)} = \frac{1}{6}\Big(\frac{1}{\hbar}V^{(3)}_{ijk}(x,y,z) + \hbar D_{ij}(x,y)\Phi_k(z) + \hbar D_{ki}(z,x)\Phi_j(y) + \hbar D_{jk}(y,z)\Phi_i(x) + \Phi_i(x)\Phi_j(y)\Phi_k(z)\Big)\ . \tag{3.16}$$

Here $D(x,y)$ describes the fully dressed propagator and $V^{(3)}(x,y,z)$ the fully dressed vertex for three-particle interactions.
Therefore, dressed quantities are treated as variables of the nPI-effective action. Moreover, the nPI-effective action is constructed such that every dressed quantity fulfills its own equation of motion, i.e.,

$$\frac{\delta\Gamma^{(nPI)}[\Phi,D,V^{(3)},\ldots]}{\delta\Phi_i} = \frac{\delta\Gamma^{(nPI)}[\Phi,D,V^{(3)},\ldots]}{\delta D_{ij}} = \frac{\delta\Gamma^{(nPI)}[\Phi,D,V^{(3)},\ldots]}{\delta V^{(3)}_{ijk}} = \ldots = 0\ . \tag{3.17}$$

The above statements shall be understood to be valid for arbitrary n. Of course one is free to choose a specific value. Depending on the number of added sources and thus of dressed quantities that appear as variables in the effective action one can therefore derive e.g. a 2PI-effective action or a 3PI-effective action etc. Since the introduction of additional source terms to our generating functional only changes the way the information of our theory is treated but does not delete any information, all effective actions obtained in this way have to agree in an untruncated set-up.

$$\Gamma^{(1PI)}[\Phi] = \Gamma^{(2PI)}[\Phi,D] = \Gamma^{(3PI)}[\Phi,D,V^{(3)}] = \ldots\ . \tag{3.18}$$

When on the other hand a truncation of the effective action, e.g. in form of a loop expansion, is performed, this equivalence does no longer persist. It is however possible to identify an equivalence of certain nPI-effective actions for each loop level separately. This leads to the following equivalence hierarchy [83]:

$$L=1 \qquad \Gamma^{(1PI)}[\Phi] = \Gamma^{(2PI)}[\Phi,D] = \Gamma^{(3PI)}[\Phi,D,V^{(3)}] = \ldots\ , \tag{3.19}$$

$$L=2 \qquad \Gamma^{(1PI)}[\Phi] \neq \Gamma^{(2PI)}[\Phi,D] = \Gamma^{(3PI)}[\Phi,D,V^{(3)}] = \ldots\ , \tag{3.20}$$

$$L=3 \qquad \Gamma^{(1PI)}[\Phi] \neq \Gamma^{(2PI)}[\Phi,D] \neq \Gamma^{(3PI)}[\Phi,D,V^{(3)}] = \ldots\ . \tag{3.21}$$

This equivalence hierarchy is very convenient for practical calculations since for a given loop expansion it prevents one from going to nPI-effective actions higher than necessary.
To give an example the 2PI effective action at one-loop reads

$$\Gamma^{(2PI)}_{L=1}[\Phi,D] = \mathcal{S}[\Phi] + \frac{\hbar}{2}\mathrm{Tr}\left[(D^0_\Phi)^{-1}D\right] + \frac{\hbar}{2}\mathrm{Tr}\log\left[D^{-1}\right] + \mathrm{const} + \mathcal{O}(\hbar^2)\,. \tag{3.22}$$

with the abbreviation

$$(D_\Phi^0)^{-1} = \left(\frac{\delta^{(2)} \mathcal{S}[\phi + \Phi]}{\delta\phi\delta\phi} \right)_{\phi=0} \tag{3.23}$$

and the trace goes over all indices and has to be understood to include integrals as well. To derive the effective actions of higher n a lot of work can be saved by exploiting the fact that Legendre transformations can be performed successively [84, 83, 85, 79]. Due to this one can start directly from higher effective actions (e.g. 2PI) so that the steps starting from the 1PI-effective action do not have to be repeated.
At first glance the nPI formalism and the DSEs bear a great resemblance to one another. Since the nPI formalism as well as DSEs are exact, i.e., they contain the full information of the theory, they must give the same results. However, things change when a truncation is introduced which is inevitable due to an infinite number of coupled correlation functions (DSEs) and source terms/Legendre transformations (nPI), respectively. Since both methods deal in different ways with the truncation and thus cut off information differently, the truncated methods do not coincide anymore in general.

3.3. The Functional Renormalization Group

The underlying idea of the Functional Renormalization Group (FRG) is that at large scales the physical system becomes independent of its microscopic degrees of freedom. An example for this – which can be found in [86] – is the alignment of spins in a ferromagnet. At the microscopic level the interaction of single spins has to be taken into account. But when one zooms out the behaviour of the spins at small distances (i.e. small compared to the correlation length) should be negligible for the description of the physical system and thus can be integrated out. The new degrees of freedom are then rather blocks of spins than single spins. In the next step, when one has further zoomed out, the system will be described by bigger blocks of spins and so on. Along this line only few parameters suffice to describe the infrared behaviour of the ferromagnet.
Already from this example two things can be deduced that are crucial for the FRG.

1. A new scale has to be introduced that determines which are the new degrees of freedom and what part of the system can be integrated out. In the example above this scale is given by the blocking step n by which the size of the spin blocks is defined.

2. The new degrees of freedom contain some of the information of the old degrees of freedom. In our case a bigger spin block is formed by some of the spins of a smaller spin block.

In the FRG-approach the first condition is fulfilled by introducing a regulator $R_k(p^2)$ that depends on a scale k. The action in the generating functional is then augmented

by the term

$$\Delta S_k[\phi] = \frac{1}{2}\int \frac{d^4q}{(2\pi)^4}\phi_i(q)R_k(q^2)\phi_i(-q)\,, \tag{3.24}$$

resulting in

$$Z_k[J] = \int D[\phi]e^{-S[\phi]-\Delta S_k[\phi]+\int d^4x\phi_i(x)J_i(x)}\,. \tag{3.25}$$

From the generating functional $Z[J]$ one can likewise write down the generating functional of the connected Green's functions

$$W_k[J] = \ln Z_k[J] = \ln\int D[\phi]e^{-S[\phi]-\Delta S_k[\phi]+\int d^4x\phi_i(x)J_i(x)}\,. \tag{3.26}$$

However, unlike the usual derivation of the effective action the Legendre transformation has now to be modified due to the appearance of the regulator term[2]:

$$\Gamma_k[\Phi] = -W_k[J] + \int d^4x J_i(x)\Phi_i(x) - \Delta S_k[\Phi]\,. \tag{3.27}$$

Since Φ is chosen to be the new variable and is thus k-independent, the source J adopts a k-dependence through

$$J_i(x) = \frac{\delta\Gamma_k[\Phi]}{\delta\Phi_i(x)} + \frac{\delta\Delta S_k[\Phi]}{\delta\Phi_i(x)} \tag{3.28}$$

There are moreover some constraints that are imposed on the method. To fulfill these conditions one demands that the regulator $R_k(p^2)$ exhibits the following properties [87, 88]:

1. To separate the fluctuations that are integrated out from those that remain unchanged $R_k(q^2)$ must behave as an IR-Regulator, that is, it should behave as

$$\lim_{q^2/k^2\to 0} R_k(q^2) > 0\,. \tag{3.29}$$

   This can be achieved in the following way:

$$R_k(q^2) \to k^2 \quad \text{for } q \ll k\,, \tag{3.30}$$
$$R_k(q^2) \to 0 \quad \text{for } q \geq k\,. \tag{3.31}$$

   Since the regulator occurs together with two fields in the term $\Delta S_k[\phi]$ it acts like a mass $\propto k^2$ for $q \ll k$. In this way the fluctuations are suppressed.

2. At a scale Λ at which all fluctuations are suppressed the classical action S should be recovered, i.e. $\Gamma_{k=\Lambda} = S$. For this purpose the regulator has to diverge in the limit $k \to \Lambda$:

$$\lim_{k^2\to\Lambda} R_k(q^2) \to \infty\,. \tag{3.32}$$

[2] Note that due to the term $\Delta S_k[\phi]$ in the Legendre transformation $\Gamma_k[\phi]$ does not need to be convex for $k \neq 0$. Only for $k \to 0$ convexity is guaranteed.

To see this we consider again (3.25) and apply the exponential function on both sides [88]

$$e^{W_k[J]} = \int D[\phi] e^{-S[\phi] - \frac{1}{2}\int \frac{d^4q}{(2\pi)^4}\phi_i(q)R_k(q^2)\phi_i(-q) + \int \frac{d^4p}{(2\pi)^4}\phi_i(p)J_i(-p)}\,. \tag{3.33}$$

Next we use (3.27) to express $W_k[J]$ and perform a variable substitution $\phi = \widetilde{\phi} + \Phi$

$$e^{-\Gamma_k[\Phi]} = \int D[\widetilde{\phi}] e^{-S[\widetilde{\phi}+\Phi] - \frac{1}{2}\int \frac{d^4q}{(2\pi)^4}\left[(\widetilde{\phi}_i(q)+\Phi_i(q))R_k(q^2)(\widetilde{\phi}_i(-q)+\Phi_i(-q)) - \Phi_i(q))R_k(q^2)\Phi_i(-q)\right]} \times$$
$$\times\, e^{\int \frac{d^4p}{(2\pi)^4}\left[(\widetilde{\phi}_i(p)+\Phi_i(p))J_i(-p) - \Phi_i(p)J_i(-p)\right]} \tag{3.34}$$

Using (3.28) we replace the source $J(q)$ by

$$J_i(q) = \frac{\delta\Gamma_k[\Phi]}{\delta\Phi_i(q)} + \Phi_i(-q)R_k(q^2) \tag{3.35}$$

and exploit the fact that

$$\int \frac{d^4q}{(2\pi)^4}\widetilde{\phi}_i(q)R_k(q^2)\Phi_i(-q) = \int \frac{d^4q}{(2\pi)^4}\Phi_i(q)R_k(q^2)\widetilde{\phi}_i(-q) \tag{3.36}$$

This gives

$$e^{-\Gamma_k[\Phi]} = \int D[\widetilde{\phi}] e^{-S[\widetilde{\phi}+\Phi] - \frac{1}{2}\int \frac{d^4q}{(2\pi)^4}\widetilde{\phi}_i(q)R_k(q^2)\widetilde{\phi}_i(-q) + \int \frac{d^4p}{(2\pi)^4}\widetilde{\phi}_i(p)\frac{\delta\Gamma_k[\Phi]}{\delta\Phi_i(-p)}} \tag{3.37}$$

When the regulator diverges the term containing the regulator corresponds to a delta functional $\delta(\widetilde{\phi})$. Herefrom follows the requested property $\Gamma_{k=\Lambda} = S$.

3. Of course the full quantum theory must be recovered when the introduced scale k vanishes, that is, when all fluctuations are integrated out. The regulator hence must obey

$$\lim_{k^2/q^2\to 0} R_k(q^2) = 0\,. \tag{3.38}$$

Apart from these conditions no further restrictions that are imposed on the regulator are necessary[3]. Therefore one can choose between a large number of different regulator forms. This allows one to implement the regulator that is best suited for the problem under consideration. Two examples for regulators are given in appendix B.1.

3.3.1. Flow Equation

It now only remains to fulfill the second condition derived from our introductory example at the beginning of section 3.3, that is, to find a way to connect the effective action at a given scale with the information at a different scale or in other words to

[3] Note, however, that the second condition is not mandatory. The effects of remaining fluctuations can be taken into account by a reparametrization of the classical action S.

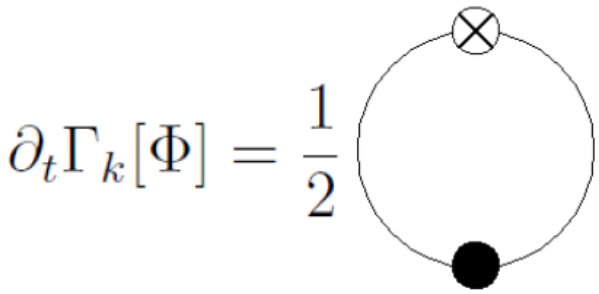

Figure 3.2.: A diagramatical representation of the flow equation. The filled blob denotes a dressed propagator (with an implicit and explicit regulator dependence). The crossed circle stands for the insertion $\dot{R}_k$

describe how $\Gamma_k[\Phi]$ varies with k. This so-called flow of the effective action $\Gamma_k[\Phi]$ is given by the Wetterich-equation [89]:

$$\frac{\partial}{\partial k}\Gamma_k[\Phi] = \frac{1}{2}\mathrm{STr}\left\{\left[\Gamma_k^{(2)}[\Phi] + R_k\right]^{(-1)}\frac{\partial}{\partial k}R_k\right\} \tag{3.39}$$

Here $\Gamma_k^{(2)}[\Phi]$ denotes the regulator dependent two-point function which is obtained by differentiating (3.27) two times with respect to Φ. The supertrace STr acts on all internal indices, which in position/momentum space corresponds to an integration. Moreover, when dealing with Grassmann-valued fields it applies the correct sign. Sometimes the flow equation is presented in a different notation in which dimensionless derivatives $\partial_t = k\frac{\partial}{\partial k}$ are used. With $\dot{R}_k = \partial_t R_k$ the equation (3.39) reads:

$$\partial_t\Gamma_k[\Phi] = \frac{1}{2}\mathrm{STr}\left\{\left[\Gamma_k^{(2)}[\Phi] + R_k\right]^{(-1)}\dot{R}_k\right\} \tag{3.40}$$

This is also the form that will be employed throughout this work.
The flow equation has a pictorial representation as Feynman diagram as it is depicted in figure 3.2. In addition to usual Feynman diagrams the derivative of the regulator $\partial_t R_k$ has to be included. This term is normally represented by a crossed circle. Furthermore, the full propagator corresponds to the expression $\left[\Gamma_k^{(2)}[\Phi] + R_k\right]^{(-1)}$, i.e. it has an implicit regulator dependence through Γ_k and an explicit dependence through R_k
From the flow equation (3.40)/(3.39) the flow equations for higher n-point functions can be derived by further differentiating with respect to Φ.
Finally, one would then start to solve the flow equation for the requested n-point function by implementing $\Gamma_{k=\Lambda}[\Phi] = S$ as an initial condition and flowing down to k=0 where the full theory is reproduced. The flow of the effective action can be illustrated in the so-called theory space. This space is spanned by all invariant operators of the field on which the effective action can depend like Φ^2, $\partial_\mu\Phi\partial_\mu\Phi$, etc. Therefore every point in theory space describes a different effective action. An example for an illustration of the effective action Γ_k in theory space is given in figure 3.3. Since different regulators can lead to different flows, the trajectories in theory space need not be the same. But since the regulator is an artificial insertion into

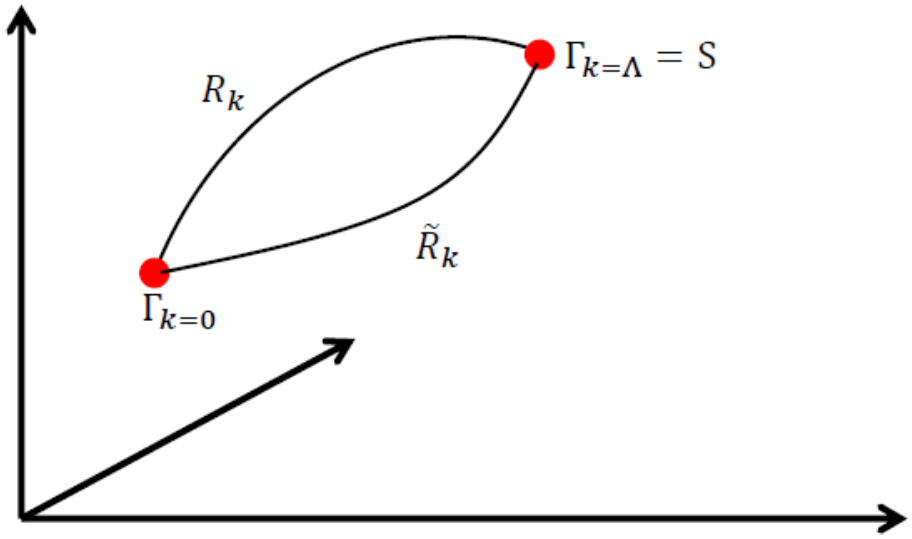

Figure 3.3.: An idealized representation of the theory space. For two different regulators $R_k(p^2)$ and $\tilde{R}_k(p^2)$ the trajectory may differ while the starting ($\Gamma_{k=\Lambda}$) and end point ($\Gamma_{k=0}$) must be the same. Note that in general the theory space is infinitely dimensional.

the theory, the effective action Γ_k has no physical interpretation anyway as long as the regulator is finite. There are only two points in theory space that are physical, namely the point $\Gamma_{k=\Lambda}[\Phi] = S$ (corresponding to a diverging regulator) where the classical action is reproduced and the point $\Gamma_{k=0}[\Phi]$ (corresponding to a vanishing regulator) where the full theory is obtained. Therefore, these both points must be the initial respectively the end point of every trajectory. In a numerical calculation a truncation needs to be employed and due to this it is possible that the result for $\Gamma_{k=0}[\Phi]$ still depends on the chosen regulator. One therefore has to check in a regulator study if the result is sensitive to a change of the regulator.

4. The quark-gluon vertex

In this chapter we will study the coupled system of quark-gluon vertex and quark propagator which make up the entire quark-sector analyzed in this thesis. In doing so we will approximate the impact of the Yang-Mills sector on the system. For the case of the Yang-Mills propagators this is achieved by using input data, i.e. results of an independent calculation ignoring effects due to back-coupling. On the other hand for the three-gluon vertex a model will be employed. It turned out that these approximations are appropriate to investigate the effects of chiral symmetry breaking [12, 10, 11, 17].
One should be aware that the DSE for the quark-gluon vertex differs from the corresponding equation in the 3PI formalism. This difference will be worked out in section 4.8. We will thus present results for both methods and show that with the employed truncation both lead to different results. Furthermore, the results of this section provide the basis for the unquenching of the three-gluon vertex in chapter 5.

4.1. The equation of the quark-gluon vertex

The diagrammatic equation for the quark-gluon vertex derived from the 3PI formalism is shown in figure 4.1. The second diagram can appear in the same form in an Abelian theory like QED, while the occurrence of the third diagram is restricted to non-Abelian theories due to the self-interaction of the gauge fields in the form of a three-gluon vertex. Consequently, both diagrams are refered to as the **Abelian** and **non-Abelian** diagram, respectively.
Regarding the DSE of the quark-gluon vertex two equations can be derived depending on which external leg is attached to the bare vertex. Attaching the gluon leg to the bare vertex (the lower equation in figure 4.2) results in the appearance of two-loop diagrams. Moreover, in this DSE version of the quark-gluon vertex all primitively divergent vertices are present. If a quark leg is attached to the bare vertex (the upper equation in figure 4.2) we arrive at an equation that resembles

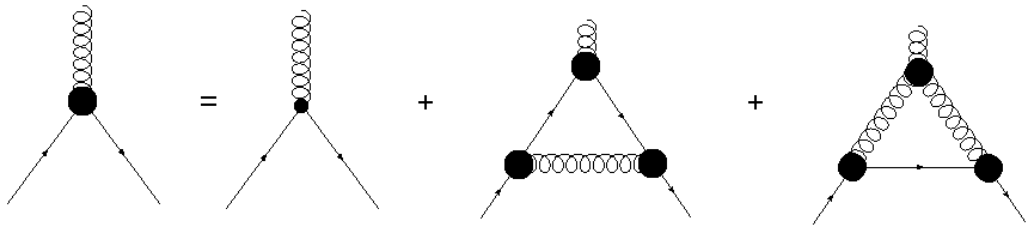

Figure 4.1.: The equation for the quark-gluon vertex in the 3PI formalism. The second and third diagrams are called the Abelian and non-Abelian diagram, respectively.

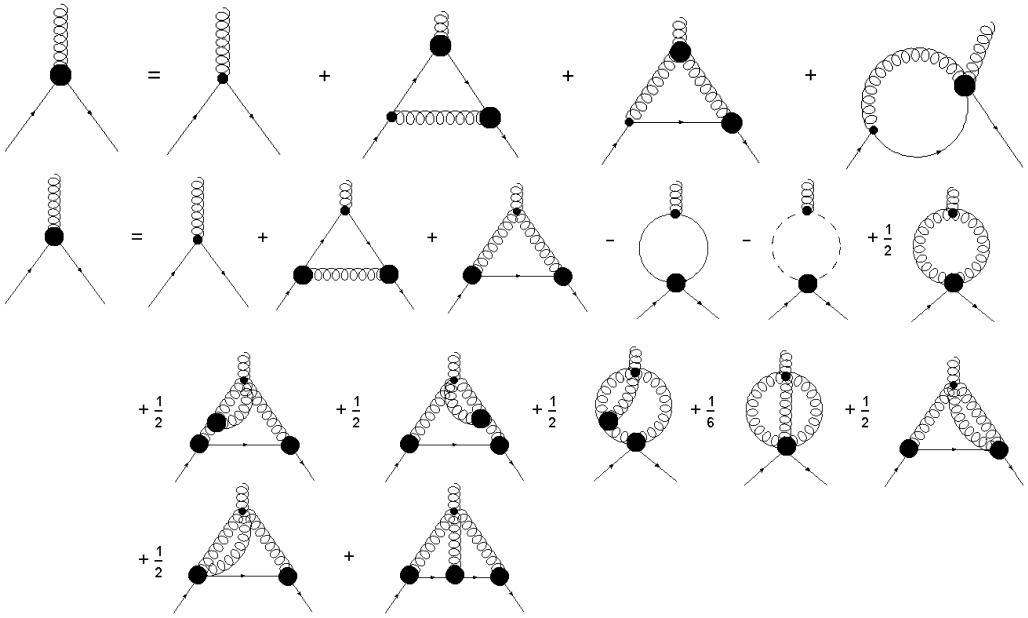

Figure 4.2.: The two DSEs of the quark-gluon vertex. In the upper equation the first derivative of the effective action is with respect to the quark field where as in the lower equation it is with respect to the gluon field.

the equation derived from the 3PI formalism. However, there are mainly two differences.
Firstly, compared to the 3PI equation there is an additional swordfish diagram with a dressed two-quark-two-gluon vertex. It was found in [14] by means of an infrared analysis that the contribution of this diagram is sizeable [1]. We will make an ansatz for the two-quark-two-gluon vertex and calculate the swordfish diagram with this model in section 4.8. Moreover, in a full DSE calculation further statements about the importance of this diagram will be made.
Secondly, in the 3PI equation all quark-gluon vertices in the Abelian and non-Abelian diagrams are dressed, whereas the DSE features a bare quark-gluon vertex in every diagram. One may therefore speculate that some of the information contained in the swordfish diagram is absorbed in the 3PI equation by dressing the bare quark-gluon vertex. In the following we will disregard the DSE with a gluon leg attached to the bare vertex and work entirely with the 3PI equation and its DSE counterpart.
Some insight into the relative contribution of each diagram to the full quark-gluon vertex can be gained by analyzing their color structure. Depicting the color factors of each diagram explicitly one arrives at the equations in figure 4.3. From these equations one becomes immediately aware that compared to the non-Abelian diagram the Abelian diagram is suppressed by a factor of N_c^2. In addition, the Abelian diagram is also suppressed dynamically. This was shown in [11] by performing the calculation in adjoint QCD. In adjoint QCD the non-Abelian diagram as well as the Abelian diagram exhibit the same color factor of $N_c/2$, but nevertheless a suppression of the Abelian diagram could be observed. The swordfish diagram in the DSE formulation of the quark-gluon vertex has a more complicated color structure due to the more intricate contribution of the two-quark-two-gluon vertex to color space.

[1] It should be mentioned however that this result refers to a so called scaling solution, whereas our calculations correspond to the decoupling solution.

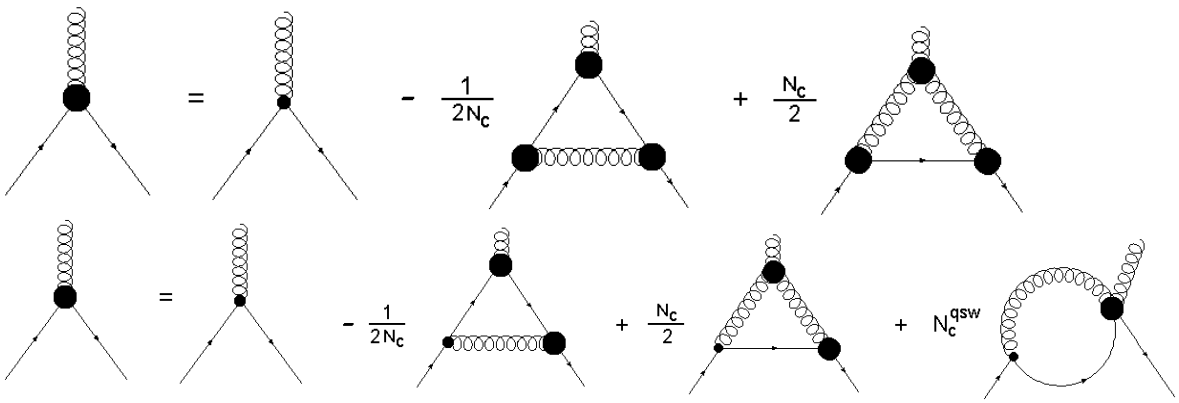

Figure 4.3.: Depicted are the 3PI equation and DSE of the quark-gluon vertex where the contribution of each diagram in the color space is made explicit. The Abelian diagram is supressed by a factor of N_c^2 compared to the non-Abelian diagram. The contribution of the swordfish diagram to color space is more complex than for the other diagrams and hence abbreviated by a generic term N_c^{qsw}.

Therefore, we combined the color factors of the swordfish diagram into a generic expression N_c^{qsw}.
Based on the aforementioned arguments we will in the following focus on the non-Abelian diagram when we work in the 3PI formalism. In contrast, the computation of the Abelian diagram in the DSE formulation is less costly, since only two instead of three fully dressed quark-gluon vertices have to be taken into account. Hence, we will consider all three diagrams of the DSE and in doing so employ a model for the two-quark-two-gluon vertex that appears in the swordfish diagram. The color structure of the two-quark-two-gluon vertex is then determined within this ansatz.

4.2. Parametrizing the quark-gluon vertex

Before we can start the actual calculation we have to think about how the information of the quark-gluon vertex that is contained in various spaces can be expressed best. Since the contribution to color space coincides with the tree-level expression, that is with the generator T^a, the only spaces that need deliberation are the momentum and Dirac space. Within a basis decomposition the information is either allocated to the dressing functions ($d^{(i)}$) or the basis tensors ($t_\mu^{(i)}$). For the quark-gluon vertex twelve basis tensors can be found which can be constructed such that eight are transverse and four are longitudinal. However, in Landau gauge the full dynamics of the theory are described by the transverse part only [90]. The reason for this is that in Landau gauge the structure of the gluon propagator is the same as for the transverse projector and that every quantity carrying a Lorentz index is finally contracted with the gluon propagator.
For the transverse quark-gluon vertex we are thus left with eight basis tensors and suppressing the color factor the vertex can be written in a generic form as

$$\Gamma_\mu^{(qgv)} = \sum_{i=1}^{8} d^{(i)}(a_1, a_2, a_3) t_\mu^{(i)} \,. \tag{4.1}$$

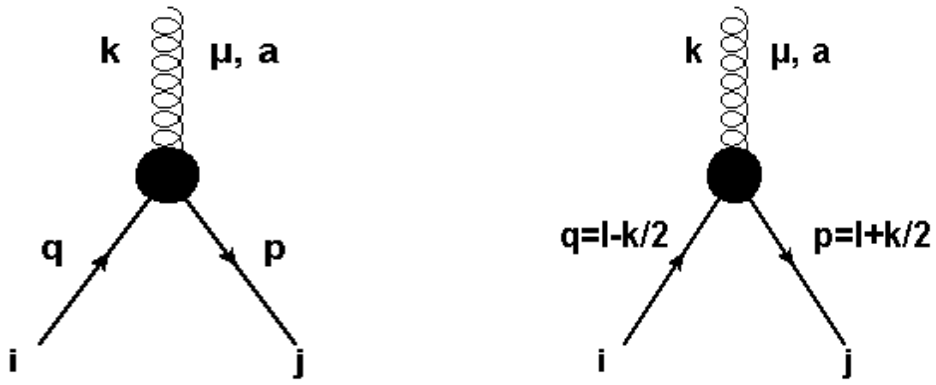

Figure 4.4.: The index conventions for the quark-gluon vertex as employed in the naive basis (left) and in the generalized Ball-Chiu basis (right). The momenta for the incoming and outgoing quark are q and p, respectively. k is the momentum of an incoming gluon and l is the relative momentum.

Our task thus translates into finding an appropriate set of basis tensors $t_\mu^{(i)}$ and a well suited parametrization of the arguments of the dressing function $d^{(i)}(a_1, a_2, a_3)$. The sets of basis tensors for the quark-gluon vertex that are proposed in the literature can be roughly classified into two groups. In the following we will call the one group the "**naive basis"** [10, 11, 17, 15] and the other group the "**generalized Ball-Chiu basis"**[91, 92, 15, 14, 93, 1, 4, 8, 94, 12, 13]. To be able to distinguish between both basis systems at first sight we will write from now on the tensors of the "naive basis" and their corresponding dressing functions as $b_\mu^{(i)}$ and $g^{(i)}$ and the tensors and dressing functions of the "generalized Ball-Chiu basis" as $X_\mu^{(i)}$ and $h^{(i)}$.
The most direct access to the quark-gluon vertex is provided by the "naive basis". In this basis a complete set of transverse basis tensors is constructed by combining all independent tensors – consisting in total of one gamma matrix and two momenta – with all independent scalars. This combination has then to be contracted by the projector

$$P_{\mu\nu}(k) = \delta_{\mu\nu} - \frac{k_\mu k_\nu}{k^2} \tag{4.2}$$

in order to project into the transverse subspace. If we choose for instance the gluon momentum k and the incoming quark momentum q (see figure 4.4) as the independent momenta in our system, the transverse basis tensors are built up from the combinations

$$P_{\mu\nu}(k) \begin{pmatrix} \gamma_\nu \\ q_\nu \end{pmatrix} \otimes \begin{pmatrix} \mathbb{1} \\ \not{q} \\ \not{k} \\ \not{k}\not{q} \end{pmatrix} , \tag{4.3}$$

where we have already taken into account that tensor structures proportional to k_ν will vanish after transverse projection. The big advantage of this basis system is the simplicity of its tensor structures. The price one has to pay for this simple structure is that the basis tensors do not exhibit certain properties like being free from kinematic singularities.
For this reason one attempted to find a set of basis tensors that are free from kine-

matic singularities. Historically this search goes back to the pioneering work of Ball and Chiu [91] who constructed a basis in QED that is free from kinematic singularities. However, Ball and Chiu worked entirely in Feynman gauge and it turned out that the basis they had constructed loses its analytical properties in other gauges. But a generalization to arbitrary gauges is possible [92].
Moreover, the basis can be written such that every single basis tensor has a definite behaviour under charge conjugation. This is in contrast to most other basis systems where this statement holds true for the whole quark-gluon vertex but not for every basis tensor alone. In order to achieve this one has to consider that charge conjugation interchanges the quark momenta

$$\begin{aligned} q &\to -p \,, \\ p &\to -q \,. \end{aligned} \tag{4.4}$$

To have a definite behaviour under charge conjugation every basis tensor has therefore to be built up from appropriate combinations of momenta. Though not necessary, it is on account of this somehow natural to work with the relative and total momenta $l = (p+q)/2$ and $k = p - q$ instead of the quark momenta q and p. With this choice the eight transverse tensors of the "generalized Ball-Chiu basis" take the form [12, 13, 94]:

$$\begin{aligned} X_\mu^{(1)} &= \gamma_\mu^{(T)} \,, & X_\mu^{(2)} &= \not{l} l_\mu^{(T)} \,, \\ X_\mu^{(3)} &= i l_\mu^{(T)} \,, & X_\mu^{(4)} &= \frac{i}{2}(l\cdot k)\left[\gamma_\mu^{(T)}, \not{l}\right] \,, \\ X_\mu^{(5)} &= \frac{i}{2}\left[\gamma_\mu, \not{k}\right] \,, & X_\mu^{(6)} &= \frac{1}{6}\left(\left[\gamma_\mu, \not{l}\right]\not{k} + \left[\not{l}, \not{k}\right]\gamma_\mu + \left[\not{k}, \gamma_\mu\right]\not{l}\right) \,, \\ X_\mu^{(7)} &= (l\cdot k)\tau_{\mu\nu}\gamma_\nu \,, & X_\mu^{(8)} &= \frac{i}{2}\tau_{\mu\nu}\left[\gamma_\nu, \not{l}\right] \,, \end{aligned} \tag{4.5}$$

where the index (T) implies a contraction with the projector (4.2) and the projector $\tau_{\mu\nu}$ is given by

$$\tau_{\mu\nu} = (l\cdot k)\delta_{\mu\nu} - l_\mu k_\nu \,. \tag{4.6}$$

Next we have to find appropriate expressions for the the three Lorentz invariants a_1, a_2 and a_3 on which the dressing functions depend. Like for the basis tensors there are different possibilities. One possibility is to use the squares of the two independent momenta in our system and the angle between them. If we choose the independent momenta to be the quark momenta p and q the three Lorentz invariants read

$$\begin{aligned} a_1 &= p^2 \,, \\ a_2 &= q^2 \,, \\ a_3 &= \frac{p\cdot q}{\sqrt{p^2 q^2}} = \cos(\alpha) \,. \end{aligned} \tag{4.7}$$

A further possibility is to derive the Lorentz invariants from the permutation group $\mathbb{S}_n$. This has been carried out for three-point functions and the group $\mathbb{S}_3$ [31, 34, 12, 13] as well as for four-point functions and the group $\mathbb{S}_4$ [95, 96]. The Lorentz

invariants in this ansatz read

$$
\begin{aligned}
a_1 = s_0 &= \frac{l^2}{3} + \frac{k^2}{4} \ , \\
a_2 = a &= \frac{l \cdot k}{\sqrt{3} s_0} \ , \\
a_3 = s &= 1 - \frac{k^2}{2 s_0} \ ,
\end{aligned} \tag{4.8}
$$

where l and k are again the relative and total momenta and we have adopted the notational convention introduced in [31]. Note that s_0 is the only dimensionful variable. a and s are angular variables that take values in the interval $[-1, 1]$. This parametrization proved to be advantageous for bound state calculations [96].
What has been said so far refers to an analysis of the quark-gluon vertex before any calculation. However, in a numerical calculation additional difficulties can arise like e.g. an imperfect cancellation of terms. With respect to this one basis may prove to be better suited than another one. In spite of its convenient analytical properties we found a calculation in the "generalized Ball-Chiu basis" rather demanding. Nonetheless, the numerical problems that arise in this basis can be circumvented and an outline how this can be done is given in appendix A.5.
We found the calculation to be easiest in a "naive basis" similar to the one that has been employed in [17][2]:

$$
\begin{aligned}
b_\mu^{(1)} &= \gamma_\nu P_{\mu\nu}(k) \ , & b_\mu^{(2)} &= i(p_\nu + q_\nu) P_{\mu\nu}(k) \ , \\
b_\mu^{(3)} &= i(\not{p} + \not{q}) \gamma_\nu P_{\mu\nu}(k) \ , & b_\mu^{(4)} &= i(\not{p} - \not{q}) \gamma_\nu P_{\mu\nu}(k) \ , \\
b_\mu^{(5)} &= -(\not{p} - \not{q})(p_\nu + q_\nu) P_{\mu\nu}(k) \ , & b_\mu^{(6)} &= (\not{p} + \not{q})(p_\nu + q_\nu) P_{\mu\nu}(k) \ , \\
b_\mu^{(7)} &= \frac{1}{2} \left[\not{p}, \not{q}\right] \gamma_\nu P_{\mu\nu}(k) \ , & b_\mu^{(8)} &= -\frac{i}{2} \left[\not{p}, \not{q}\right] (p_\nu + q_\nu) P_{\mu\nu}(k) \ ,
\end{aligned} \tag{4.9}
$$

where we choose the two independent momenta to be p and q and thus $k = p - q$. For the dressing functions $g^{(i)}$ we use the parametrization (4.7). The full decomposition of the quark-gluon vertex thus has the form:

$$
T^a \Gamma_\mu^{(qgv)}(p, q) = T^a \sum_{i=1}^{8} g^{(i)}(p^2, q^2, \cos(\alpha)) b_\mu^{(i)} \ . \tag{4.10}
$$

For later it is useful to separate the basis tensors into chirally symmetric and chiral symmetry breaking subsets. This can be easily done by counting the number of gamma matrices in every tensor. The tensors with an odd number of gamma matrices belong to the set $G_{\chi sym}$ that respects chiral symmetry and those with an even number of gamma matrices break chiral symmetry and thus belong to the set $G_{\chi SB}$. We have

$$
G_{\chi sym} = \left\{ b_\mu^1, b_\mu^5, b_\mu^6, b_\mu^7 \right\} \ , \tag{4.11}
$$

$$
G_{\chi SB} = \left\{ b_\mu^2, b_\mu^3, b_\mu^4, b_\mu^8 \right\} \ . \tag{4.12}
$$

[2] Note that in our convention the momentum of the antiquark p is outgoing, whereas in [17] all momenta are incoming.

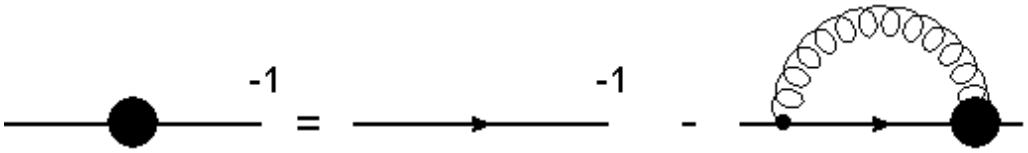

Figure 4.5.: The quark propagator DSE

4.3. The quark propagator

Coupled to the equation of the quark-gluon vertex is the quark propagator and vice versa the quark-gluon vertex appears in the DSE of the quark propagator (figure 4.5). The latter case plays a crucial role in dynamical chiral symmetry breaking, since a certain strength for the quark-gluon vertex is necessary for triggering this mechanism as we will discuss below.
The dynamical breaking of chiral symmetry reflects itself also in the dressing functions of the quark propagator

$$S(p) = Z_f(p^2)\frac{i\not{p} + M(p^2)}{p^2 + M^2(p^2)} \ . \tag{4.13}$$

The dressing function $Z_f(p^2)$ is called the wave function renormalization and $M(p^2)$ is the mass function which comprises the mass that is generated by chiral symmetry breaking. In this thesis we are working entirely in the chiral limit and consequently $M(p^2)$ will tend to zero at high momenta. Going from high momenta towards the infrared chiral symmetry will break at around $1\,GeV$ and mass is dynamically generated. The function $M(p^2)$ will thus rise until it adopts its final value of around $300 - 400\,MeV$. For the actual calculation we will however use a different notation for the quark propagator

$$S(p) = \frac{1}{-i\not{p}A(p^2) + B(p^2)} \ . \tag{4.14}$$

Since this is merely a further parametrization of the same quantity one can relate the dressing functions $A(p^2)$ and $B(p^2)$ to the wave function renormalization and the mass function

$$Z_f(p^2) = \frac{1}{A(p^2)} \ , \tag{4.15}$$

$$M(p^2) = \frac{B(p^2)}{A(p^2)} \ . \tag{4.16}$$

To project out the dressing function $B(p^2)$ we take the Dirac trace of the quark propagator DSE directly, whereas projecting out $A(p^2)$ requires a multiplication with $\not{p}$ before taking the Dirac trace. The equations then read

$$A(p^2) = Z_2 + Z_{1F}\frac{g^2}{4ip^2}C_F \int \frac{d^4k}{(2\pi)^4}\mathrm{Tr}[\not{p}\gamma_\mu D_{\mu\nu}(k)S(p+k)\Gamma^{(qgv)}_\nu(p,p+k)] \ , \tag{4.17}$$

$$B(p^2) = Z_{1F}\frac{g^2}{4}C_F \int \frac{d^4k}{(2\pi)^4}\mathrm{Tr}[\gamma_\mu D_{\mu\nu}(k)S(p+k)\Gamma^{(qgv)}_\nu(p,p+k)] \ . \tag{4.18}$$

Here, we have already divided by the terms from the left-hand side. The color factors are absorbed in $C_F = \frac{N_c^2-1}{2N_c}$, where a factor $\frac{N_c^2-1}{2}$ stems from the color trace of the loop and the left-hand side contributes with the factor N_c. Z_2 and Z_{1F} are the renormalization constants of the quark field and the quark-gluon vertex. The fully dressed gluon propagator $D_{\mu\nu}(k)$ is given by

$$D_{\mu\nu}(k) = \left(\delta_{\mu\nu} - \frac{k_\mu k_\nu}{k^2}\right) \frac{Z(k^2)}{k^2}\,, \tag{4.19}$$

where $Z(k^2)$ is the gluon dressing function.
It should be noted that in the general case of non-vanishing quark masses a term $Z_2 Z_m m$ has to be added to (4.18), which drops out in the chiral limit.

4.4. Renormalization

There are mainly two ways how the renormalization can be performed. In the first variant one employs a MOM scheme in which one subtracts from the equation in question the equation evaluated at a specific point. This method was introduced in [97, 98, 99] and frequently applied henceforth (see e.g. [100]).
The second possibility consists in using the Slavnov-Taylor identities, which relate renormalization constants to each other. However, it should be stressed that this is only useful if the exact value of some renormalization constants is already known. Typically, one calculates the renormalization constants of the fields from the propagator equations by using the MOM scheme described above and then exploits the STIs to get the renormalization constants of the vertices. This method can be combined with so-called renormalization group improvement terms [101], which we will employ when we calculate the three-gluon vertex in chapter 5.
In figure 4.6 the 3PI equation and the DSE are shown again, but this time the renormalization constants are displayed explicitly. In the 3PI equation we have already discarded the Abelian diagram since we will not consider it in the following.
For the 3PI equation we will use the MOM scheme. Schematically one may write the 3PI equation as follows

$$g_i(p^2, q^2, \cos(\alpha)) = \left\{ Z_{1F} \;\; \mathbf{treelevel} + \mathbf{loop}(p^2, q^2, \cos(\alpha)) \right\}_i \,. \tag{4.20}$$

Most of the notation is self-explanatory, however, we have to comment on the curly brackets. The eight dressing functions of the quark-gluon vertex demand that we project the equation eight times which results in eight equations. However, we do not project out the dressing functions directly but rather use a method which corresponds to a matrix multiplication (see Appendix A.4 for technical details) and therefore the information about a specific dressing function is scattered over different projections. The matrix combines these projections such that the dressing function is recovered. The curly brackets shall indicate that the matrix multiplication has already been performed and that hence the right-hand side contains all information corresponding to dressing function g_i in a proper way.
The only dressing function that is UV-divergent and thus needs renormalization is the tree-level dressing function g_1. The subtraction scheme then requires that we assign a certain value to g_1 at a specific point. For this we use the condition that

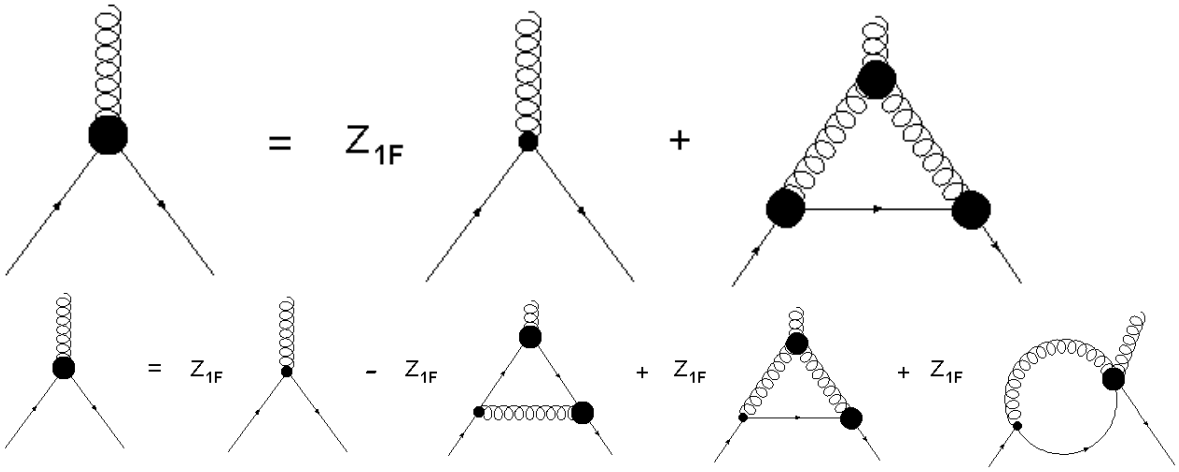

Figure 4.6.: The quark-gluon vertex in the 3PI and DSE formalism. The renormalization constants are depicted explicitly. Note that the Abelian diagram in the 3PI equation has already been droped.

the running coupling derived from the quark-gluon vertex

$$\alpha_{qgv}(p^2) = \alpha(\mu^2) g_1(p^2, p^2, 0.5)^2 Z(p^2) A(p^2)^{-2} \tag{4.21}$$

matches the running coupling from the ghost and gluon propagators [35].

$$\alpha_{ghgl}(p^2) = \alpha(\mu^2) Z(p^2) G(p^2)^2 \,. \tag{4.22}$$

Here $\alpha(\mu^2)$ is the coupling at the renormalization point μ^2. From $\alpha_{qgv}(\mu^2) = \alpha_{ghgl}(\mu^2)$ we obtain the following condition

$$\begin{aligned} g_1(\mu^2, \mu^2, 0.5)^2 Z(\mu^2) A(\mu^2)^{-2} &= Z(\mu^2) G(\mu^2)^2 \,, \\ \Rightarrow g_1(\mu^2, \mu^2, 0.5) &= G(\mu^2) A(\mu^2) \,. \end{aligned} \tag{4.23}$$

In contrast to propagators there is a multitude of points at which vertices can be subtracted. In our case we have chosen the symmetric point. Moreover, the value of the ghost dressing function $G(\mu^2)$ is fixed by the input we use for the Yang-Mills propagators and the value for the dressing function of the quark propagator will be set to $A(\mu^2) = 1$.
Evaluating (4.20) at the scale μ^2 we can solve for the renormalization constant

$$Z_{1F} = \frac{g_1(\mu^2, \mu^2, -0.5) - \{\mathbf{loop}(\mu^2, \mu^2, -0.5)\}_1}{\{\mathbf{treelevel}\}_1} \,. \tag{4.24}$$

This value for Z_{1F} will then be updated in each iteration step.
Regarding the equations for the two dressing functions of the quark propagator (4.17) and (4.18) the only unknown renormalization constant is Z_2 in the equation for $A(p^2)$. Here again we will employ the subtraction method, but since we are not interested in the exact value of Z_2 we will this time subtract the equation for $A(p^2)$ evaluated at μ^2 from (4.17). The value of the dressing function $A(p^2)$ at the scale μ^2 has already been set for the calculation of Z_{1F} and is given by $A(\mu^2) = 1$. With

this we finally have to calculate the equation

$$A(p^2) = 1 + Z_{1F}\left(\mathbf{loopA}(p^2) - \mathbf{loopA}(\mu^2)\right) \ , \tag{4.25}$$

where we have introduced the abbreviation

$$\mathbf{loopA}(p^2) = \frac{g^2}{4ip^2} C_F \int \frac{d^4k}{(2\pi)^4} \mathrm{Tr}[\not{p}\gamma_\mu D_{\mu\nu}(k) S(p+k) \Gamma^{(qgv)}_\nu(p, p+k)] \ . \tag{4.26}$$

With respect to the DSE we proceed in reversed order. We calculate Z_{1F} in the quark propagator equation and then use the result for the quark-gluon vertex. Here the starting point is equation (4.17). However, this time we make use of the STIs to reexpress the renormalization constant Z_2:

$$Z_2 = \frac{\widetilde{Z}_3 Z_{1F}}{\widetilde{Z}_1} \ . \tag{4.27}$$

The value of $\widetilde{Z}_3$ is known from the independent calculation of the Yang-Mills propagators that we use as input.
Applying an argument by Taylor [102] the renormalization constant of the ghost-gluon vertex is equal to one in certain renormalization schemes, $\widetilde{Z}_1 = 1$ [3]. This is also referred to as the "non-renormalization theorem". One of the renormalization schemes, in which this statement is valid, is the $\overline{MS}$ scheme. We therefore employ the MiniMOM scheme [104], which is a hybrid renormalization scheme that uses momentum subtraction for the propagators and the $\overline{MS}$ scheme for the ghost-gluon vertex. All remaining renormalization constants are then determined via the STIs. On account of this we are able to set $\widetilde{Z}_1 = 1$ in (4.27). Plugging the resulting expression for Z_2 into (4.17) and solving for Z_{1F} then leads to

$$Z_{1F} = \frac{1}{\widetilde{Z}_3 + \mathbf{loopA}(\mu^2)} \ . \tag{4.28}$$

Having found an expression for Z_{1F} we are then in a position to calculate the quark propagator and the quark-gluon vertex.

4.5. Results for the quark-gluon vertex from the 3PI formalism

At this point we would like to summarize the setup and specify which input enters the system. The quark-gluon vertex and the quark propagator are solved dynamically and hence the only unknown quantities in the equations for the quark-gluon vertex (Figure 4.6, top) and the quark propagator (Figure 4.5) are the three-gluon vertex and the gluon propagator. Indirectly, also the ghost propagator contributes via the model which we will employ for the three-gluon vertex.
This model was introduced in [101] and is constructed such that it fulfills Bose symmetry and reproduces the correct anomalous dimension of the three-gluon vertex.

[3] It should be emphasized that this statement is not true in arbitrary renormalization schemes, see [103].

It consists of an infrared and an ultraviolet term

$$D^{A^3}(p,q,-p-q) = D^{A^3,IR}(p,q,-p-q) + D^{A^3,UV}(p,q,-p-q) \;, \tag{4.29}$$

where we have adopted the notation of [101]. The UV-part consists of an appropriate combination of the ghost and gluon dressing functions $G(p^2)$ and $Z(p^2)$,

$$D^{A^3,UV}(p,q,-p-q) = G\left(\frac{p^2+q^2+(p+q)^2}{2}\right)^{\alpha} Z\left(\frac{p^2+q^2+(p+q)^2}{2}\right)^{\beta} \;. \tag{4.30}$$

The parameters α and β are not free but fixed by two requirements:

1. The UV-part of the model shall give the correct anomalous dimension of the three-gluon vertex: $\gamma_{3g} = 1+3\delta$, with δ being the ghost anomalous dimension.
2. The model shall not interfere with the infrared, that is, it shall be IR-finite.

With these conditions two equations can be set up from the UV-running [42] and IR-running [105, 106, cf. references in [90]] of the Yang-Mills propagators and α and β can be determined solely in terms of δ (using $\gamma = -1-2\delta$ for the anomalous dimension of the gluon if necessary). A complete calculation is carried out in chapter 5. Here, we only specify the result which reads for the decoupling solution

$$\alpha = \frac{3\delta+1}{\delta} \quad , \quad \beta = 0 \qquad \text{(decoupling)} \;. \tag{4.31}$$

One guideline for the construction of the IR-part is the zero-crossing which is a prominent feature of the three-gluon vertex. In order not to affect the ultraviolet damping functions are incorporated into $D^{A^3,IR}(p,q-p-q)$ which are of the form

$$f_{\Lambda_{3g}}(p^2) = \frac{\Lambda_{3g}^2}{\Lambda_{3g}^2+p^2} \;. \tag{4.32}$$

The IR-part of the model then reads

$$D^{A^3,IR}(p,q-p-q) = h_{IR} G(p^2+q^2+(p+q)^2)^3 (f_{\Lambda_{3g}}(p^2) f_{\Lambda_{3g}}(q^2) f_{\Lambda_{3g}}((p+q)^2))^{n_{3g}} \;. \tag{4.33}$$

Compared to the UV-part $D^{A^3,IR}(p,q-p-q)$ exhibits three free parameters h_{IR}, Λ_{3g} and n_{3g}. A negative h_{IR} leads to a zero crossing and n_{3g} is typically assigned a value of $n_{3g} = 4$. The position of the zero crossing can be adjusted by Λ_{3g}. This model for the three-gluon vertex will be employed in the non-Abelian diagram of the quark-gluon vertex. If not stated otherwise, we will use $h_{IR} = -0.1$ and $\Lambda_{3g} = 0.12\,GeV$. For the gluon propagator we will use the result of a separate calculation of the Yang-Mills propagators as input. For this purpose the coupled system of ghost and gluon DSE is solved. An important role in this calculation plays the three-gluon vertex model (4.29) which is employed in the gluon loop of the gluon propagator DSE. The parameters of the model can be adjusted in such a way that the ghost and gluon propagators can be brought into agreement with quenched Lattice results [107]. The Lattice data then also sets the scale of our system. Finally, from this calculation the values for the renormalization constants Z_3 and $\widetilde{Z}_3$ can be extracted. For further details of the calculation the reader is referred to appendix A.3.

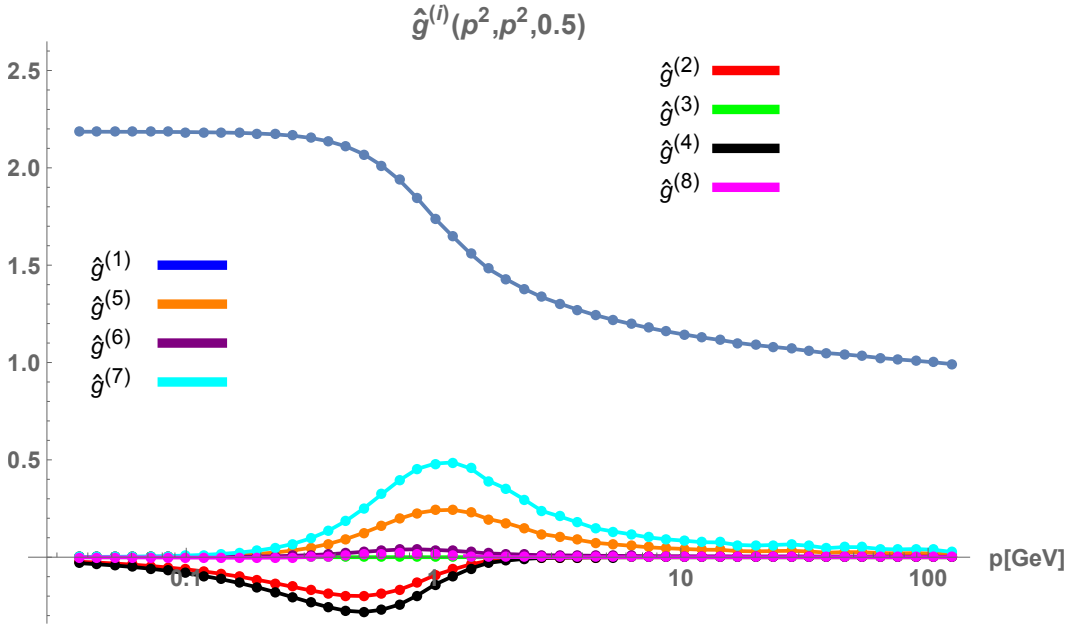

Figure 4.7.: The dressing functions of the quark-gluon vertex at the symmetric point. The dressing functions in the legend on the left-hand side belong to the chirally symmetric group $G_{\chi sym}$ and the one in the legend on the right-hand side to the group $G_{\chi SB}$ that breaks chiral symmetry.

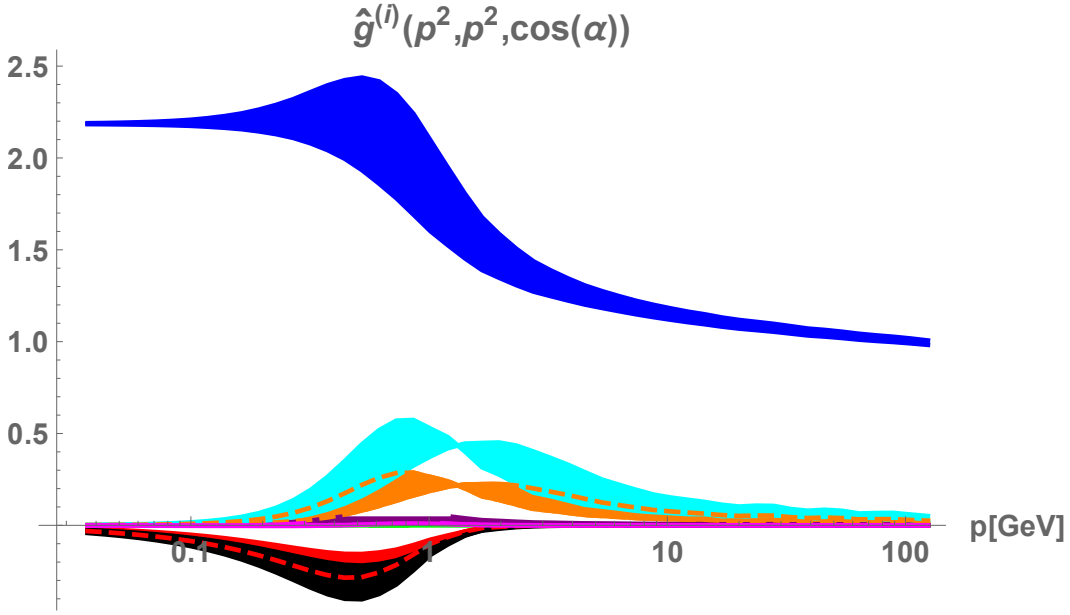

Figure 4.8.: The dressing functions at different values of $\cos(\alpha)$. The bands in this plot indicate the range in which the dressing functions vary with respect to the angle.

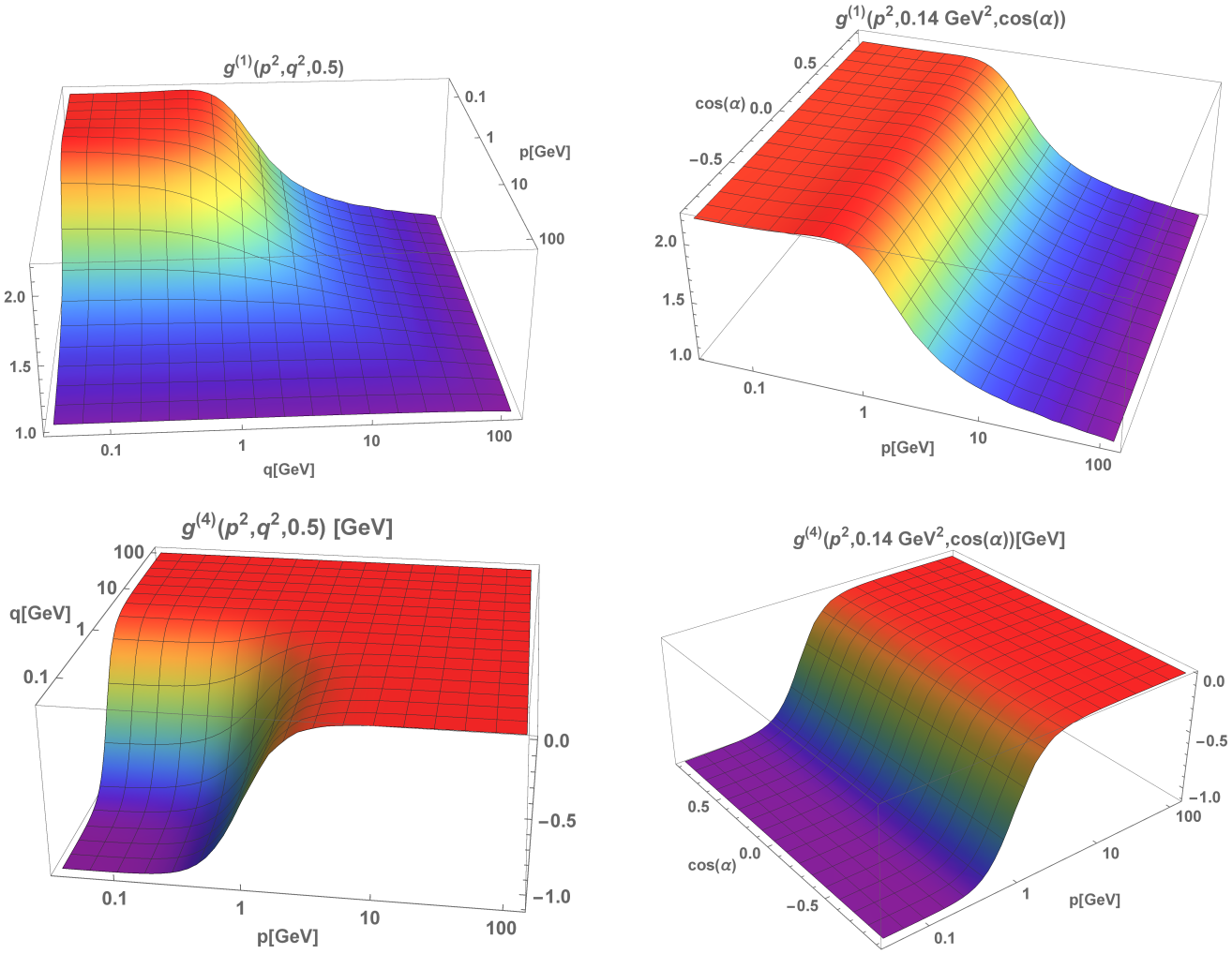

Figure 4.9.: Three-dimensional plots of the dressing functions $g^{(1)}$ and $g^{(4)}$. On the left-hand side $\cos(\alpha)$ and on the right-hand side q^2 have been set to a fixed value.

Having fixed the unknown quantities we are in a position to solve the coupled system of quark-gluon vertex and quark propagator. In figure 4.7 the quark-gluon vertex is depicted at the symmetric point with $p^2 = q^2$ and $\cos(\alpha) = 0.5$. Since all basis tensors except for the tree-level tensor are dimensionful, the corresponding dressing functions are dimensionful as well in order to render the whole vertex dimensionless. It is therefore convenient to project out the dimensions of the dressing functions in order to make a meaningful comparison possible. For this purpose we used appropriate powers of the average momentum

$$\bar{p}_{(qgv)} = \sqrt{\frac{p^2 + q^2 + (p-q)^2}{3}}\,. \tag{4.34}$$

The dressing functions, with respect to which the dimensions have been projected out, will be denoted by $\hat{g}^{(i)}$.
Not surprisingly, the biggest contribution stems from the tree-level dressing func-

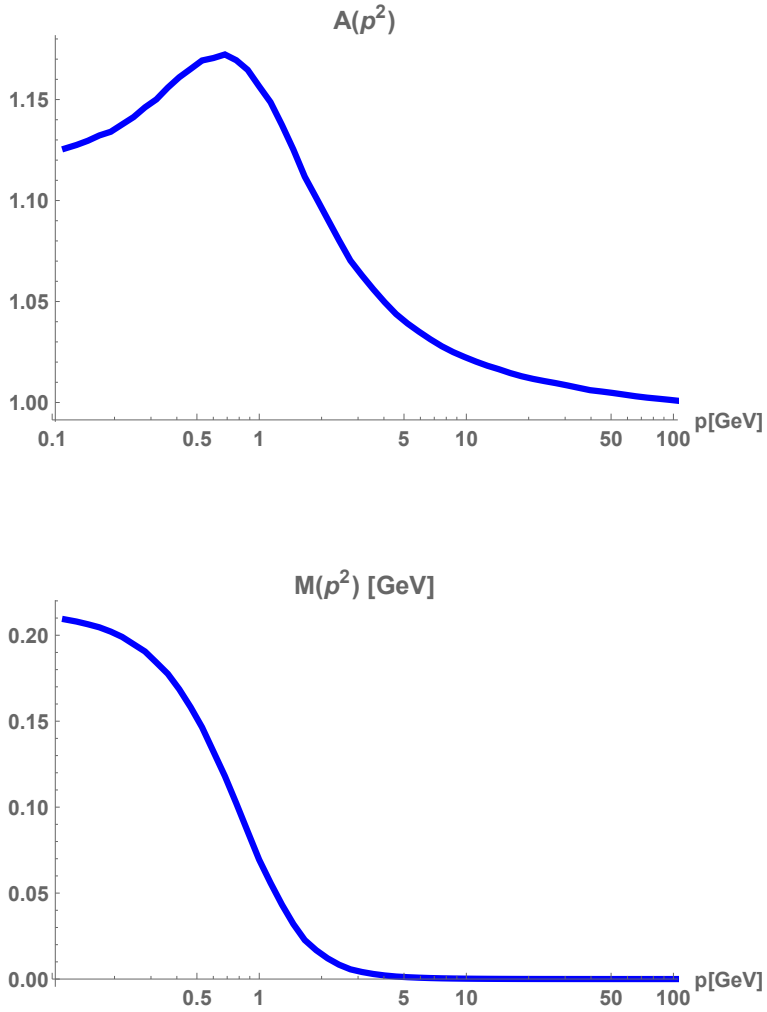

Figure 4.10.: The dressing functions $A(p^2)$ and $M(p^2)$ of the quark propagator.

tion. More interesting is the behaviour of the other dressing functions. Since there exists no tree-level expression for these dressing functions they have to approach zero in the UV regime. Running down from the UV towards smaller momenta their size increases before it again tends towards zero in the IR regime. The most dominant contribution in the midmomentum regime stem from the dressing functions $\hat{g}^{(5)}, \hat{g}^{(7)}, \hat{g}^{(2)}$ and $\hat{g}^{(4)}$, where the former two belong to the chirally symmetric set $G_{\chi sym}$ and the latter two to the chiral symmetry breaking set $G_{\chi SB}$. The dressing functions $\hat{g}^{(2)}$ and $\hat{g}^{(4)}$ are hence of special interest, since their increase at $\mathcal{O}(1GeV)$ indicates that chiral symmetry is broken.
Figure 4.9 shows three-dimensional plots of the dressing functions $g^{(1)}$ and $g^{(4)}$ which are the dominant functions of the groups $G_{\chi sym}$ and $G_{\chi SB}$, respectively. In the plots on the left-hand side the angle $\cos(\alpha)$ is held fixed, whereas on the right-hand side the momentum q^2 is fixed. It should be remarked that this time the dimension of $g^{(4)}$ is not projected out. From figures 4.9 and 4.8 one can also infer that there is a non-negligible dependence of the dressing functions on the angle with the biggest variation in the midmomentum regime.
The results for the dressing functions of the quark propagator are depicted in figure 4.10. It is apparent that the mass generated due to chiral symmetry breaking, $M(p^2 = 0)$, is much smaller than the expected value of $300 - 400\,MeV$. We found that the quark-gluon vertex is very sensitive to the Yang-Mills input, i.e., to the

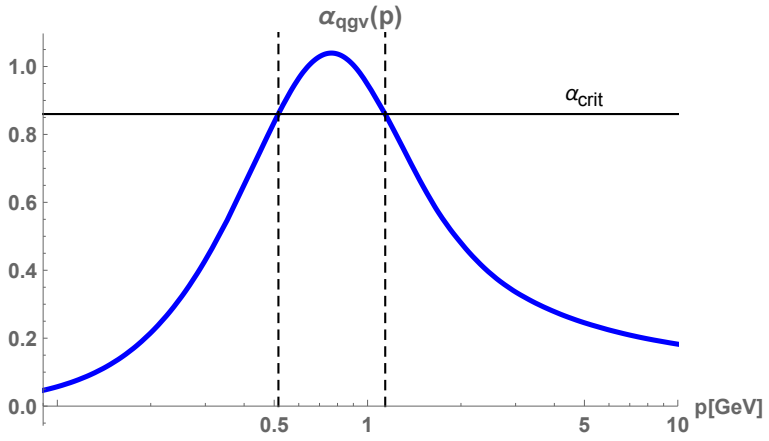

Figure 4.11.: The running coupling derived from the quark-gluon vertex.

gluon propagator and three-gluon vertex. However, slight changes of the quark-gluon vertex have a big impact on the quark propagator ([18, 108]). This indicates that one has to calculate the three-gluon vertex very precisely to obtain the correct generated mass. We will substantiate this further in the next chapter when we couple the three-gluon vertex to the quark-gluon vertex. A further quantity that is of decisive importance for chiral symmetry breaking is the running coupling derived from the quark-gluon vertex (4.21). If the running coupling stays below a critical value of $\alpha_{crit} = 0.86$ no chiral symmetry breaking appears [17, 109, 18]. The running coupling obtained from our calculation is shown in figure 4.11.

At the end of this section we would like to make a remark regarding the comparability of our results with the results obtained in other basis systems. Since the dressing functions of different basis systems in general differ from each other, it is inevitable to compare the dressing functions in the same basis. For this a basis transformation has to be performed which is possible for our basis and other basis systems of the "naive basis"-type [4]. However, a transformation from the "naive basis" to the "generalized Ball-Chiu basis" turns out to be problematic. The reason is that the transformation matrix possesses singularities that are amplified by the numerical treatment. In this way a direct comparison between our results and the results in the "generalized Ball-Chiu basis" is made difficult.

4.6. Impact of the three-gluon vertex model

In this section we investigate how sensitive the results of the quark-gluon vertex are to different parameters of the three-gluon vertex model. For this purpose we have varied the parameters h_{IR} and Λ_{3g}^2 and kept one of both parameters fixed (see figure 4.12).

If we vary h_{IR} and keep Λ_{3g} fixed at a value of $\Lambda_{3g} = 1.17\,GeV$ we arrive at the results for the quark-gluon vertex and quark propagator depicted in figure 4.13. Later we will also compare calculations for $\Lambda_{3g} = 1.17\,GeV$ and $\Lambda_{3g} = 0.12\,GeV$ at fixed h_{IR} to see how the position of the zero crossing of the three-gluon vertex affects the quark-gluon vertex. Regarding the quark-gluon vertex we focus on the depiction

[4] For a comparison with [17] one should be aware that – following a common FRG convention – the definition of the dressing functions in [17] differs slightly from our definition.

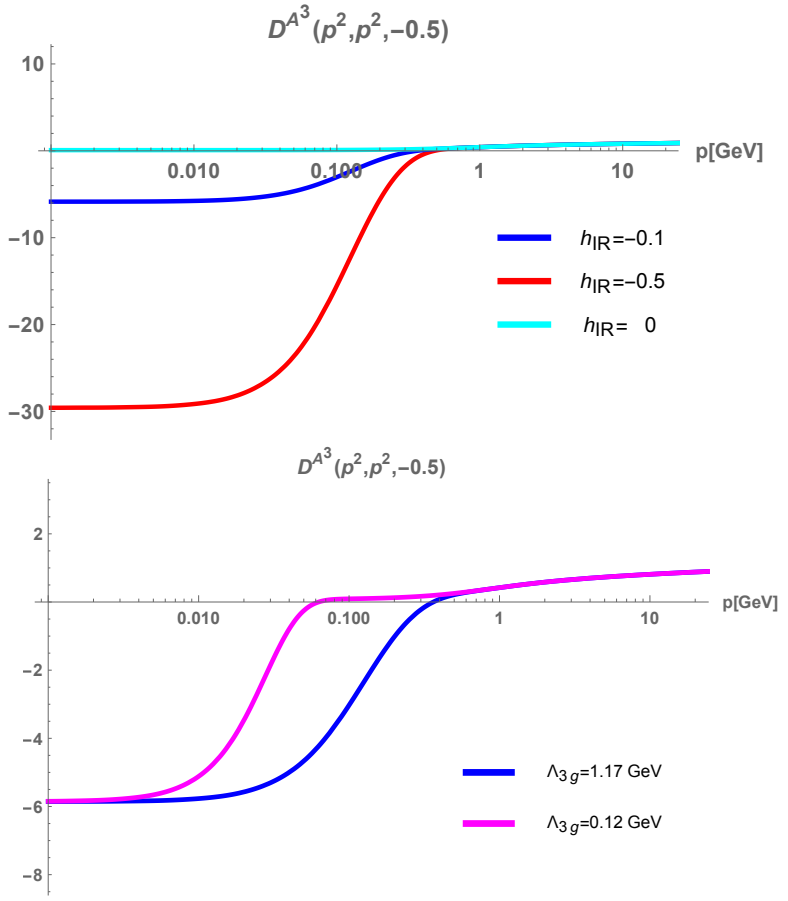

Figure 4.12.: The three-gluon vertex model for fixed $\Lambda_{3g} = 1.17\,GeV$ (top) and fixed $h_{IR} = -0.1$ (bottom).

of the tensor structures $\hat{g}^{(1)}$, $\hat{g}^{(7)}$ and $\hat{g}^{(4)}$ which are the leading contributions of the chiral symmetric and chiral symmetry breaking basis tensors. The plot at the top of figure 4.13 reveals that an enhanced infrared behaviour of the three-gluon vertex results in a sign flip of the non-tree-level dressing functions. This behaviour has been observed as well in [11]. The change in the quark-gluon vertex also affects the generation of mass in the quark propagator. In a second comparison shown in the middle of figure 4.13 we have switched off the infrared part of the three-gluon vertex in one of the quark-gluon vertices ($h_{IR} = 0$). In this way we can study the effect of the zero crossing in the three-gluon vertex on the quark-gluon vertex. From this and the previous comparison we can deduce that the zero crossing of the three-gluon vertex bends down the tree-level dressing function in the infrared. However, the other dressing functions only change quantitatively but not qualitatively.
In a further calculation we kept h_{IR} unaltered at $h_{IR} = -0.1$ and changed Λ_{3g} (see figure 4.14). This allows us to investigate how the position of the zero crossing of the three-gluon vertex impacts the quark-gluon vertex. The purple curves correspond to a calculation with $\Lambda_{3g} = 0.12\,GeV$ that is the zero crossing of the three-gluon vertex is shifted towards the infrared. The result resembles the calculation above with vanishing infrared part of the three-gluon vertex, e.g. the tree-level dressing function does not bend down in the infrared. One can therefore argue that the infrared part of the three-gluon vertex has no effect on the quark-gluon vertex if the zero crossing lies too deep in the infrared.

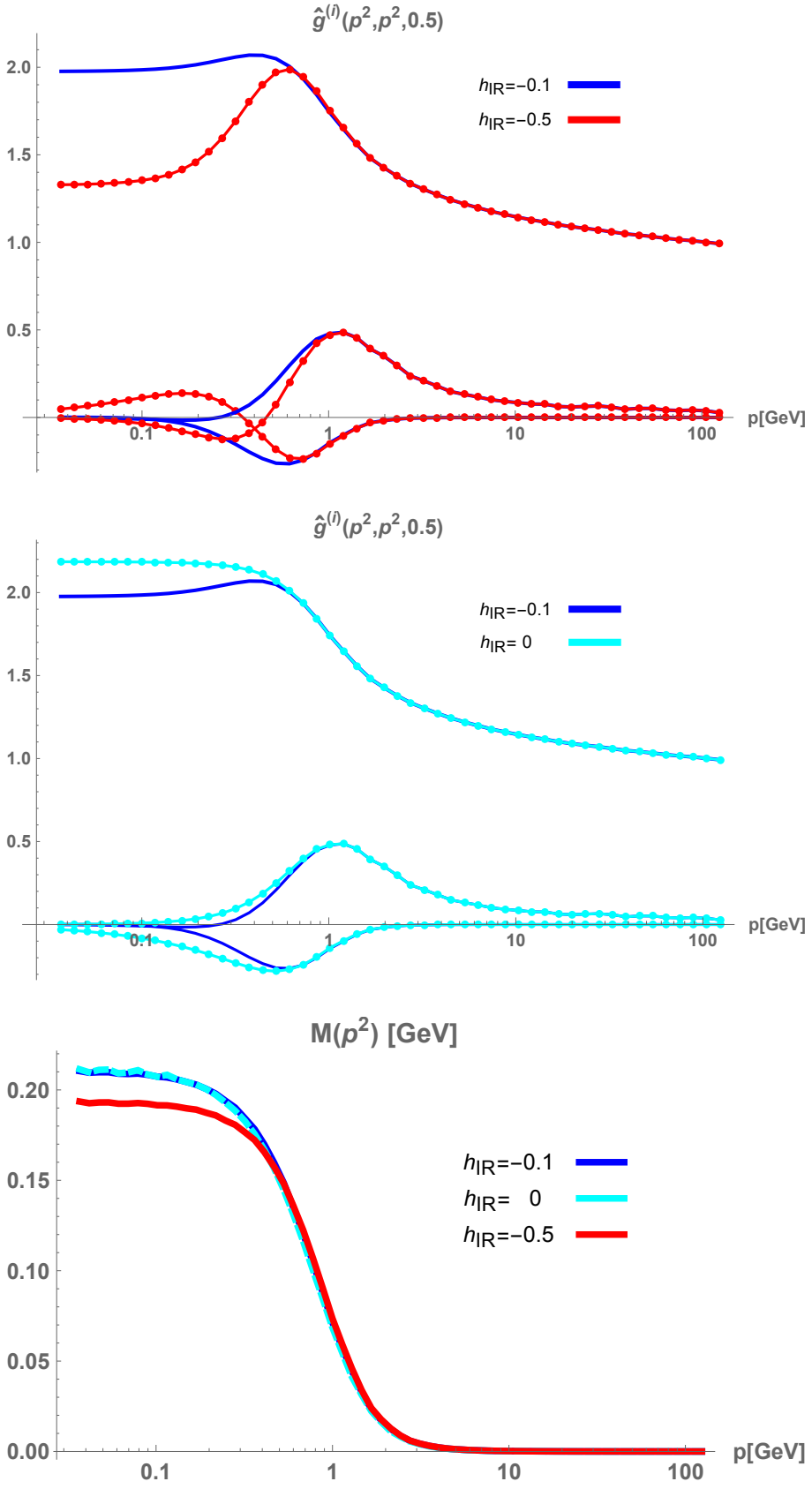

Figure 4.13.: Results for the quark-gluon vertex and quark propagator for different h_{IR} and $\Lambda_{3g} = 1.17\,GeV$. An enhanced infrared part of the three-gluon vertex leads to a sign flip in the quark-gluon vertex and has an effect on the generation of mass.

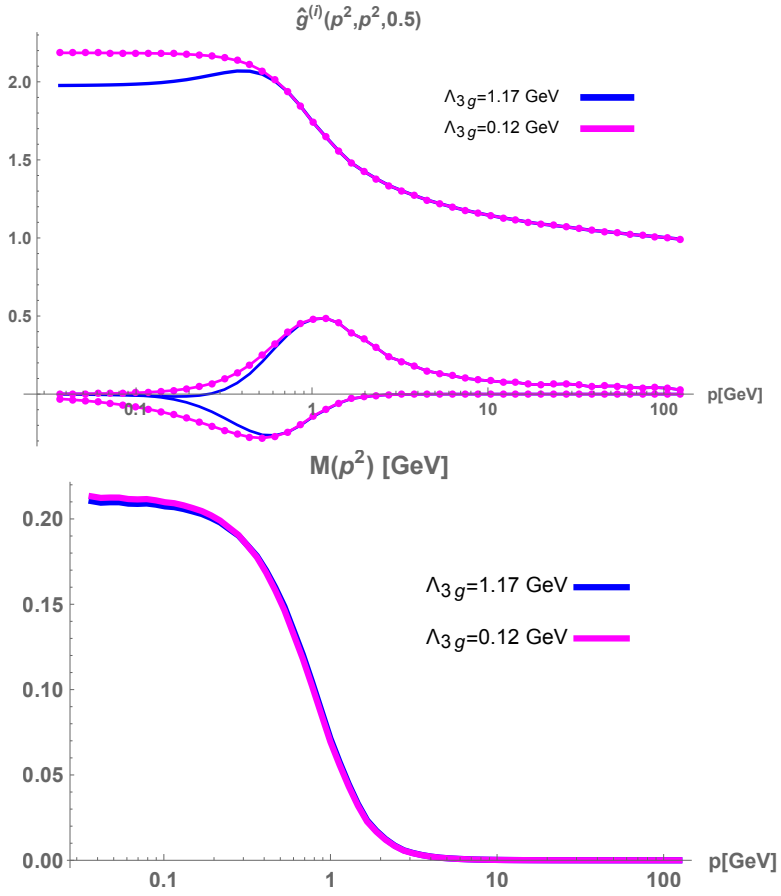

Figure 4.14.: The quark-gluon vertex and mass function for fixed $h_{IR} = -0.1$ and $\Lambda_{3g} = 0.12\,GeV$ and $\Lambda_{3g} = 1.17\,GeV$.

4.7. A model for the two-quark-two-gluon vertex

Usually, the construction of a model is guided by the consideration that the dominant contribution stems from the tree-level form of the correlation function. Further information like the UV-behaviour gained from perturbation theory may additionally constrain the form of the model. By following this approach the models for the three-gluon and four-gluon vertices that are used in this thesis have been constructed.
Concerning the two-quark-two-gluon vertex (figure 4.15) the situation is different. The two-quark-two-gluon vertex has no tree-level counterpart and thus it is a priori unknown which tensor structure gives the main contribution.
We will therefore adopt the model that was introduced in the FRG study [17] for DSE calculations [110]. In this ansatz the tensor structure is derived from arguments regarding gauge invariance. However, this model has to be viewed as a first, more or less speculative ansatz for the two-quark-two-gluon vertex. It is therefore not to be expected that it will reproduce the strength of the full two-quark-two-gluon vertex correctly and we will assess the quality of the model on account of the following calculations. Recently, there has been made progress in the calculation of the four-point functions in perturbation theory [111] and also a first non-perturbative calculation of the two-quark-two-gluon vertex seems to be feasible in the near future

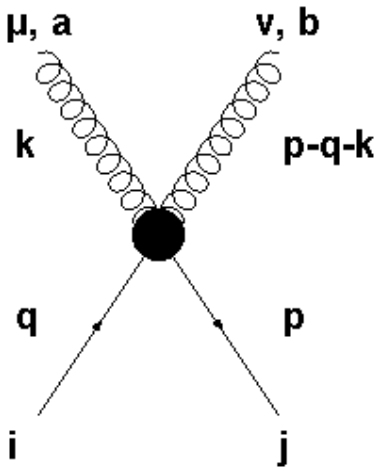

Figure 4.15.: The two-quark-two-gluon vertex.

[5].

The derivation of the two-quark-two-gluon vertex model is based on what in [17] is called a "gauge-invariant completion". The underlying idea is the following: the (hypothetical) occurence of the basis tensors of the quark-gluon vertex (4.9) in the action would violate gauge invariance. However, by adding suitable terms to the action gauge invariance can be preserved. An instructive example given in [17] is the "gauge-invariant completion" of the tree-level tensor and in order to illustrate the general idea we will recapitulate it at this place.
In the action the tree-level tensor structure of the quark-gluon vertex is identified in the term $\bar{q}\not{A}q$. This term clearly breaks gauge invariance. Fortunately, it does not appear alone in the Lagrangian but together with a further term $\bar{q}\not{\partial}q$. Both terms together form the covariant derivative $\bar{q}\not{D}q$ which is gauge invariant.
In the same way gauge invariance can be obtained for the remaining tensor structures of the quark-gluon vertex. We will however concentrate on the tensor structures $b^{(5)}$ and $b^{(7)}$ as defined in (4.9) which are the most dominant of the beyond-treelevel tensors. Essential for the following argument is that the term that has to be added in order to restore gauge invariance does not only contribute at the level of the quark-gluon vertex $\mathcal{O}(\bar{q}Aq)$ but also at the level of the two-quark-two-gluon vertex $\mathcal{O}(\bar{q}AAq)$ and the two-quark-three-gluon vertex $\mathcal{O}(\bar{q}AAAq)$. The term $\mathcal{L}^{(STI)}_{(qgv)}$ required for "gauge-invariant completion" reads [17]:

$$\begin{aligned}
\mathcal{L}^{(STI)}_{(qgv)} =& \bar{q}(p)\left\{-igT_{\mu\nu\rho}\left[p_\nu p_\rho - q_\nu q_\rho + q_\nu p_\rho\right]\right\} A^a_\mu(p-q)T^a q(q) && : \mathcal{O}(\bar{q}Aq) \\
&+ \\
&\bar{q}(p)\left\{ig^2 T_{\mu\nu\rho}(k-p)_\rho\right\} A^b_\nu(p-q-k)T^b A^a_\mu(k)T^a q(q) && : \mathcal{O}(\bar{q}AAq) \\
&+ \\
&\bar{q}(p)\left\{ig^3 T_{\mu\nu\rho}\right\} A^a_\mu(p-q-k-r)T^a A^c_\rho(r)T^c A^b_\nu(k)T^b q(q) && : \mathcal{O}(\bar{q}AAAq)
\end{aligned} \tag{4.35}$$

[5] While writing this thesis results of a calculation of the two-quark-two-gluon vertex have been published in [18].

The tensor $T_{\mu\nu\rho}$ is given by $T_{\mu\nu\rho} = \{[\gamma_\mu, \gamma_\nu], \gamma_\rho\}$[6].
Since the first term in (4.35) gives a contribution to the quark-gluon vertex it can be constructed by appropriate combinations of the tensors of our quark-gluon vertex basis (4.9). In order to investigate how much every basis tensor contributes to the structure $\mathcal{O}(\bar{q}Aq)$ we define a set of orthonormal projectors with the following properties:

$$R_\mu^{(i)} b_\mu^{(j)} = \begin{cases} 1, \text{ for } i = j \\ 0, \text{ for } i \neq j \end{cases} \quad \text{with } i, j = 1, \ldots, 8 \,. \tag{4.36}$$

Projecting with $R_\mu^{(i)}$ onto the vertex derived from the $\mathcal{O}(\bar{q}Aq)$ component of $\mathcal{L}_{(qgv)}^{(STI)}$the only non-zero expressions are $R_\mu^{(5)} b_\mu^{(5)} = \frac{1}{2}$ and $R_\mu^{(7)} b_\mu^{(7)} = 1$. Hence, only the basis tensors $b_\mu^{(5)}$ and $b_\mu^{(7)}$ contribute at a ratio of $1:2$. This reflects a property that can be found for the dressing functions, namely the relation $2g^{(5)} = g^{(7)}$[7].
The next step is based on the assumption that the whole structure $\mathcal{L}_{(qgv)}^{(STI)}$ is dressed by a single dressing function $\lambda^{(STI)}$. But on account of what has just been said we can deduce from the $\mathcal{O}(\bar{q}Aq)$ contribution of $\mathcal{L}_{(qgv)}^{(STI)}$ that either $\lambda^{(STI)}(p^2, q^2, \cos(\alpha)) = g^{(7)}(p^2, q^2, \cos(\alpha))$ or equivalently $\lambda^{(STI)}(p^2, q^2, \cos(\alpha)) = 2g^{(5)}(p^2, q^2, \cos(\alpha))$.
We are now able to set up a complete model for the two-quark-two-gluon vertex. From the second term in (4.35) we obtain the tensor structure and for the dressing function we will set $\lambda^{(STI)} = g^{(7)}$. There is however one last problem that needs to be tackled. The two-quark-two-gluon vertex has four legs and consequently one would expect its dressing function to depend on four momenta instead of the three momenta of the quark-gluon vertex. In order to resolve the missing momentum we will use the average momentum

$$\bar{p}_{(2q2A)} = \sqrt{\frac{p^2 + q^2 + k^2 + (p - q - k)^2}{4}} \tag{4.37}$$

and evaluate the dressing function at a specific point, e.g. the symmetric point. Putting all the pieces together the model for the two-quark-two-gluon vertex has the form

$$\Gamma_{\mu\nu}^{(2q2gl,ab)}(p, q, k, p - q - k) = -\frac{i}{4} g^2 \lambda^{(STI)}(\bar{p}_{(2q2A)}) T_{\mu\nu\rho} \left[(k - p)_\rho T^b T^a + (k + q)_\rho T^a T^b \right]$$

$$\text{with} \quad \lambda^{(STI)}(\bar{p}_{(2q2A)}) = g^{(7)}(\bar{p}^2_{(2q2A)}, \bar{p}^2_{(2q2A)}, 0.5) \,. \tag{4.38}$$

4.8. Results for the quark-gluon vertex from the DSE formalism

With the model for the two-quark-two-gluon vertex we are able to compute the full DSE of the quark-gluon vertex (figure 4.3) by approximating the contribution

[6] Note that the tensor $T_{\mu\nu\rho}$ is negative under odd commutations of its indices, $T_{\mu\nu\rho} = -T_{\mu\rho\nu} = T_{\rho\mu\nu}$. By exploiting this property the expressions in [17] can be simplified considerably.

[7] In [17] also the relation $2b^{(2)} = b^{(4)}$ was found. This relation is not realized exactly in our results.

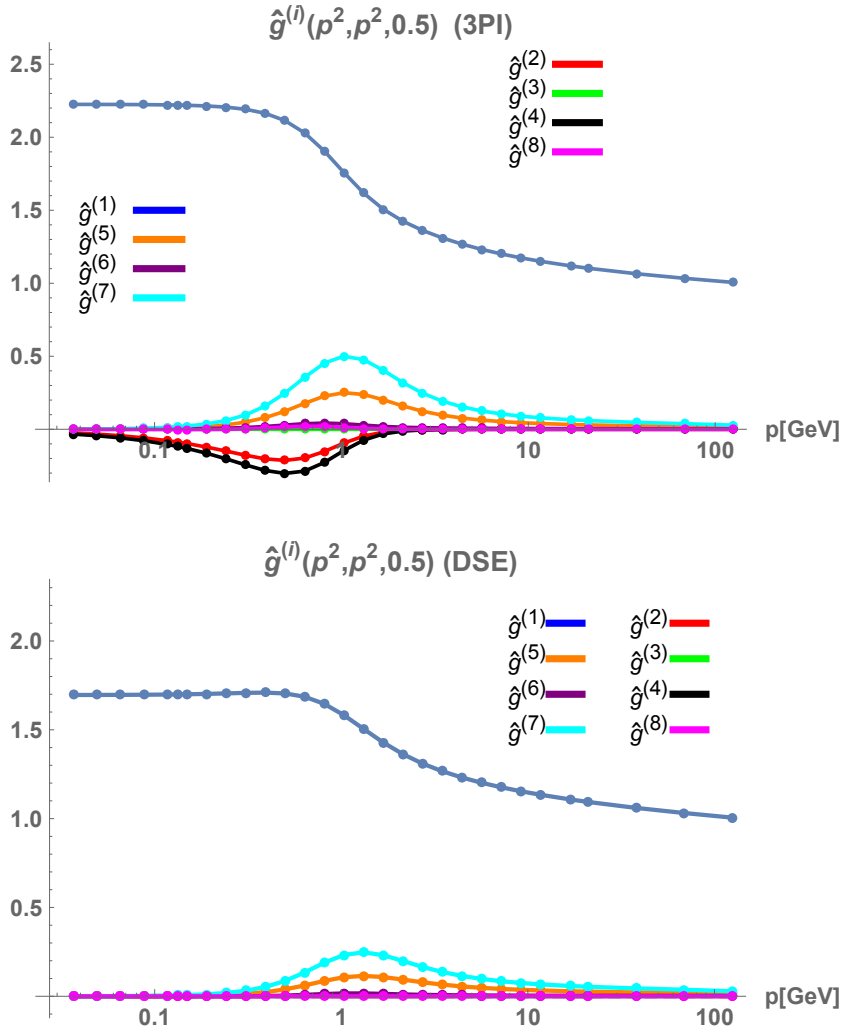

Figure 4.16.: The quark-gluon vertex as obtained from the 3PI formalism (top) and its DSE (bottom).

of the swordfish diagram. In doing so we expressed the renormalization constants by their STIs. To make a comparison with the results from the 3PI formalism possible we redid the corresponding 3PI calculation but this time with the same renormalization prescription as in the DSE case. The results obtained from both methods are depicted in figure 4.16 and figure 4.17 shows the contribution of each diagram of the DSE.
One immediately recognizes that the dressing functions that correspond to the chiral symmetry breaking tensor structures vanish and that the overall strength of the other dressing functions is diminished. A deeper analysis reveals that the contribution of the Abelian diagram is insignificant compared to the non-Abelian diagram as was argued above. Since the non-Abelian diagram exhibits one dressed quark-gluon vertex less than its 3PI counterpart the missing strength has to come from the swordfish diagram. However, with the employed model for the two-quark-two-gluon vertex the swordfish diagram itself is negligible. This hints to the fact that the used model underestimates the strength of the two-quark-two-gluon vertex. One may surmise that with additional strength stemming from a full inclusion of the two-quark-two-gluon vertex chiral symmetry breaking could be recovered. However, further studies are required in order to make a definitive statement.

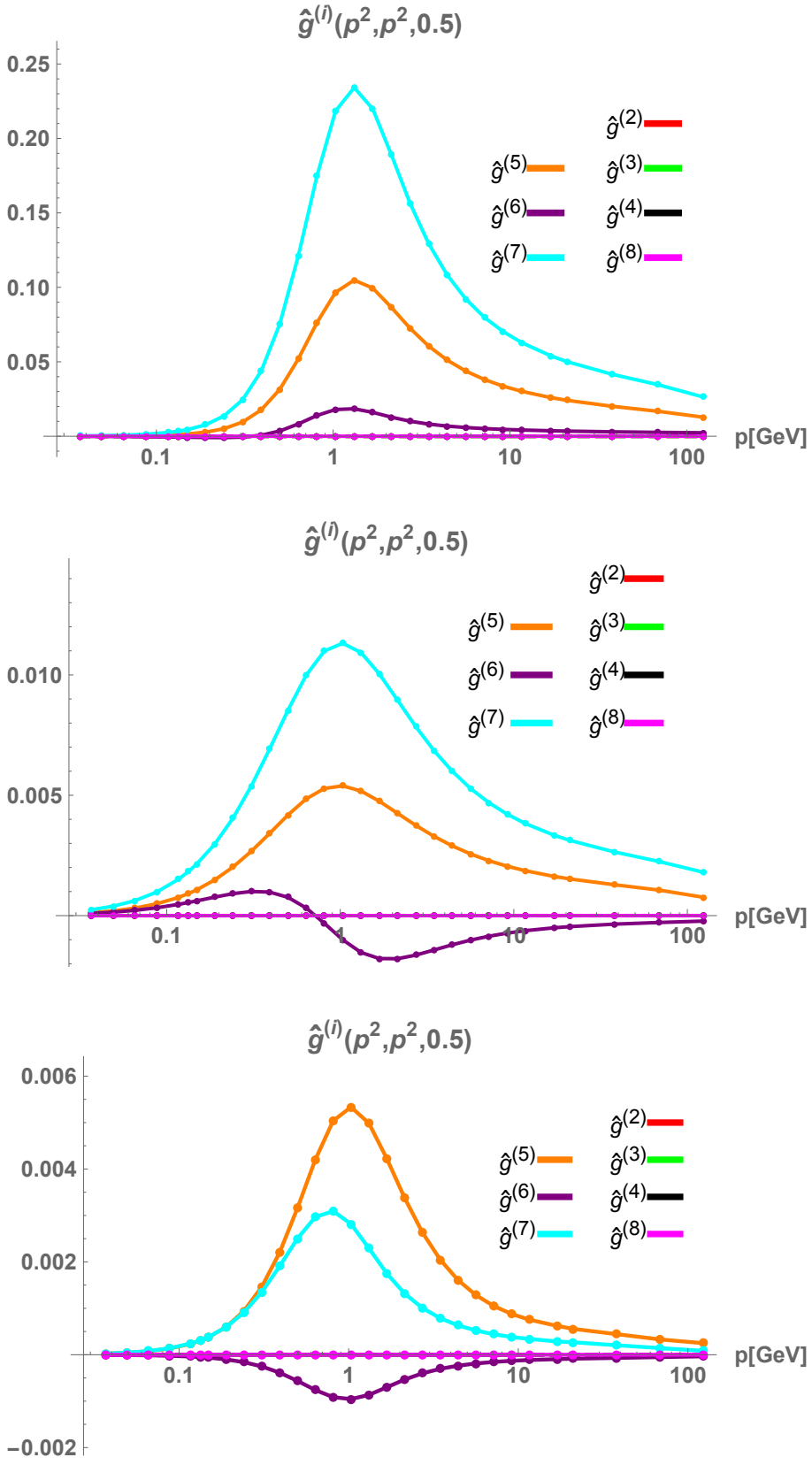

Figure 4.17.: Contribution of the non-Abelian (top), Abelian (middle) and swordfish (bottom) diagrams to the beyond tree-level dressing functions of the quark-gluon vertex. As anticipated the influence of the Abelian diagram is negligible and nearly the full strength is carried by the non-Abelian diagram. Contrary to expectations the contribution of the swordfish diagram is insignificant.

5. The unquenched three-gluon vertex

The final goal of this chapter is the calculation of the coupled system of quark-gluon vertex, quark propagator and three-gluon vertex. To achieve this the investigation will be performed gradually. In a first step the three-gluon vertex of Yang-Mills theory will be considered. In this step the employed basis system of the three-gluon vertex will be introduced and issues of the calculation will be addressed. This serves as the basis for the next step in which we augment the three-gluon vertex with the diagrams of the quark sector. In a first computation of the unquenched three-gluon vertex the results for the quark-gluon vertex presented in the previous chapter will be used. In this calculation backcoupling effects of the three-gluon vertex on the quark-gluon vertex will be ignored. Finally, the coupled system of both vertices and the quark propagator will be solved. At the end of this chapter we will be in a position to answer the questions which impact unquenching has on the position of the zero crossing of the three-gluon vertex and how a dynamic three-gluon vertex influences dynamical chiral symmetry breaking.

5.1. The Yang-Mills three-gluon vertex

We start with the full DSE of the three-gluon vertex in Yang-Mills theory which is depicted in figure 5.1. Applying the standard truncation, i.e., neglecting two-loop diagrams and diagrams with non-primitively divergent vertices, leaves us with the diagrams at the bottom in figure 5.1. Apart from the tree-level diagram there are three swordfish diagrams (diagrams 4 to 6 on the r.h.s.), one ghost triangle diagram (diagram 2) and one gluon triangle diagram (diagram 3).
Analogous to the steps carried out for the quark-gluon vertex we have first of all to find a suitable parametrization for the three-gluon vertex. In contrast to the quark-gluon vertex the color content of the three-gluon vertex is more complex. A complete basis of the color space is given by the antisymmetric structure constant f^{abc} and the symmetric structure constant d^{abc}. However, it can be shown analytically that the terms proportional to d^{abc} have to vanish and that the color content of the full three-gluon vertex is solely described by f^{abc} [112]. A proof of this statement will be given in appendix A.7.
In momentum space there are in general four transverse and ten longitudinal tensor structures. In order to find a convenient basis we can again exploit that in Landau gauge the transverse part describes the full dynamics of the system [90]. This would leave us then with four tensor structures. However, the calculation can be simplified even further due to the observation made in [31] that the contribution of the three non tree-level tensor structures is negligible.

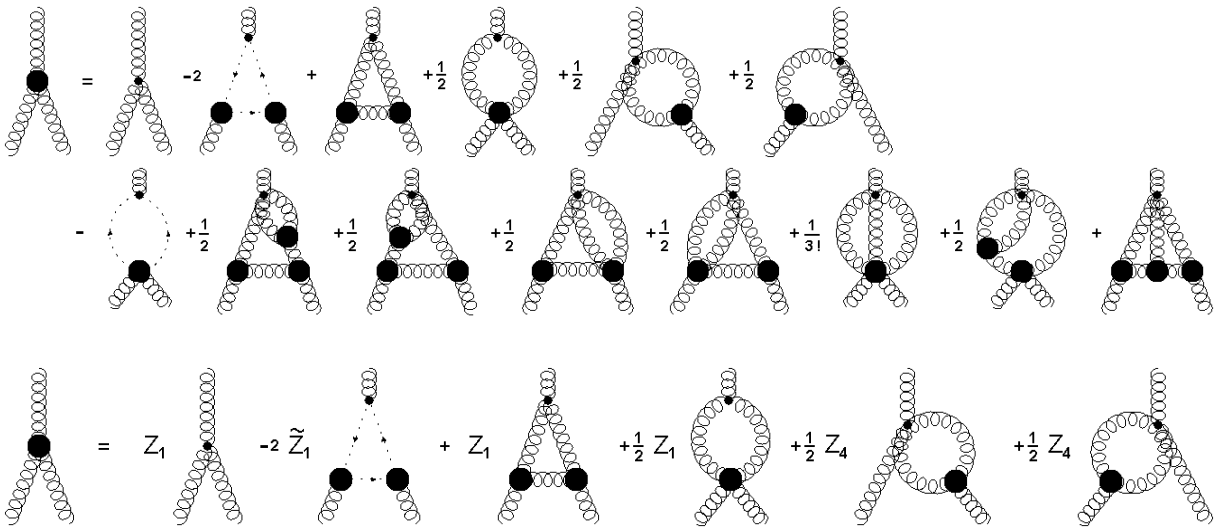

Figure 5.1.: Top: The full DSE of the three-gluon vertex in Yang-Mills theory. Bottom: the truncated DSE with an explicit depiction of the renormalization constants.

With this in mind we employ the following parametrization of the three-gluon vertex:

$$\Gamma^{abc}_{\mu\nu\rho}(p,q,-p-q) = D^{A^3}(p^2,q^2,\cos(\alpha)) f^{abc} \Gamma^{(0)}_{\mu\nu\rho}(p,q,-p-q) \;, \tag{5.1}$$

where D^{A^3} denotes the dressing function and $\Gamma^{(0)}_{\mu\nu\rho}$ is the tree-level tensor structure of the three-gluon vertex. There are two further issues that need to be settled before the actual calculation can be performed. The first issue concerns renormalization and the other issue is related to the question, how the unknown quantities that enter the three-gluon vertex DSE shall be approximated.
We will tackle the problem of renormalization first. The dependence of the three-gluon vertex on the renormalization constants is shown in figure 5.1. Because the loop diagrams depend on different renormalization constants a direct application of the subtraction method described in section 4.4 is difficult. One solution would be to replace the renormalization constants by their corresponding STIs [31]. One should however bear in mind that due to the truncation of the DSE the anomalous dimensions are in general not correctly reproduced. We therefore pursue a different strategy and replace the renormalization constants by so-called renormalization group improvement terms [97]. In doing so we follow [30, 113]. The underlying

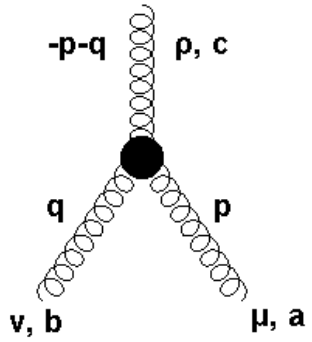

Figure 5.2.: The dressed three-gluon vertex.

idea is to construct the respective anomalous dimension in terms of the anomalous dimensions of the ghost δ and gluon $\gamma = -1 - 2\delta$ (cf. the construction of the UV part of the three-gluon vertex model in section 4.5 and in [101]). There are three different renormalization constants that enter the DSE of the three-gluon vertex. The renormalization constant of the ghost-gluon vertex is $\tilde{Z}_1 = 1$ in Landau gauge using the MiniMOM renormalization scheme. The renormalization constants of the three-gluon vertex Z_1 and the four-gluon vertex Z_4 are then replaced by appropriate RG improvement terms. With these considerations in mind a sensible ansatz for the RG improvement terms is given by

$$D^{A^3}_{RG}(p,q,-p-q) = G(\bar{x}_{(3gl)})^{\alpha_{3g}} Z(\bar{x}_{(3gl)})^{\beta_{3g}} \,, \tag{5.2}$$

$$D^{A^4}_{RG}(p,q,k,-p-q-k) = G(\bar{x}_{(4gl)})^{\alpha_{4g}} Z(\bar{x}_{(4gl)})^{\beta_{4g}} \,, \tag{5.3}$$

with

$$\bar{x}_{(3gl)} = \frac{p^2+q^2+(p+q)^2}{2} \,, \tag{5.4}$$

$$\bar{x}_{(4gl)} = \frac{p^2+q^2+k^2+(p+q+k)^2}{2} \,. \tag{5.5}$$

We can now proceed in the same way as we did for the three-gluon vertex model and constrain the possible values for the exponents by demanding that the RG improvement terms shall be finite in the infrared and that they run with the anomalous dimension of the three-gluon vertex $\gamma_{3g} = 1 + 3\delta$ and four-gluon vertex $\gamma_{4g} = 1 + 4\delta$ in the ultraviolet. Additionally, we exploit that the behaviour of the ghost and gluon propagators is known for the IR and UV regime. In resummed perturbation theory one finds

$$\begin{aligned} Z(p^2) &= Z(\mu^2)\left[\omega \log\left(\frac{p^2}{\mu^2}\right)+1\right]^{\gamma} \,, \\ G(p^2) &= G(\mu^2)\left[\omega \log\left(\frac{p^2}{\mu^2}\right)+1\right]^{\delta} \,, \end{aligned} \tag{5.6}$$

where μ is the renormalization point and

$$\omega = \frac{11 N_c \alpha(\mu^2)}{12\pi} \,. \tag{5.7}$$

In the infrared the ghost and gluon dressing functions are described by a power law behaviour

$$\begin{aligned} G(p^2) &= c_{gh}\,(p^2)^{\kappa^{gh}_{IR}} \,, \\ Z(p^2) &= c_{gl}\,(p^2)^{\kappa^{gl}_{IR}} \,. \end{aligned} \tag{5.8}$$

For the decoupling solution the infrared exponents are $\kappa^{gh}_{IR} = 0$ and $\kappa^{gl}_{IR} = 1$. With this information we can set up the following equations

UV running	IR finiteness
$\alpha_{3g}\delta + \beta_{3g}\gamma = \gamma_{3g}$	$\kappa^{gh}_{IR}\alpha_{3g} + \kappa^{gl}_{IR}\beta_{3g} = 0$
$\alpha_{4g}\delta + \beta_{4g}\gamma = \gamma_{4g}$	$\kappa^{gh}_{IR}\alpha_{4g} + \kappa^{gl}_{IR}\beta_{4g} = 0$

Solving these equations for α_{3g} (α_{4g}) and β_{3g} (β_{4g}) we get

$$\alpha_{3g} = \frac{3\delta + 1}{\delta},\ \beta_{3g} = 0\ , \tag{5.9}$$

$$\alpha_{4g} = \frac{4\delta + 1}{\delta},\ \beta_{4g} = 0\ . \tag{5.10}$$

With these exponents the RG improvement terms (5.2) and (5.3) are completely determined and we can make the replacements

$$\begin{aligned} Z_1 &\to D^{A^3}_{RG}(p, q, -p - q)\ , \\ Z_4 &\to D^{A^4}_{RG}(p, q, k, -p - q - k)\ . \end{aligned} \tag{5.11}$$

At this place it is worth looking at the above treatment of the renormalization constants from a different perspective. It is assumed that if all bare vertices in the loop diagrams were dressed, the anomalous dimensions would be automatically reproduced correctly. With this assumption we can think of the above replacements as virtually dressing the bare vertices:

$$\begin{aligned} \Gamma^{(0)}_{\mu\nu\rho}(p, q, k) &\to \frac{1}{Z_1} D^{A^3}_{RG}(p, q, k)\Gamma^{(0)}_{\mu\nu\rho}(p, q, k)\ , \\ \Gamma^{(0)}_{\mu\nu\rho\lambda}(p, q, k, r) &\to \frac{1}{Z_4} D^{A^4}_{RG}(p, q, k, r)\Gamma^{(0)}_{\mu\nu\rho\lambda}(p, q, k, r)\ . \end{aligned} \tag{5.12}$$

It should, however, be noted that the RG improvement terms have a quantitative impact on the result compared to a calculation in which the renormalization constants are expressed by their STIs. A discussion of the differences between both methods can be found in [34].
The only renormalization constant that cannot be treated this way is the one that belongs to the tree-level diagram. We will express this constant by its STI

$$Z_1 = \frac{Z_3}{\widetilde{Z}_3}\ , \tag{5.13}$$

where $\widetilde{Z}_1 = 1$ has been used.
Having solved the issue of renormalization we can now focus our attention on the yet undefined n-point functions in the three-gluon vertex DSE.
Like for the quark-gluon vertex we use for the Yang-Mills propagators the results of a separate calculation detailed in appendix A.3. This calculation also provides us with the renormalization constants Z_3 and $\widetilde{Z}_3$.
A further not yet specified quantity is the dressed ghost-gluon vertex. Although an inclusion of the fully dressed ghost-gluon vertex is in principle possible and has already been performed [30, 13], we will approximate it by the bare vertex in order to simplify calculations. Since the dressed ghost-gluon vertex shows only in the midmomentum regime a small deviation from its bare expression this proved to be a reasonable approximation [114, 115, 36, 116, 117, 101].
The last n-point function that needs consideration is the dressed four-gluon vertex which appears in one of the swordfish diagrams. A special attention is required for this vertex for it plays a crucial role in the balance between the gluon triangle and the swordfish diagram. With each iteration step the gluon triangle increases and in order to enable a stable iteration this enhancement has to be counteracted by the

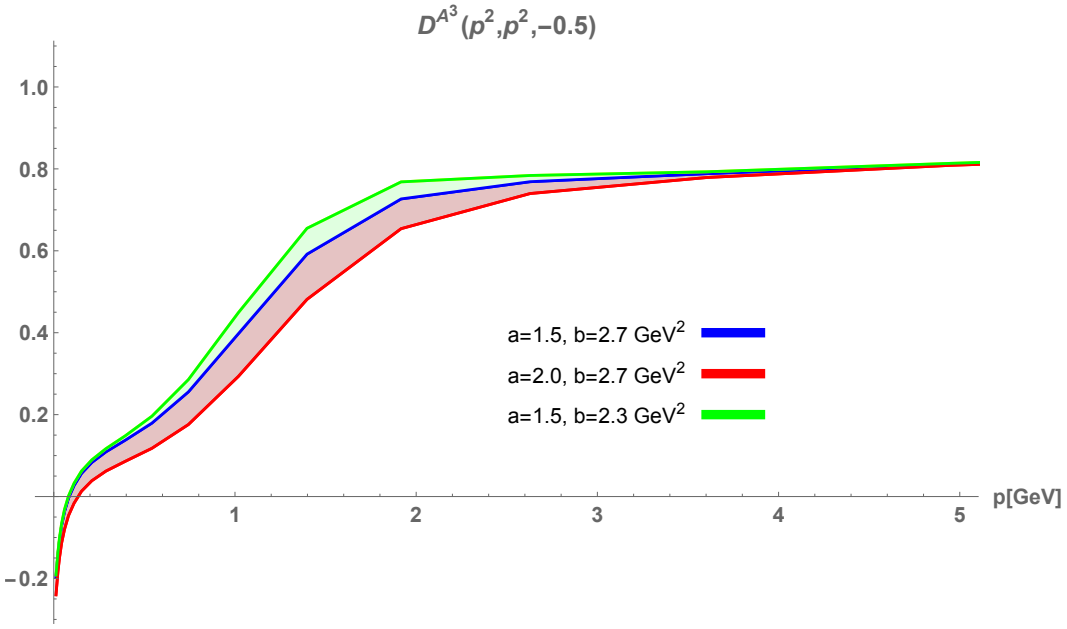

Figure 5.3.: The three-gluon vertex at the symmetric point. Due to the freedom of choosing values for the parameters a and b in the four-gluon vertex model more than one solution can be found.

swordfish diagram. For this to be possible we need to provide the four-gluon vertex model with enough strength. Our ansatz reads [30]

$$\Gamma_{\mu\nu\rho\lambda}(p,q,k,r) = \left[a \tanh\left(\frac{b}{\bar{x}_{(4gl)}}\right) + 1\right] D^{A^4}_{RG}(p,q,k,r)\Gamma^{(0)}_{\mu\nu\rho\lambda}(p,q,k,r)\ . \qquad (5.14)$$

According to what we have learned from renormalizing the three-gluon vertex we "dress" the bare four-gluon vertex with a RG-improvement term $D^{A^4}_{RG}$ in order to obtain the correct UV running. The strength of our model ansatz is then controlled by the term in squared brackets and can be adjusted by the free parameters a and b. The model that we find in this way agrees with first results for the four-gluon vertex [118].

Figure 5.3 shows the result for the three-gluon vertex at the symmetric point. Due to the truncation of the three-gluon vertex DSE Bose symmetry is not manifest anymore and thus we have Bose symmetrized the equation by hand. From what has just been said it should be clear that by varying the parameters of the four-gluon vertex model we obtain a band of solutions rather than a single solution. However, the width of this band is restricted by the fact that not for all possible parameters the iteration is stable [1].

One property of the three-gluon vertex that has attracted much attention since its first discovery in (two and three dimensional) Lattice calculations is the zero crossing [119, 36]. Hereafter it could be reproduced by means of other methods as well [120, 30, 31, 27, 35, 25]. The zero crossing owes its existence to the ghost-triangle diagram which is negative and gives the dominant contribution in the infrared [121]. It moreover serves as a guideline for the impact the three-gluon vertex has on hadronic properties. The relevant scale for hadrons lies at several hundred MeV and the

[1] It should be stressed that figure 5.3 does not show the full possible band.

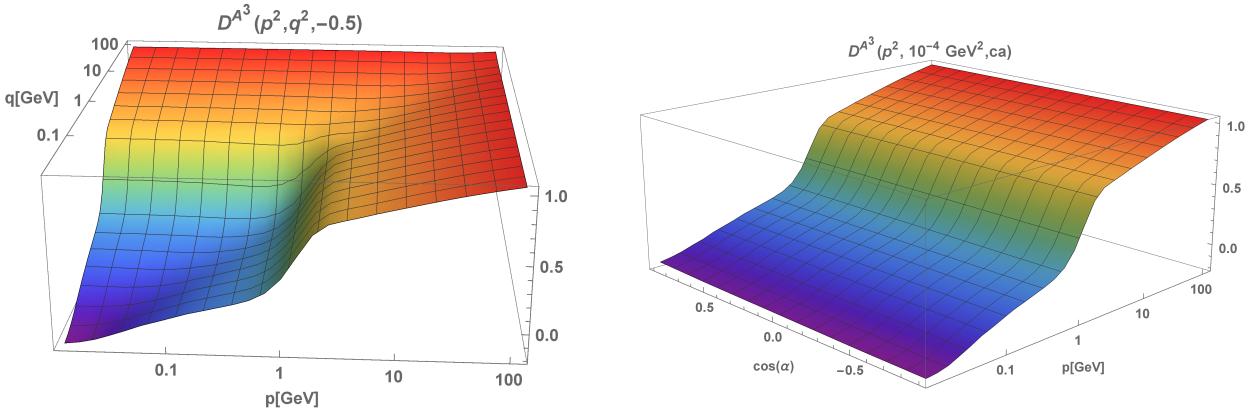

Figure 5.4.: The three-gluon vertex plotted at fixed angle $\cos(\alpha) = -0.5$ (left) and fixed momentum $q^2 = 10^{-4}\,GeV^2$ (right)

strength of the three-gluon vertex in this area affects hadronic observables. From figure 5.3 we can therefore deduce that a shift of the zero crossing towards the infrared regime would lead to an increase of the strength of the three-gluon vertex in the relevant region whereas a shift towards the ultraviolet regime would lead to a decrease.
One drawback of the above calculation is that on account of the ambiguitiy of the parameters in the four-gluon vertex model the exact position of the zero crossing cannot be determined precisely. However, the solutions lie in a narrow range around $0.1\,GeV$ [2]. A more accurate determination of the position of the zero crossing has been the subject of recent Lattice calculations [38, 37].

5.2. Unquenching the three-gluon vertex with a static quark sector

To unquench the Yang-Mills three-gluon vertex we have to augment the DSE by three diagrams, two triangle diagrams and one swordfish diagram (see figure 5.5). There are no further two-loop diagrams that would be affected by the truncation and consequently the whole impact of the quark sector is encoded in merely three diagrams. Before we will deal with the computation of the quark diagrams it is worthwhile to have a closer look at the two quark triangle diagrams.
Since every quark possesses a corresponding antiquark we obtain two diagrams one with the internal lines being formed by quarks and one where the internal lines are formed by antiquarks or equally one diagram with the loop going clockwise and one diagram with the loop going counterclockwise. A similar situation exists in QED where it is long known that according to Furry's theorem [122] diagrams with a fermion loop with an odd number of vertices cancel each other. However, in QCD the case is more elaborate due to the non-trivial color space. The quark-triangle diagrams are directly proportional to both the antisymmetric structure constant f^{abc} as well as the symmetric structure constant d^{abc}. If one defines charge cojugation for non-Abelian theories an equivalent to Furry's theorem can be formulated. In

[2] Note that the position of the zero-crossing changes if the STIs are used for the renormalization constants instead of the RG-improvement terms [31].

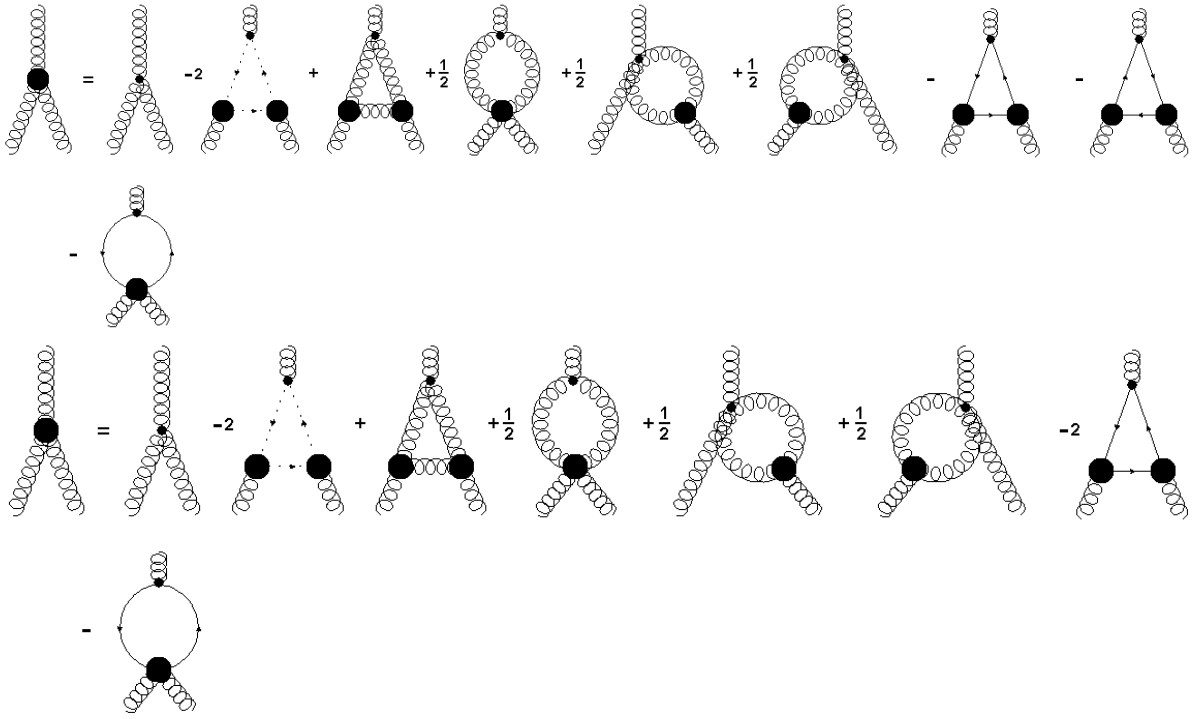

Figure 5.5.: The DSE for the unquenched three-gluon vertex. Compared to the Yang-Mills three-gluon vertex three diagrams have to be added: two quark triangle diagrams and one quark swordfish diagram (top). By applying an non-Abelian analogue of Furry's theorem one can show that both quark triangle diagrams give the same contribution (bottom).

this manner one can show that the terms proportional to d^{abc} cancel – which is in line with the above statement that only the antisymmetric structure constant contributes to the three-gluon vertex – and that the terms proportional to f^{abc} are added up [123]. An in-depth analysis of this statement can be found in appendix A.7, here we will focus on its practical implication which leads to the DSE of the unquenched three-gluon vertex shown at the bottom of figure 5.5.
With the quark triangle and quark swordfish diagrams we now have two further diagrams that need renormalization. Both diagrams are renormalized via the renormalization constant Z_{1F} for which we will employ the constant calculated in the quark sector.
There is one further thing we would like to remark. The quark diagrams in the three-gluon vertex are proportional to the number of flavours N_f. In a truncation that includes correlation functions up to the level of three-point functions the gluon propagator is the only other quantity for which this is the case. It is hence possible to study the behaviour of the three-gluon vertex in the limit of large N_f as it was done for the gluon propagator in the past.

In a first attempt we use the quark-gluon vertex and quark propagator from the calculation presented in the last chapter where a model for the three-gluon vertex was employed. This implies that we ignore effects due to the backcoupling of the three-gluon vertex onto the quark-gluon vertex for the moment. For the two-quark-two-gluon vertex that appears in the quark swordfish diagram we will use the model that was introduced in section 4.7.

Figure 5.6 shows the results of this calculation which are best depicted over a log-

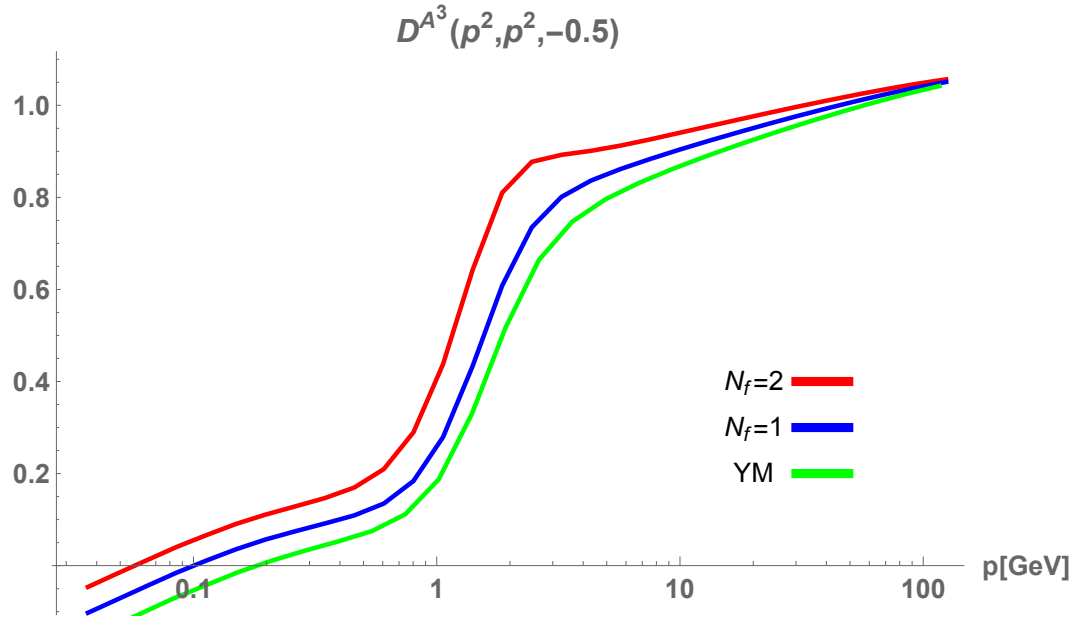

Figure 5.6.: The unquenched three-gluon vertex with a static input for the quark sector. In this plot the results for $N_f = 2$ and $N_f = 1$ and the Yang-Mills three-gluon vertex are compared.

arithmic momentum axis. In this plot the three-gluon vertices for $N_f = 2, N_f = 1$ and $N_f = 0$, i.e. the Yang-Mills case, are compared to each other. It should be noted that the quark sector interferes with the cancellation mechanism between swordfish diagram and gluon triangle so that the parameters of the four-gluon vertex model have to be adjusted accordingly. In our case we use the parameters $a = 2$ and $b = 5.4\,GeV^2$ which are employed in all calculations to make a comparison between the different results possible. As we can see from figure 5.6 both unquenched results lie above the Yang-Mills three-gluon vertex and the unquenched three-gluon vertex for $N_f = 2$ lies above the one for $N_f = 1$ [3]. This can be understood from figure 5.7 where the contribution from the quark triangle diagram and the quark swordfish diagram for $N_f = 1$ are depicted. Both diagrams are static, that is, they do not contain the three-gluon vertex and are therefore not updated within each iteration step [4]. The quark triangle diagram is entirely positive and gives a small but significant contribution. Therefore the unquenched three-gluon vertex becomes enhanced compared to the Yang-Mills calculation with an enhancement that is proportional to N_f. On the other hand the contribution of the quark-swordfish diagram is negligible which could again be due to the fact that the model might underestimate the strength of the two-quark-two-gluon vertex. The effect observed here that the unquenched quantity is above the quenched one is opposite to what can be seen for the gluon propagator where the unquenched gluon propagator lies below the quenched propagator [100, 124, 125, 126].
We can therefore now give an answer to the question how the unquenching of the three-gluon vertex alters the position of the zero crossing. It is shifted towards the

[3] A similar result but by using the 3PI equation instead of the DSE for the three-gluon vertex was found in [13].

[4] We would like to remark that the UV behaviour of the quark-gluon vertex is of high importance for the renormalization of the quark triangle diagram. A too slow decrease of the non tree-level dressing functions results in cutoff dependent divergencies.

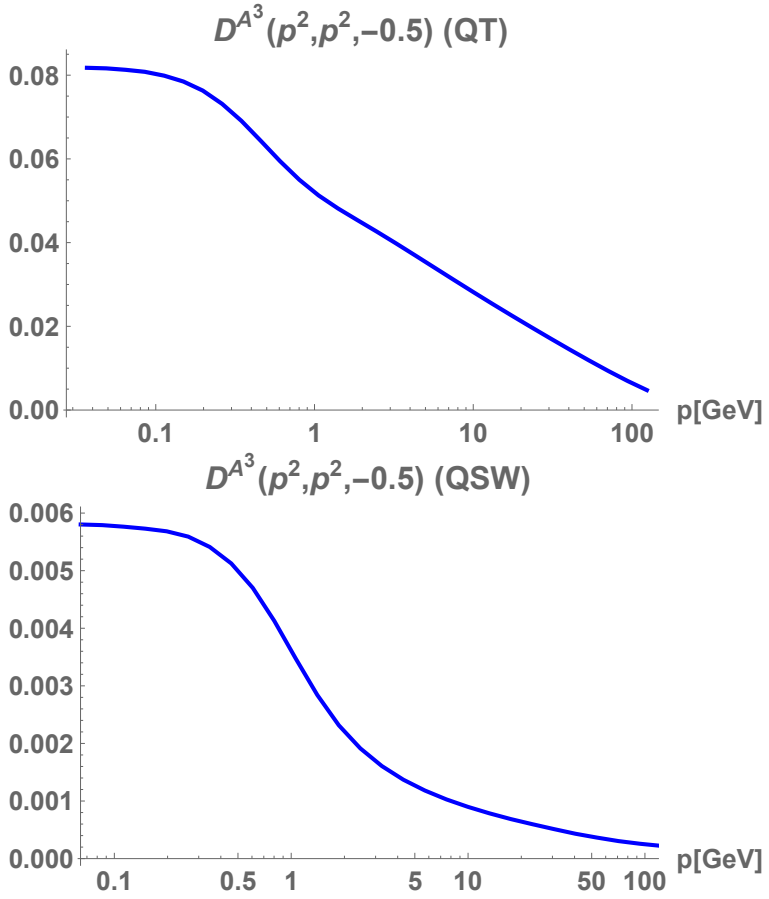

Figure 5.7.: The contributions from the quark triangle diagram (top) and the quark swordfish diagram (bottom) for $N_f = 1$.

infrared regime and consequently the strength of the three-gluon vertex at the for hadrons relevant scale of several hundred MeV increases.

5.3. The coupled system of quark-gluon vertex, quark propagator and three-gluon vertex

Finally, we couple the equations for the quark-gluon vertex and quark propagator as discussed in the last chapter to the three-gluon vertex and calculate the system of quark-gluon vertex, quark propagator and three-gluon vertex. With respect to this set-up it is especially interesting to see how a dynamical three-gluon vertex rather than a model influences the mechanism of chiral symmetry breaking in the quark sector.

In figure 5.8 the result for the quark-gluon vertex is shown. Depicted are the dressing functions of the quark-gluon vertex for a calculation with $N_f = 2$ (top) and $N_f = 1$ (middle) in the three-gluon vertex DSE and a comparison between both calculations (bottom) in terms of the dressing functions $\hat{g}^{(1)}, \hat{g}^{(4)}$ and $\hat{g}^{(7)}$, which are the most dominant dressing functions of the quark-gluon vertex. The dressing functions of the calculation with $N_f = 2$ have overall more strength than the one of the calculation with $N_f = 1$ and it is therefore to be expected that they also give rise to a more pronounced generation of mass in the quark propagator.

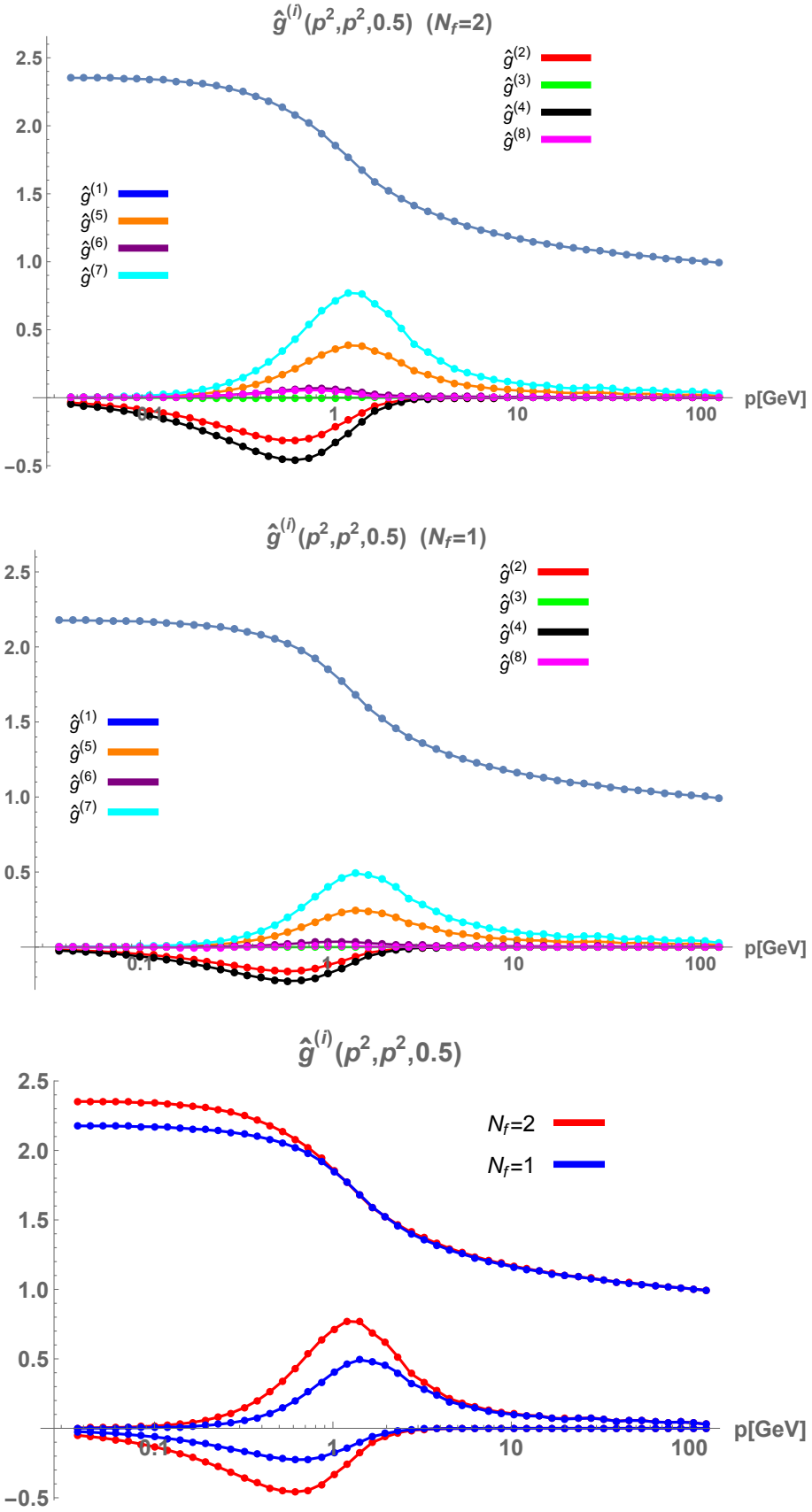

Figure 5.8.: The quark-gluon vertex from a calculation with a dynamical three-gluon vertex. The plot at the top refers to a calculation with $N_f = 2$ in the three-gluon vertex DSE and the plot in the middle to a calculation with $N_f = 1$. At the bottom the dressing functions $\hat{g}^{(1)}$, $\hat{g}^{(4)}$ and $\hat{g}^{(7)}$ of both calculations are compared.

This assumption is confirmed by figure 5.9 which compares the dressing functions $A(p^2)$ and $M(p^2)$ of a calculation with a dynamical three-gluon vertex with $N_f = 2$ and $N_f = 1$ with the result of the last chapter, where a three-gluon vertex model was used. The calculation with $N_f = 2$ shows the biggest difference to the other results. Regarding the dressing function $A(p^2)$ it does not bend down in the infrared in contrast to the other results. Moreover, the result for $N_f = 2$ exhibits the biggest value for $M(p^2 = 0)$ in the range of 350 MeV as one would expect. The result for $N_f = 1$ has a much smaller generated mass, yet it lies above the one of the calculation with a three-gluon vertex model. The reason for these differences have to be searched for in the three-gluon vertex.
In figure 5.10 we see the results for the three-gluon vertex ($N_f = 2$ and $N_f = 1$) from a calculation with a dynamical quark sector. As a guideline the three-gluon vertex of a Yang-Mills calculation is depicted as well. As already observed in the last section the unquenched results lie above the Yang-Mills result and in turn the result for $N_f = 2$ is above the one with $N_f = 1$. Having the results of the quark sector in mind we can deduce that the stronger the three-gluon vertex the stronger the quark-gluon vertex and the more mass is generated in the quark propagator. The biggest impact seems to stem from the range of several GeV where the difference between the result for $N_f = 2$ and $N_f = 1$ is most pronounced.
With this observation we can substantiate the assumption formulated in the last chapter that the quark-gluon vertex and with it chiral symmetry breaking is very sensitive to the Yang-Mills sector. A precise knowledge of the gluon propagator and the three-gluon vertex seems therefore to be inevitable [5].
However, we would like to remark that our finding that the generated mass increases with increasing number of flavours is in contradiction with present Lattice results. On the Lattice it was found that the addition of quark loops rather leads to a small decrease of the generated mass [127, 124]. A possible explanation of the difference could be that we have not included the gluon propagator dynamically. As mentioned above unquenching diminishes the strength of the gluon propagator, whereas it leads to an enhancement of the three-gluon vertex. In such a way the gluon propagator could counteract effects due to the unquenching of the three-gluon vertex. For a definitive statement a full inclusion of the gluon propagator is therefore essential.

[5] A similar conclusion was drawn in [18].

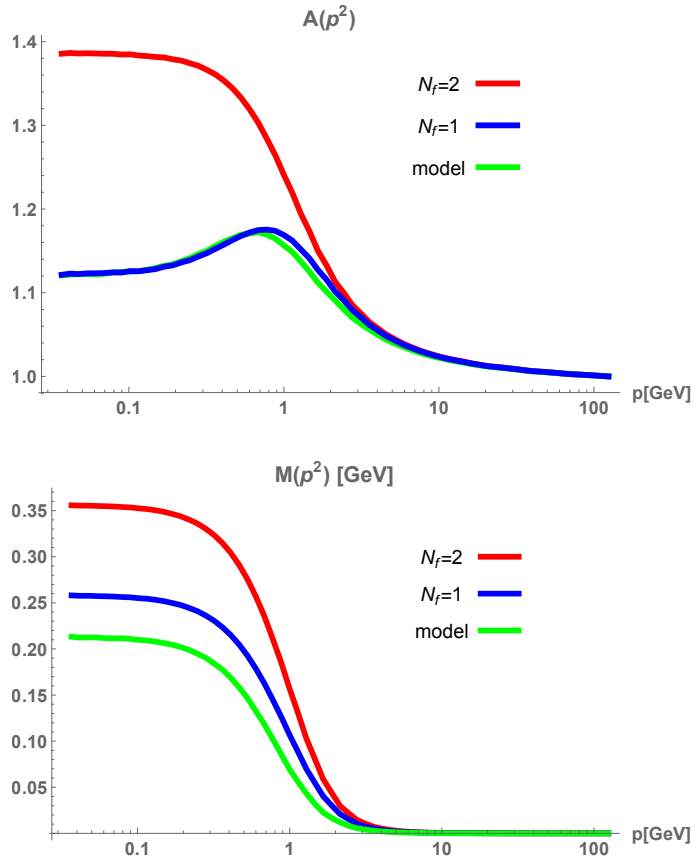

Figure 5.9.: The dressing function $A(p^2)$ (top) and the mass function $M(p^2)$ (bottom) of the quark propagator. In this figure the results of a calculation with a dynamical three-gluon vertex ($N_f = 2$ and $N_f = 1$) are compared with the results of the previous chapter where a model for the three-gluon vertex was employed.

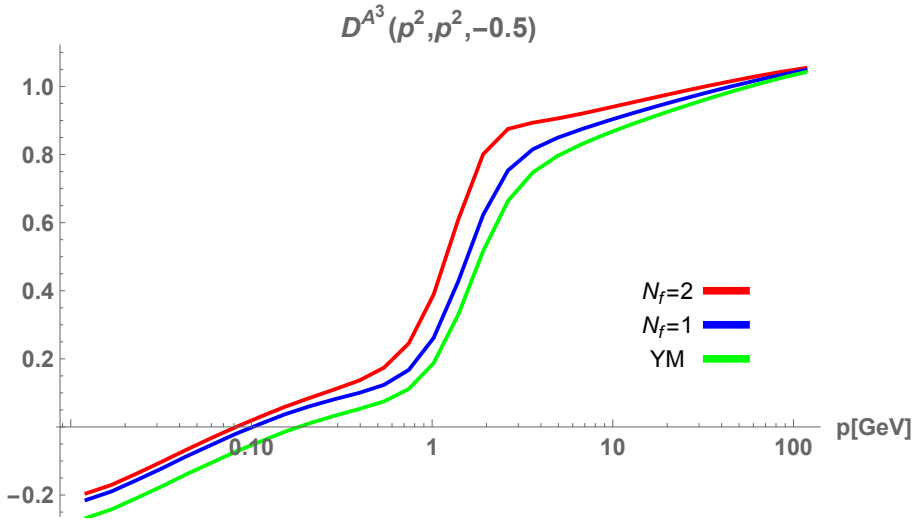

Figure 5.10.: The three-gluon vertex from a calculation with a dynamical quark-gluon vertex ($N_f = 2$ and $N_f = 1$) and in Yang-Mills theory.

6. Conclusion and Outlook

The main goal of our work is the unquenching of the three-gluon vertex in a dynamical set-up consisting of quark-gluon vertex, quark propagator and three-gluon vertex. To achieve this we took small steps and considered the quark sector and the three-gluon vertex separately before coupling them. For the quark-gluon vertex we took all eight transverse basis tensors into account and considered the 3PI equation of the quark-gluon vertex as well as its DSE. Regarding the 3PI equation the focus was solely on the calculation of the non-Abelian diagram, whereas for the quark-gluon vertex DSE all three diagrams (non-Abelian, Abelian and swordfish diagram) were included. In doing so we employed a model [17] for the two-quark-two-gluon vertex that occurs in the swordfish diagram. Moreover, for the Yang-Mills propagators we used input that is in agreement with quenched Lattice data. We approximated the three-gluon vertex by a model [101] whose impact on the result was analyzed by varying the model parameters. Finally, we calculated the coupled system of quark-gluon vertex and quark propagator. For the 3PI equation we found a generated mass of around $210\,MeV$ which is smaller than what one would expect. On the other hand in the DSE calculation the generated mass vanishes completely. Comparing the diagrams of the 3PI equation with its DSE counterpart one may speculate that the reason for this is that the swordfish diagram needs to have a certain strength to enable chiral symmetry breaking. This would then hint to the fact that the model underestimates the strength of the two-quark-two-gluon vertex. However, this argument is not compelling and a definitive statement has to rely on further investigations. As expected we found the contribution of the Abelian diagram to be insignificant which confirms earlier investigations of the Abelian diagram in the 3PI equation [11].
The quark sector in the three-gluon vertex is reflected in the quark triangle diagram and the quark swordfish diagram, where for the latter we used once more the two-quark-two-gluon vertex model. By defining charge conjugation for non-Abelian theories we were able to show that the three-gluon vertex has to be proportional to the antisymmetric structure constant f^{abc} and that the part proportional to the symmetric structure constant d^{abc} has to vanish. Moreover, we could demonstrate in a way similar to Furry's theorem that the color symmetric parts of both quark triangle diagrams cancel each other and that the color antisymmetric parts add up. As a consequence only one quark triangle diagram needs to be calculated.
Crucial for the stability of the three-gluon vertex is the cancellation mechanism between one swordfish diagram and the gluon-triangle diagram. This has to be taken account of by the four-gluon vertex model in the swordfish diagram. Unfortunately, a change of the parameters of this model affects the position of the zero crossing of the three-gluon vertex.
In the calculation of the coupled system of quark propagator, quark-gluon vertex and three-gluon vertex the mutual impact of the quark sector and three-gluon vertex onto each other can be studied. There are mainly two findings:

1. Although the position of the zero crossing of the three-gluon vertex cannot be determined precisely due to the arbitrariness introduced by the four-gluon vertex model, it is possible to make a statement about how the zero crossing is affected by unquenching effects. We could see that the unquenched three-gluon vertex lies above the three-gluon vertex of a pure Yang-Mills calculation and that consequently the position of the zero-crossing is shifted towards the infrared regime. This in turn implies that the strength of the three-gluon vertex increases at a scale relevant for hadron physics.

2. Dynamical chiral symmetry breaking is very sensitive to the value of the three-gluon vertex that enters the equation of the quark-gluon vertex. From our calculation we could see that a stronger three-gluon vertex leads to more generated mass in the quark propagator, where the calculation for flavour number $N_f = 2$ in the three-gluon vertex gives a value of around $350\,MeV$ in accordance with expectations. Especially the part of the three-gluon vertex around $1 - 5\,GeV$ seems to play an important role for this.

Of course our calculations are subject to truncation effects. It will therefore be the task of future work to examine how much our results are affected by the truncation. However, some steps to ameliorate the set-up can already now be specified:
Instead of quenched input for the Yang-Mills propagators one should use input that matches unquenched Lattice data. Moreover, the bare ghost-gluon vertex should be replaced by a dressed ghost-gluon vertex. Since the transverse ghost-gluon vertex has only one dressing function which is relatively easy to calculate, this seems to be comparatively easy.
We have seen that there is a difference between the non-Abelian diagram in the 3PI equation, where all quark-gluon vertices are dressed, and the non-Abelian diagram in the DSE, where one quark-gluon vertex is bare. It would therefore be interesting to see, if the same is true for the quark-triangle diagram in the three-gluon vertex. One should therefore perform a comparison between a calculation of the three-gluon vertex in the 3PI formalism and a calculation of the three-gluon vertex DSE.
So far only the tree-level tensor of the three-gluon vertex has been taken into account since in a Yang-Mills calculation the other tensor structures were found to be negligible [31]. However, a considerable contribution of the beyond tree-level tensor structures to the quark-triangle diagram cannot be excluded a priori.
In the long run, the gluon propagator should be included dynamically, since it is expected that effects due to the unquenching of the gluon propagator counteract effects due to the unquenching of the three-gluon vertex. In order to see which of both effects prevails a dynamical inclusion of the gluon propagator is inevitable.
The calculations presented here may serve as starting point for further research ranging from a calculation of the quark-gluon vertex at finite temperature and/or finite chemical potential to a calculation of bound states. A particularly interesting field of application is the physics at large N_f and the conformal window which is of importance for some theories of technicolor that demand a walking behaviour for the running coupling. A possible future project could therefore be an extension of the investigation done in [128]. In this study the gluon propagator at large N_f was examined employing a model for the quark-gluon vertex. The authors point out that an inclusion of a full quark-gluon vertex may improve the prediction of the number N_f^{crit} at which the conformal behaviour sets in.
So far most of the previous research focused either on the quark sector **or** on pure

Yang-Mills theory. Building up on this groundwork it became recently possible to study the interplay between both sectors [13, 18]. Already a notable result of this research is that dynamical chiral symmetry breaking is less robust than anticipated. It is clear that this finding deserves further investigations and one may expect interesting results from this research topic in the years to come.

7. Symmetry-broken phase of ϕ^4-theory from the FRG

This chapter differs widely from the preceding investigation. The biggest difference is that the theory under consideration will be a $O(N)$-symmetric scalar field theory instead of QCD. $O(N)$-symmetric scalar field theories have been intensively studied in the past. The reason for their application is that they allow for a comparatively easy calculation of the critical exponents. Moreover, due to their simple form they are the ideal tool to become acquainted with the FRG and investigate the behaviour of a theory at finite temperature in the symmetric and symmetry broken phase.
In this chapter we will consider ϕ^4-theory with the aim to research the symmetry broken phase employing a Local Potential Approximation (LPA). In doing so we will rely on a method that was invented in [129], in which the potential is expanded around a constant rather than around its minimum. In this way this work complements [130].
In the following most steps will be performed for general N. However, in the actual calculation we will restrict ourselves to $N = 1$, which corresponds to the universality class of the Ising model.

7.1. The Local Potential Approximation

We consider the Lagrangian

$$\mathcal{L} = \frac{1}{2}\partial_\mu\phi\partial_\mu\phi + \frac{1}{2}m^2\phi^2 + \frac{\lambda}{24}\phi^4 \ .$$

This Lagrangian is symmetric under $O(N)$ symmetry and ϕ denotes a N-component real field

$$\phi = \begin{pmatrix} \phi_1 \\ \phi_2 \\ \vdots \\ \phi_N \end{pmatrix} \ . \tag{7.1}$$

With this Lagrangian we can derive the effective action Γ_k as outlined in section 3.3, in which the FRG was introduced. The next step thus consists in finding an appropriate truncation. We will employ a so-called *derivative expansion*. How this works for the FRG is best seen in momentum space. From the flow equation (3.40) we can deduce that on account of the condition (3.31) only loop momenta q smaller than k result in a non-vanishing flow. For small external momenta one can therefore expand the effective action in terms of q^2/k^2 and p_i^2/k^2, where p_i are the external momenta which have to fulfill the condition $p_i^2 < k^2$. In position space this

corresponds to an expansion in terms of field derivatives which gave this truncation scheme its name. A drawback of this truncation scheme is that in the limit $k \to 0$ the expansion is only reasonable for vanishing external momenta [1]. But since we are mainly interested in thermodynamical quantities this does not pose a strong restriction.
Applying the derivative expansion to the effective action up to the order $\mathcal{O}(\partial^2)$ yields [132]

$$\Gamma_k[\Phi_k] = \int d^4x \left(V_k(\rho_k) + \frac{1}{2} Z_k(\rho_k)(\partial\Phi_k)^2 + \frac{1}{4} Y_k(\rho_k)(\Phi_k \partial\Phi_k)^2 + \mathcal{O}(\partial^4) \right) . \quad (7.2)$$

Here $V_k(\rho)$ is the potential, $Z_k(\rho)$ is the wave-function renormalization [2] and $\rho = \frac{1}{2}\Phi^2$. Moreover, the quantities V_k, Z_k and Y_k have to depend on ρ since due to the $O(N)$-symmetry the exponents of the field must be even. For $O(N = 1)$ the term proportional to Y_k can be absorbed by the term Z_k.
The *Local Potential Approximation* (LPA) consists now in setting $Y_k(\rho) = 0$ and $Z_k(\rho) = 1$:

$$\Gamma_k[\Phi_k] = \int d^4x \left(V_k(\rho_k) + \frac{1}{2} (\partial\Phi_k)^2 \right) . \quad (7.3)$$

This approximation shows a quick convergence and good approximations of thermodynamic quantities can be obtained. But due to the fact that $Z_k(\rho)$ has been set equal to one, it is not possible to calculate the anomalous dimension. However, there exists an extension of this scheme called LPA$'$ in which a field-independent wave-function renormalization Z_k is considered [132].
Typically, in a further approximation the potential is expanded around its minimum $\rho_{0,k}$ [130]

$$V_k(\rho_k) = \lambda_{0,k} + \lambda_{1,k}(\rho_k - \rho_{0,k}) + \frac{\lambda_{2,k}}{2}(\rho_k - \rho_{0,k})^2 + \mathcal{O}(\rho^3) . \quad (7.4)$$

One should bear in mind that due to the flow of the potential also the minimum changes and therefore depends on the scale. Note that in section 7.3 we will employ a different ansatz in which the potential is expanded around a constant. However, we state this formula here to allow for a comparison between both methods.
For the case of $\rho_{0,k} = 0$ we can rewrite the coefficients to obtain the form of the classical ϕ^4 potential

$$V_k(\rho_k) = V_{0,k} + m_k^2 \rho_k + \frac{\lambda_k}{6} \rho_k^2 , \quad (7.5)$$

where we can identify $\lambda_{1,k} = m_k^2$ and $\lambda_{2,k} = \frac{\lambda_k}{3}$. In the following we will thus often refer to $\lambda_{1,k}$ and $\lambda_{2,k}$ as the mass and the coupling.
Since we are mainly interested in thermodynamical quantities rather than in the dynamics of the field we can project the potential out of the effective action. This is usually done by choosing a constant uniform field in order to get rid of the derivatives

[1] An improvement of the derivative expansion is given by the BMW method which allows for the calculation of n-point functions at non-vanishing momenta [131].
[2] In DSE-language this corresponds to the inverse dressing function.

in the effective action

$$\Phi_k = \begin{pmatrix} \Phi_k^{const} \\ 0 \\ \vdots \\ 0 \end{pmatrix} . \tag{7.6}$$

From this we obtain (up to a volume factor) the flow equation for the potential. If we split up the propagator on the right-hand side of the Wetterich equation into its transverse and longitudinal part (see appendix B.2), we get

$$\partial_t V_k(\rho_k) = \frac{1}{2} \int \frac{d^4q}{(2\pi)^4} \dot{R}_k(q) \left[G_{trans}(q)(N-1) + G_{long}(q) \right] , \tag{7.7}$$

where G_{trans} and G_{long} are abbreviations for

$$\begin{aligned} G_{trans}(p) &= \frac{1}{(p^2 + V_k'(\rho_k) + R_k(p))} , \\ &= \frac{1}{p^2 + \lambda_{1,k} + \lambda_{2,k}(\rho_k - \rho_{0,k}) + R_k(p)} , \\ G_{long}(p) &= \frac{1}{(p^2 + V_k'(\rho_k) + 2\rho_k V_k''(\rho_k) + R_k(p))} , \\ &= \frac{1}{p^2 + \lambda_{1,k} + 3\rho_k \lambda_{2,k} - \lambda_{2,k}\rho_{0,k} + R_k(p)} \end{aligned} \tag{7.8}$$

Here the prime stands for differentiating with respect to ρ_k. In the following we will set $N = 1$ which implies that the transverse part drops out.
The flow equation of the effective potential gives direct access to the pressure, since in our approximation one finds

$$P_k = -\left(V_k^T(\rho_k = \rho_{0,k}) - V_k^{T=0}(\rho_k = \rho_{0,k}) \right) , \tag{7.9}$$

where the normalization has been chosen such that the pressure vanishes in the vacuum $P_{k=0}^{T=0} = 0$ [3].

The flow equations for the parameters $\lambda_{1,k}$ and $\lambda_{2,k}$ are obtained by differentiating the potential with respect to ρ_k and evaluating it at the minimum.
Moreover, the flow equation for the minimum can be derived from the relation

$$\partial_t V_k'(\rho_{0,k}) = \dot{V}_k'(\rho_{0,k}) + V_k''(\rho_{0,k})\dot{\rho}_{0,k} = 0 . \tag{7.10}$$

[3] In principle one could also finetune the potential $V_{k=\Lambda}$ such that the value of the pressure in the vacuum vanishes $P_{k=0}^{T=0} = 0$. However, this procedure is numerically challenging since it involves cancellations over several orders of magnitude [133].

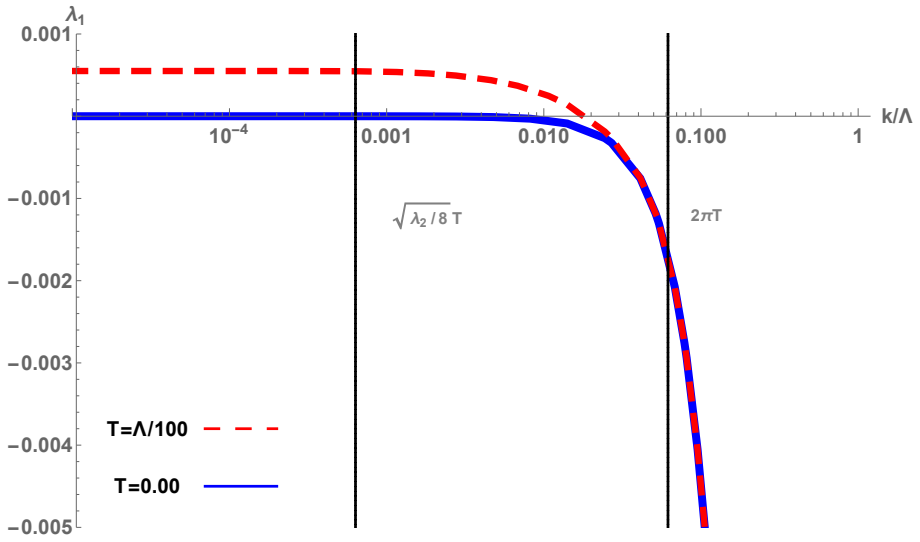

Figure 7.1.: $\lambda_{1,k}$ plotted over the scale k/Λ. The blue, solid line refers to a calculation in the vacuum and the red, dashed line to a calculation at finite temperature. The vertical lines shall indicate the points $\sqrt{\lambda_{2,k}/8}\mathrm{T}$ and $2\pi\mathrm{T}$.

The coupled system of flow equations for $N = 1$ therefore reads

$$\dot{P}_k = -\frac{1}{2}\sum\!\!\!\!\!\!\int \frac{\dot{R}_k(q)}{q^2 + \lambda_{1,k} + 2\lambda_{2,k}\rho_{0,k} + R_k(q)}\,, \tag{7.11}$$

$$\dot{\lambda}_{1,k} = -\frac{1}{2}\sum\!\!\!\!\!\!\int \frac{3\lambda_{2,k}\dot{R}_k(q)}{(q^2 + \lambda_{1,k} + 2\lambda_{2,k}\rho_{0,k} + R_k(q))^2} - \lambda_{2,k}\dot{\rho}_{0,k}\,, \tag{7.12}$$

$$\dot{\lambda}_{2,k} = 9\sum\!\!\!\!\!\!\int \frac{\lambda_{2,k}^2\dot{R}_k(q)}{(q^2 + \lambda_{1,k} + 2\lambda_{2,k}\rho_{0,k} + R_k(q))^3}\,, \tag{7.13}$$

$$\dot{\rho}_{0,k} = -\frac{\dot{\lambda}_{1,k}}{\lambda_{2,k}}\,. \tag{7.14}$$

Here we have introduced the notation

$$\sum\!\!\!\!\!\!\int = \begin{cases} \int \frac{d^4q}{(2\pi)^4} & \text{for } T = 0\,, \\ T\sum\limits_{\omega_n}\int \frac{d^3q}{(2\pi)^3} & \text{for } T \neq 0\,, \end{cases} \tag{7.15}$$

in order to differentiate between the theory in the vacuum and at finite temperature. ω_n refers to the Matsubara frequencies $\omega_n = 2\pi nT$.
These flow equations close on themselves, but they are coupled to each other in different ways. For example the minimum $\rho_{0,k}$ couples back to all other flow equations. In section 7.3 we will investigate which problems can arise from this and how they can be circumvented.

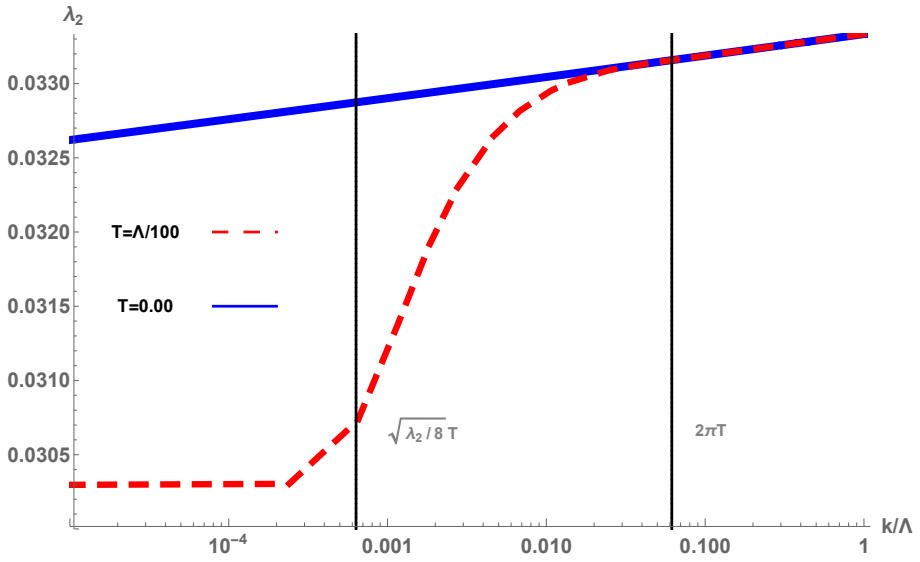

Figure 7.2.: $\lambda_{2,k}$ plotted over the scale k/Λ. The blue, solid line refers to a calculation in the vacuum and the red, dashed line to a calculation at finite temperature. The vertical lines shall indicate the points $\sqrt{\lambda_{2,k}/8}\mathrm{T}$ and $2\pi\mathrm{T}$.

7.2. The Symmetric Phase

In the unbroken theory we have $\rho_{0,k} = 0$ which simplifies the system of flow equations. Especially no back coupling of the minimum has to be taken into account.
In principle one could now start to solve the coupled system of flow equations. However, one faces the problem that the initial values for the parameters $\lambda_{1,k}$ and $\lambda_{2,k}$ have to be chosen carefully so that one stays in the symmetric phase, i.e., that $V'(\rho_k = 0) = \lambda_{1,k} = 0$[4]. Therefore we proceed in two steps [134]:

1. We start at $k = \Lambda$ in the vacuum with fixed $\lambda_{2,k=\Lambda}$ and finetune the value for $\lambda_{1,k=\Lambda}$ in such a way that we arrive at $\lambda_{1,k=0} = 0$.

2. With the values for $\lambda_{1,k=\Lambda}$ and $\lambda_{2,k=\Lambda}$ obtained in the first step we then flow down from $k = \Lambda$ to $k = 0$ at finite temperature.

In figures (7.1) and (7.2) the results for $\lambda_{1,k}$ and $\lambda_{2,k}$ for the vacuum and for finite temperature for $N = 1$ are depicted. For these calculations the exponential regulator has been employed. In contrast the use of the optimized regulator is more problematic, since due to the theta function $\Theta(k^2 - q^2)$ the impact of single Matsubara frequencies becomes visible which leads to an oscillatory behavior of the flow [5].
With respect to thermal effects three different domains can be distinguished:

k=Λ to k=2πT : Since effects due to finite temperature arise at scales below the first Matsubara frequency $2\pi T$ the behaviour at large scales is not affected

[4] In principle the parameters can be chosen such that $V'(\rho_k = 0) > 0$ as well. However, the advantage of fine-tuning $\lambda_{1,k}$ such that $V'(\rho_k = 0) = 0$ is that the symmetry broken phase can be reached by small changes of $\lambda_{1,k}$.

[5] Cf. the discussion in [135]

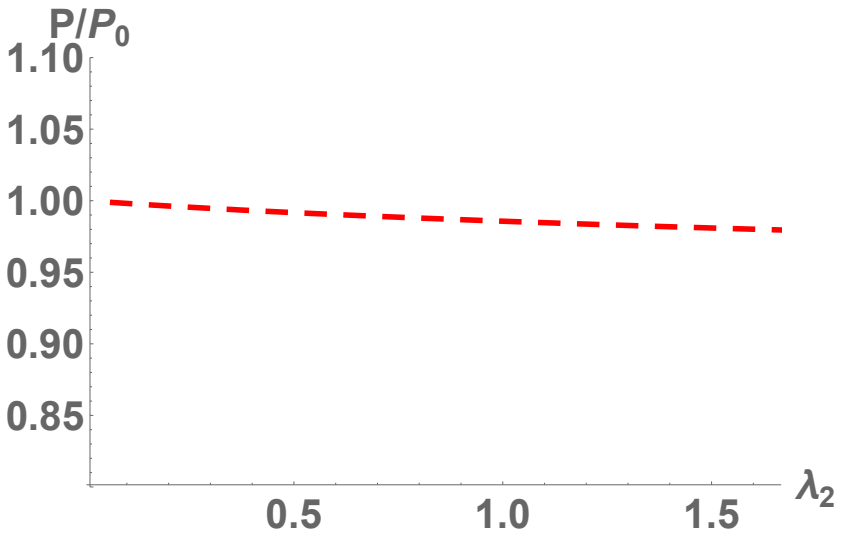

Figure 7.3.: The pressure P/P_0 plotted over the coupling λ_2. The pressure is normalized to the Stefan-Boltzmann pressure P_0.

by $T \neq 0$.

k=2πT to k=$\sqrt{\lambda_{2,k}/8}$T : In this domain thermal effects come into play. While the vacuum mass continues running logarithmically to the finetuned value $\lambda_{1,k=0} = 0$, at finite temperature the system starts generating a thermal mass due to thermal fluctuations. The size of the thermal mass can be estimated by Perturbation Theory which gives to first order $m^2_{therm} = (\lambda_{1,k})_{therm} = \frac{\lambda_{2,k}}{8}T^2$ [136][6]. In the same way the coupling $\lambda_{2,k}$ starts to deviate from the vacuum solution in this regime on account of thermal fluctuations and the backcoupling of the thermal mass to the flow of the coupling.

k=$\sqrt{\lambda_{2,k}/8}$T to k=0 : The creation of a thermal mass $(\lambda_{1,k})_{therm}$ is counteracted by the fact that in the flow equation $\lambda_{1,k}$ appears in the denominator and hence an increasing mass slows down the flow. When the scale k=$\sqrt{\lambda_{2,k}/8}$T is reached, $\lambda_{1,k}$ and $\lambda_{2,k}$ start to freeze out at their final value.

In figure (7.3) the pressure over the coupling $\lambda_{2,k}$ is depicted. The pressure is normalized to the Stefan-Boltzmann free pressure $P_0 = \frac{\pi^2}{90}T^4$. At vanishing coupling constant $\lambda_{2,k}$ all energy is kinetic energy and thus the pressure coincides with the Stefan-Boltzmann pressure. With increasing coupling strength parts of the kinetic energy are absorbed by the interaction and consequently the pressure decreases. The results for the symmetric phase presented in this section are in agreement with the results found in [133, 130].

[6] Sometimes a different convention for the coupling is used so that $g^2 = \frac{\lambda_{2,k}}{8}$. In this case the thermal mass is given by $m^2_{therm} = g^2T^2$.

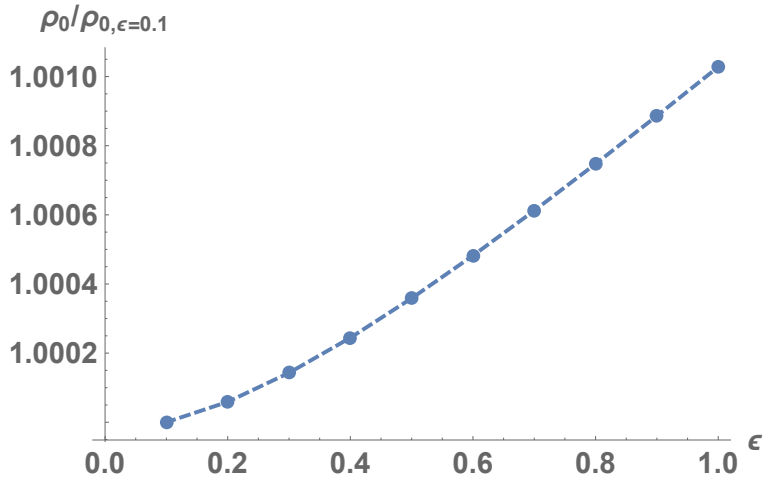

Figure 7.4.: The ratio $\rho_0(\epsilon)/\rho_0(\epsilon = 0.1)$ as a function of ϵ. The minimum changes very slowly with varying ϵ which proves the employed method to be reliable.

7.3. The Symmetry Broken Phase

In the symmetry broken phase the minimum does not vanish and consequently the back coupling of the flow equation of the minimum (7.14) to the system of equations (7.11)-(7.13) has to be considered. In this way every numerical inaccuracy that appears in the flow equation of the minimum is carried over to all other equations. In order to avoid this effect we employ a method that was developed in [129]. This method is based on the idea that the minimum is a characteristic point for the potential but not for the evolution of the flow. Therefore we can expand around an arbitrary and fixed point κ that lies close to the potential minimum:

$$\kappa = (1 + \epsilon)\rho_{0,k=0}\,, \tag{7.16}$$

with ϵ being small and positive. The reason for the latter is that the potential becomes convex at $k = 0$ and hence it is flat for $\rho < \rho_0$. If ϵ was negative we would therefore expand in a flat region which leads to a loss of information about the theory.
One has nevertheless to bear in mind that every physical quantity (like the pressure) has to be evaluated at the potential minimum. However, this does not pose a problem since the potential minimum can always be determined a posteriori through the condition $V'(\rho_0) = 0$.
With this the following system of equations has to be solved:

$$\dot{P}_k = -\frac{1}{2}\sum\int \frac{\dot{R}_k(q)}{q^2 + \lambda_{1,k} + 2\lambda_{2,k}\kappa + R_k(q)}\,, \tag{7.17}$$

$$\dot{\lambda}_{1,k} = -\frac{1}{2}\sum\int \frac{3\lambda_{2,k}\dot{R}_k(q)}{(q^2 + \lambda_{1,k} + 2\lambda_{2,k}\kappa + R_k(q))^2}\,, \tag{7.18}$$

$$\dot{\lambda}_{2,k} = 9\sum\int \frac{\lambda_{2,k}^2\dot{R}_k(q)}{(q^2 + \lambda_{1,k} + 2\lambda_{2,k}\kappa + R_k(q))^3}\,. \tag{7.19}$$

In this equations the minimum is replaced by the constant κ. In general κ can be

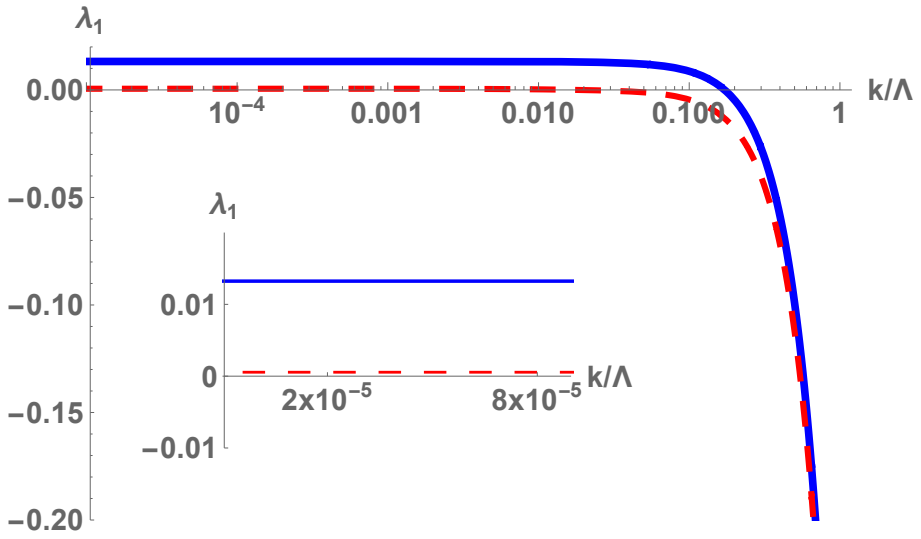

Figure 7.5.: Results for λ_1 at $T = \Lambda/100$ in the symmetry broken (blue, continuous line) and in the symmetric phase (red, dashed line). In the symmetry broken phase more thermal mass is generated.

chosen arbitrarily as long as it lies close to the minimum. This is demonstrated in figure 7.4 where it is plotted how the position of the minimum changes for different values of ϵ. The deviation of the minimum from its value at $\epsilon = 0.1$ increases with growing ϵ but remains even for $\epsilon = 1$ negligible. In the actual calculation one would therefore choose a value for κ and check it distance to the calculated minimum in the end.

In figure 7.5 and 7.6 the results for λ_1 and λ_2 at finite temperature in the symmetry broken phase are shown in comparison with the respective results for the symmetric phase. In the symmetry broken phase more thermal mass is generated than in the symmetric phase. As discussed in the previous section an increasing mass slows down the flow and therefore in the symmetry broken phase λ_2 freezes out much faster.

We are also able to calculate the pressure as a function of the temperature. The plot is shown in figure 7.7 where T_c corresponds to the critical temperature where the symmetric phase is restored. The pressure rises very quickly with temperature before it flattens out. It finally adapts the value of $P/P_0 = 1$ which corresponds to an interaction free theory. Regarding the calculation itself there are two things one should be aware of. Since the position of the minimum changes with the temperature, one has to adapt the value of κ accordingly. Additionally one faces the problem that at temperatures close to the critical temperature the flow equation becomes very stiff. It is therefore recommended to use algorithms that are better suited for this like e.g. the algorithm of Bulirsch-Stoer.

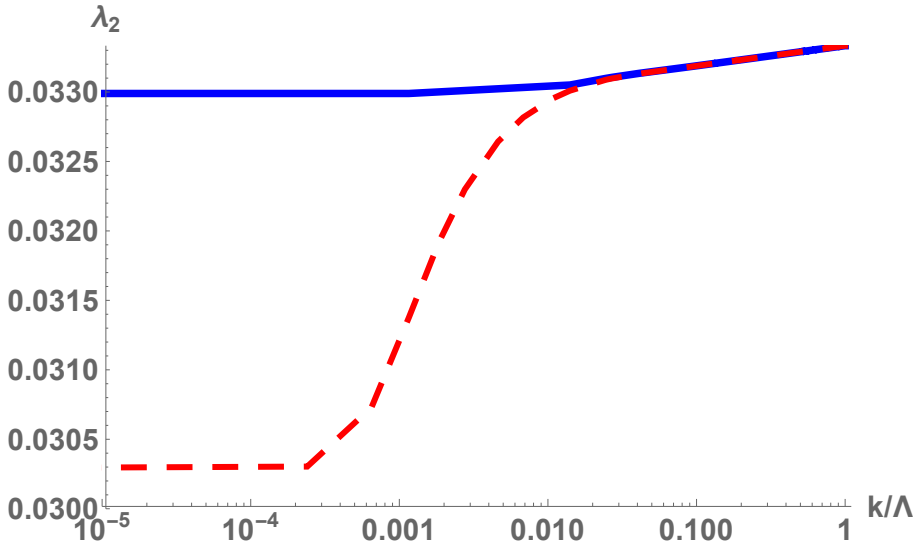

Figure 7.6.: Results for λ_2 at $T = \Lambda/100$ in the symmetry broken (blue, continuous line) and in the symmetric phase (red, dashed line). In the symmetry broken phase λ_2 freezes out much faster as a consequence of the bigger thermal mass.

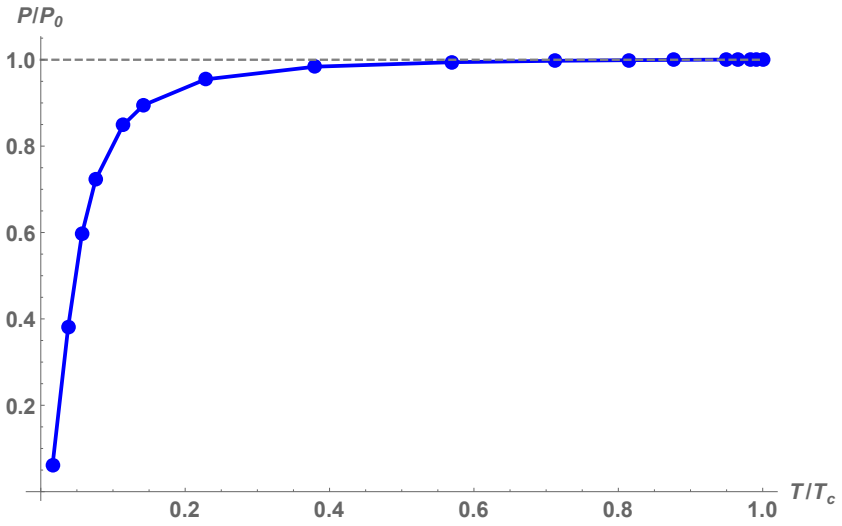

Figure 7.7.: The pressure as a function of the temperature. P_0 is the Stefan-Boltzmann pressure and T_c refers to the critical temperature at which the symmetric phase is restored.

7.4. Conclusion and Outlook

We have studied the $O(N)$-symmetric ϕ^4-theory for $N = 1$. As truncation a Local Potential Approximation was employed. In the calculation the symmetric as well as the symmetry broken phase in the vacuum and at finite temperature was researched. In doing so we avoided the back-coupling of the minimum to all other flow equations by expanding around a constant which lies close to the exact minimum [129]. The position of the minimum depends only weakly on this constant which proved this ansatz a posteriori to be reliable. We calculated the mass and the coupling and could study how thermal mass is generated and how it impacts the flow of both quantities.
We computed the pressure as a function of the temperature in the symmetry broken phase, which is – to our knowledge – the first time that such a calculation has been performed. Furthermore, we could point out problems like the stiffness of the flow equation near the critical temperature and gave possible solutions.
In a further step one could go to N higher than $N = 1$. In this way the transverse modes are included as well. For this purpose, our investigation may serve as groundwork and starting from the considerations done here an extension to arbitrary N is possible. Moreover, higher orders in the derivative expansion can be included so that also the anomalous dimension can be researched.

Acknowledgements

I am grateful to many people who in a direct or indirect way contributed to this work.
First of all I would like to thank Reinhard Alkofer for the topic of my thesis, his support and the many discussions we had about chiral symmetry breaking and other questions. I'm deeply grateful to Markus Huber for our long-lasting cooperation. It's no exaggeration to say that I owe him almost everything I know about Dyson-Schwinger equations. Moreover, I would like to thank Richard Williams for taking the time to give me some helpful advices about the quark-gluon vertex. Also the inspiring discussions with Gernot Eichmann, Mario Mitter, Andreas Windisch, Markus Hopfer, Walid Mian and Pascal Törek should not remain unmentioned.
During my project I worked at two different institutes abroad. I would like to take the chance to thank Jean-Paul Blaizot, Leonard Fister and all the other members (and guests) of the IPhT in Saclay for their great hospitality and the fruitful collaboration. It was an unforgettable experience. The same applies to Christian Fischer and my colleagues from the physics institute in Gießen who took care of me during my stay there. I thank Claudia Spidla and Fanny Maetz for their help with everything that concerns administration.
Finally, I would like to thank my family for their support at any time.

This work was supported by the Austrian Science Fund (FWF) through the Doctoral Program on "Hadrons in Vacuum, Nuclei and Stars" (FWF DK-W1203).

Appendices

A. Calculation of the quark-gluon and three-gluon vertices

A.1. Notation and Conventions

Throughout this thesis we worked entirely in Euclidean space-time. Regarding the gamma matrices the connection between Minkowski and Euclidean spacetime is given by

$$\gamma_\mu^{(E),k} = -i\gamma_\mu^{(M),k} \quad \text{for } k = 1,2,3 \,, \tag{A.1}$$

$$\gamma_\mu^{(E),4} = \gamma_\mu^{(M),0} \,. \tag{A.2}$$

Since there is no likelihood of confusion, the index E is omitted most of the time. The Clifford algebra is then given by

$$\{\gamma_\mu, \gamma_\nu\} = 2\delta_{\mu\nu} \,, \tag{A.3}$$

with the metric tensor of Euclidean space-time $\delta_{\mu\nu}$.
Moreover, we did all calculation in the quark sector in the chiral limit, i.e., the quark masses were set to zero.
The local gauge transformations of color SU(3) is given by

$$\Omega(x) = e^{-ig\theta^a(x)T^a} \tag{A.4}$$

with the generators T^a. Under this transformation the quark and gluon fields transform according to

$$q \to \Omega(x)q \,, \tag{A.5}$$

$$\overline{q} \to \overline{q}\Omega(x)^{-1} \,, \tag{A.6}$$

$$A \to \Omega(x)A_\mu\Omega(x)^{-1} + \frac{i}{g}(\partial_\mu\Omega(x))\Omega(x)^{-1} \,. \tag{A.7}$$

Sometimes we used for the integrals the shorthand notation

$$\int AB = \int d^4x A(x)B(x) \,. \tag{A.8}$$

A.2. Propagators and Vertices

In the following we present a collection of propagators and vertices that have been used in the calculations. With respect to the vertices we will focus on the transverse tensor structures if not stated otherwise.

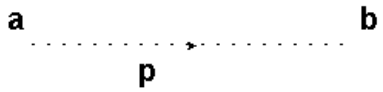

bare ghost propagator:

$$D^{(0)}_{gh}(p^2) = -\delta^{ab}\frac{1}{p^2}\ .$$

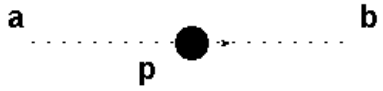

dressed ghost propagator:

$$D_{gh}(p^2) = -\delta^{ab}\frac{G(p^2)}{p^2}\ .$$

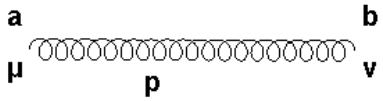

bare gluon propagator:

$$D^{(0)}_{\mu\nu}(p^2) = \delta^{ab}\frac{1}{p^2}\left(\delta_{\mu\nu} - \frac{p_\mu p_\nu}{p^2}\right)\ .$$

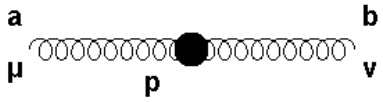

dressed gluon propagator:

$$D_{\mu\nu}(p^2) = \delta^{ab}\frac{Z(p^2)}{p^2}\left(\delta_{\mu\nu} - \frac{p_\mu p_\nu}{p^2}\right)\ .$$

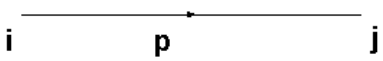

bare quark propagator:

$$S^{(0)}(p^2) = \delta^{ij}\frac{1}{m - i\not{p}}\ .$$

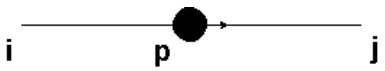

dressed quark propagator:

$$S(p^2) = \delta^{ij} \frac{1}{B(p^2) - iA(p^2)\not{p}} ,$$
$$= \delta^{ij} \frac{B(p^2) + iA(p^2)\not{p}}{B(p^2)^2 + A(p^2)^2 p^2} .$$

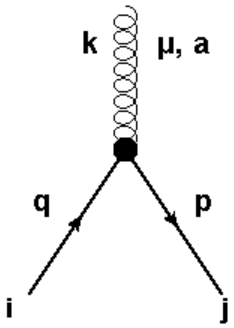

bare quark-gluon vertex:

$$\Gamma_\mu^{(qgv,0),a}(p,q) = igT_{ij}^a \gamma_\mu$$

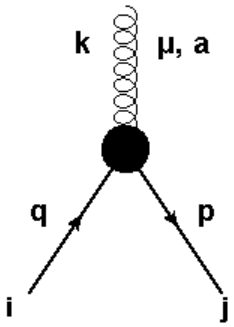

dressed quark-gluon vertex:

$$\Gamma_\mu^{(qgv),a}(p,q) = igT_{ij}^a \sum_{i=1}^{8} g^{(i)}(p^2, q^2, \cos(\alpha)) b_\mu^{(i)} ,$$

with $b_\mu^{(i)}$ as in (4.9).

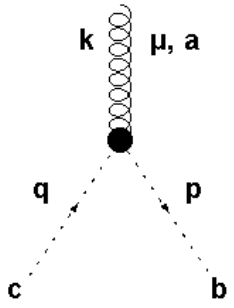

bare ghost-gluon vertex:

$$\Gamma_\mu^{(ghgv,0),abc}(p) = igf^{abc} p_\mu$$

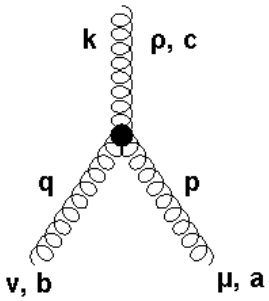

bare three-gluon vertex:

$$\Gamma^{(0),abc}_{\mu\nu\rho}(p,q,k) = -igf^{abc}[\delta_{\mu\nu}(p_\rho - q_\rho) + \delta_{\nu\rho}(q_\mu - k_\mu) + \delta_{\mu\rho}(k_\nu - p_\nu)]$$

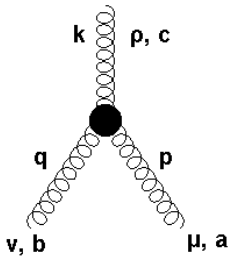

dressed three-gluon vertex:

$$\Gamma^{abc}_{\mu\nu\rho}(p,q,k) = D^{AAA}(p^2,q^2,\cos(\alpha))\,\Gamma^{(0),abc}_{\mu\nu\rho}(p,q,k)$$

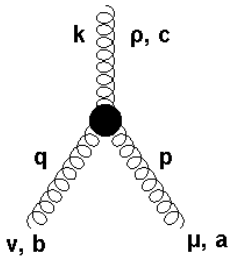

three-gluon vertex model:

$$\Gamma^{(model),abc}_{\mu\nu\rho}(p,q,k) = D^{AAA}_{model}(p^2,q^2,\cos(\alpha))\,\Gamma^{(0),abc}_{\mu\nu\rho}(p,q,k)$$

with D^{AAA}_{model} as in 4.29

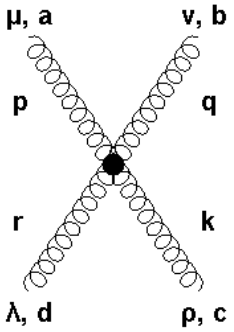

bare four-gluon vertex:

$$\begin{aligned}\Gamma^{(0),abcd}_{\mu\nu\rho\lambda}(p,q,k,r) = & g^2\Big[-\delta_{\mu\nu}\delta_{\rho\lambda}(f^{ade}f^{bce} + f^{ace}f^{bde}) \\ & +\delta_{\mu\rho}\delta_{\nu\lambda}(f^{ade}f^{bce} - f^{abe}f^{cde}) \\ & +\delta_{\mu\lambda}\delta_{\nu\rho}(f^{ace}f^{bde} + f^{abe}f^{cde})\Big]\end{aligned}$$

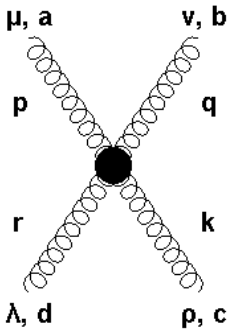

four-gluon vertex model:

$$\Gamma^{abcd}_{\mu\nu\rho\lambda}(p,q,k,r) = \left[a\tanh(\frac{b}{\bar{x}_{(4gl)}}) + 1\right] D^{A^4}_{RG}(p,q,k,r) \times \Gamma^{(0),abcd}_{\mu\nu\rho\lambda}(p,q,k,r)$$

$$\bar{x}_{(4gl)} = \frac{p^2+q^2+k^2+r^2}{2}$$

with $D^{A^4}_{RG}(p,q,k,r)$ as in (5.3)

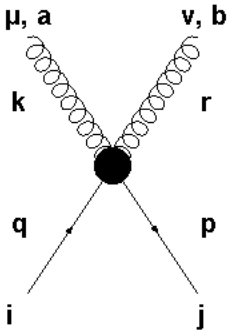

two-quark-two-gluon vertex model:

$$\Gamma^{2q2gl,ab}_{\mu\nu}(p,q,k,r) = -\frac{ig^2}{4} g^{(7)}(\bar{p}^2_{(2q2A)}, \bar{p}^2_{(2q2A)}, 0.5) T_{\mu\nu\rho} \times \left[(k-p)_\rho T^b T^a + (k+q)_\rho T^a T^b\right]$$

with

$$\bar{p}_{(2q2A)} = \sqrt{\frac{p^2+q^2+k^2+(p-q-k)^2}{4}}$$

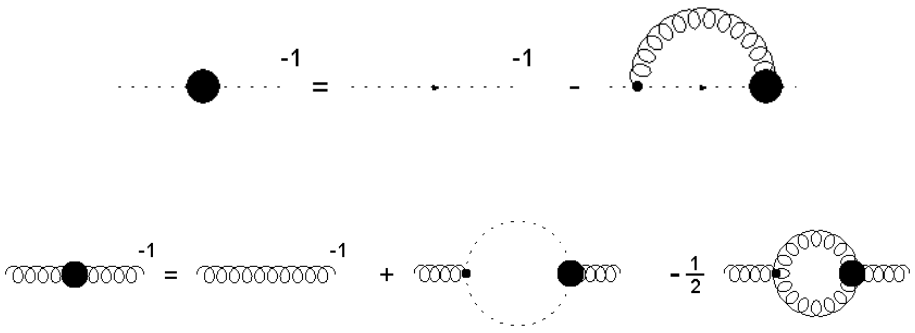

Figure A.1.: The (truncated) DSEs for the ghost and gluon propagator. The gluon equation is truncated by neglecting the two-loop diagrams. The second and third diagrams of the gluon DSE are called the ghost and gluon loop, respectively.

A.3. Calculation of the Yang-Mills input

As mentioned in the main text we calculated the coupled system of (quenched) ghost and gluon propagator DSE (figure A.1) and used the result as input for every further calculation. Crucial for this calculation is the use of the three-gluon vertex model (4.29) in the gluon loop of the gluon propagator DSE. This model was introduced in section 4.5 and for the convenience of the reader we write it down again

$$D^{A^3}(p,q,-p-q) = D^{A^3,IR}(p,q,-p-q) + D^{A^3,UV}(p,q,-p-q) \ ,$$

with

$$D^{A^3,UV}(p,q,-p-q) = G\left(\frac{p^2+q^2+(p+q)^2}{2}\right)^{\alpha} Z\left(\frac{p^2+q^2+(p+q)^2}{2}\right)^{\beta} \ ,$$

$$D^{A^3,IR}(p,q-p-q) = h_{IR} G(p^2+q^2+(p+q)^2)^3 (f_{\Lambda_{3g}}(p^2) f_{\Lambda_{3g}}(q^2) f_{\Lambda_{3g}}((p+q)^2))^{n_{3g}} \ ,$$

$$f_{\Lambda_{3g}}(p^2) = \frac{\Lambda_{3g}^2}{\Lambda_{3g}^2 + p^2} \ .$$

The parameters α and β take the fixed values $\alpha = \frac{3\delta+1}{\delta}$ and $\beta = 0$. On the other hand the parameters h_{IR}, Λ_{3g} and n_{3g} are free. In order to account for the correct UV running of the gluon propagator we multiply $D^{A^3}(p,q,-p-q)$ with an RG-improvement term

$$D^{A^3}_{RG}(p,q,-p-q) = \frac{1}{Z_1} D^{A^3,UV}(p,q,-p-q) \tag{A.9}$$

and obtain for the full model

$$\Gamma^{A^3}_{model}(p,q,-p-q) = D^{A^3}_{RG}(p,q,-p-q) D^{A^3}(p,q,-p-q) \Gamma^{(0),abc}_{\mu\nu\rho}(p,q,-p-q) \ , \tag{A.10}$$

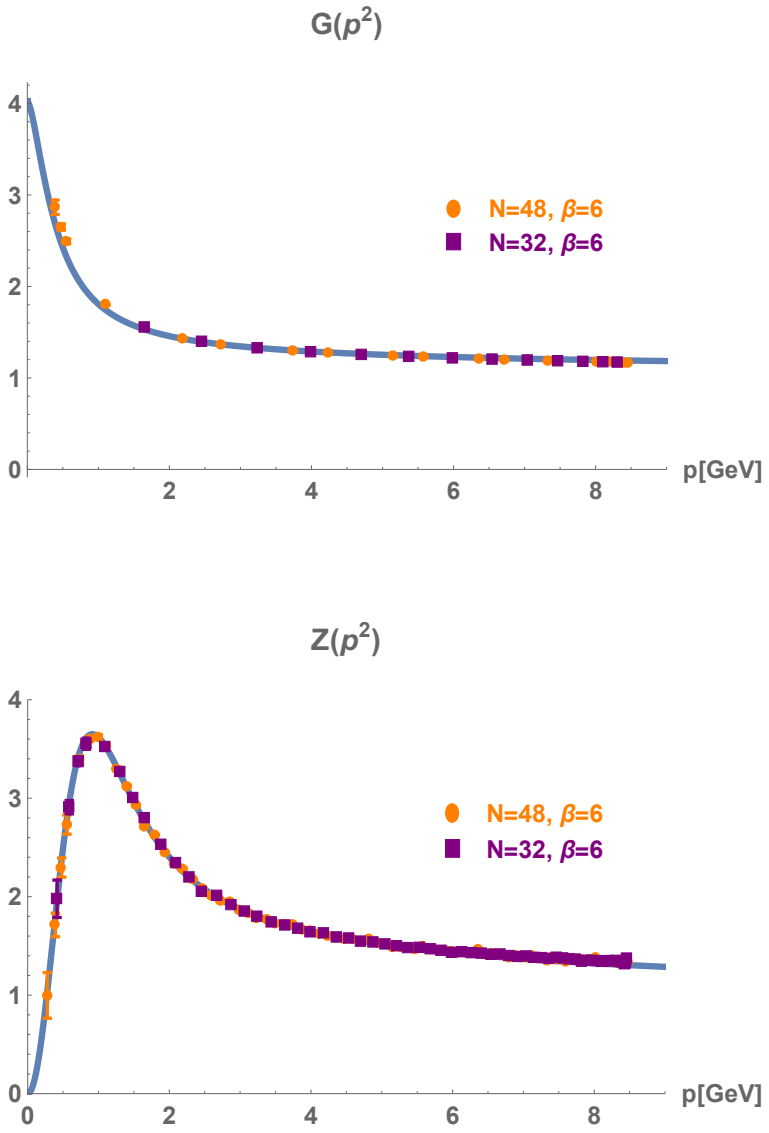

Figure A.2.: Using the parameters $h_{IR} = -1$, $\Lambda_{3g} = 0\,GeV$ and $n_{3g} = 4$ in the three-gluon vertex model the ghost and gluon propagators match Lattice data. The Lattice results are taken from [107].

with the tree-level tensor of the three-gluon vertex $\Gamma^{(0),abc}_{\mu\nu\rho}$.

For the renormalization we use a MOM-subtraction scheme. Subtracting the ghost and gluon equations evaluated at the subtraction points s^2_{gh} and s^2_{gl} from the unevaluated equations results in

$$G(p^2)^{-1} = G(s^2_{gh})^{-1} + loop_{gh}(p^2) - loop_{gh}(s^2_{gh}) \,, \tag{A.11}$$

$$Z(p^2)^{-1} = Z(s^2_{gl})^{-1} + loop_{gl}(p^2) - loop_{gl}(s^2_{gl}) \,. \tag{A.12}$$

The values of the dressing functions at the subtraction point are set to $G(s^2_{gh} = 0\,GeV^2) = 3.9$ and $Z(s^2_{gl} = 13577\,GeV^2) = 1$.
There is yet a further subtlety in form of spurious quadratic divergences hidden in the gluon DSE. These divergences are linked to the explicit breaking of gauge invariance due to the cutoff regularisation and have to be subtracted in addition to the usual renormalization process. For this several subtraction methods have been worked out (see e.g. [137] for an overview). We apply a method in which the value

of the gluon propagator is fixed in the infrared and a second subtraction of the gluon DSE is performed [138].
As part of the truncation prescription the two-loop diagrams in the gluon DSE are neglected. However, it was found that their contribution is seizable [1]. By choosing appropriate values for the free parameters we can tune the three-gluon vertex model such that it effectively compensates the missing strength from the two-loop diagrams. Choosing $h_{IR} = -1$, $\Lambda_{3g} = 0\,GeV$ and $n_{3g} = 4$ the results for the ghost and gluon dressing functions coincide with Lattice data (figure A.2). The Lattice results then set the scale in our system.
The advantage of this method over a direct fit of the Lattice data is that we are now able to calculate the renormalization constants $\widetilde{Z}_3$ and Z_3 as well. They are given by

$$\begin{aligned} \widetilde{Z}_3 &= G(p^2)^{-1} - loop_{gh}(p^2) \,, \\ Z_3 &= Z(p^2)^{-1} - loop_{gl}(p^2) \,. \end{aligned} \tag{A.13}$$

Since now $\widetilde{Z}_3$ and Z_3 are known and $\widetilde{Z}_1 = 1$ in Landau gauge all further renormalization constants can be determined via the STIs.

[1] This is in particular the case for the so-called squint diagram [139, 11]. The contribution of the second two-loop diagram, the sunset diagram, is however negligible [140].

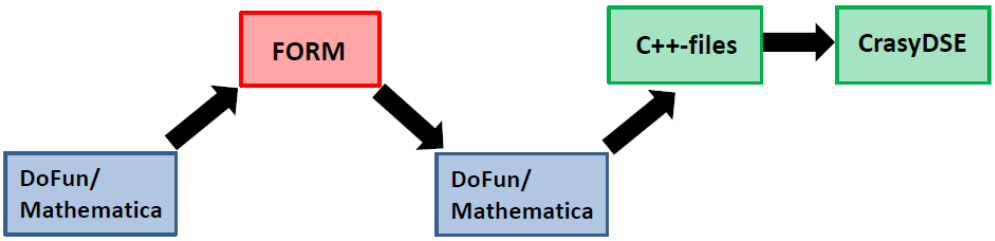

Figure A.3.: Schematic diagram of the computation process.

A.4. Steps for the calculation of the quark-gluon vertex

This section of the appendix is devoted to the technicalities that are necessary to calculate the quark-gluon vertex.
The integration kernels have been generated using the *Mathematica* package *DoFun* [76, 141]. The Lorentz contractions and the Dirac trace were performed with the help of *FORM* [142] and *ParFORM* [143]. The fully contracted kernels were then reimported into *Mathematica* where further manipulations were executed before the final expressions were transferred to a *C++*-file. The equations were numerically solved using the *C++*-program *CrasyDSE* [144]. To speed up the programm the code was parallelized using *MPI* .

A key question one has to answer is the question of how to project out the information that is located in the dressing functions of the quark-gluon vertex. There are in principle two possibilities. One way is to construct the projectors such that each dressing function is projected out directly. The advantage of this method is certainly that the eight equations that result from the projection do not need further manipulation. This can for example be achieved by using an orthonormal basis system, which was employed in [10, 11]. However, the elements of the orthonormal basis are comparatively big and thus they lead to rather complex kernels in the loop integration. In [10, 11] it was attempted to cope with this by using a second non-orthonormal basis system in the integration kernels and perform a basis transformation within each iteration step. Using an orthonormal basis system is one possibility to project out the dressing functions directly, but there is no necessity to use an orthonormal basis. In principle one can use any basis as long as the projectors themselves are constructed accordingly. In any case the clear disadvantage of this method is that the projectors are quite lengthy. Having performed the projection the lengthy terms that belong to the projectors cannot be separated from the integration kernels and therefore are called every time the integrand is evaluated. Since this is the case for every combination of internal and external points the calculation can be slowed down considerably.
We will therefore use a second method which corresponds to solving a matrix equation. In this ansatz the used basis and projectors can be chosen at will and therefore one can pick a basis where the basis tensors are relatively small. In our case we will employ the basis elements themselves as projectors. The projectors then mix the information of different dressing functions, i.e., after the projection with a certain

projector more than one dressing function may remain on the left-hand side. For example the second projector results in terms proportional to the second and third dressing function,

$$\begin{aligned}\mathrm{proj}_\mu^{(2)}(p,q)\Gamma_\mu^{(qgv)}(p,q) =& \mathrm{proj}_\mu^{(2)}(p,q)\sum_{i=1}^{8} g^{(i)}(p^2,q^2,\cos(\alpha))b_\mu^{(i)} \\ &\propto c^{(2,2)}(p,q)g^{(2)}(p^2,q^2,\cos(\alpha)) + c^{(3,2)}(p,q)g^{(3)}(p^2,q^2,\cos(\alpha))\ .\end{aligned} \tag{A.14}$$

Consequently, one can set up a 8×8 Matrix M with the elements $M^{(i,j)} = c^{(i,j)}(p,q)$ and arrives at the following matrix equation:

$$M\begin{pmatrix} g^{(1)} \\ g^{(2)} \\ \vdots \\ g^{(8)} \end{pmatrix} = \begin{pmatrix} \mathrm{proj}_\mu^{(1)}\Gamma_\mu^{(qgv,0)} \\ \mathrm{proj}_\mu^{(2)}\Gamma_\mu^{(qgv,0)} \\ \vdots \\ \mathrm{proj}_\mu^{(8)}\Gamma_\mu^{(qgv,0)} \end{pmatrix} + \int \frac{d^4k}{(2\pi)^4} \begin{pmatrix} \mathrm{proj}_\mu^{(1)}\mathbf{loop}_\mu \\ \mathrm{proj}_\mu^{(2)}\mathbf{loop}_\mu \\ \vdots \\ \mathrm{proj}_\mu^{(8)}\mathbf{loop}_\mu \end{pmatrix} \tag{A.15}$$

$$\Downarrow$$

$$\begin{pmatrix} g^{(1)} \\ g^{(2)} \\ \vdots \\ g^{(8)} \end{pmatrix} = (M)^{-1}\left\{ \begin{pmatrix} \mathrm{proj}_\mu^{(1)}\Gamma_\mu^{(qgv,0)} \\ \mathrm{proj}_\mu^{(2)}\Gamma_\mu^{(qgv,0)} \\ \vdots \\ \mathrm{proj}_\mu^{(8)}\Gamma_\mu^{(qgv,0)} \end{pmatrix} + \int \frac{d^4k}{(2\pi)^4} \begin{pmatrix} \mathrm{proj}_\mu^{(1)}\mathbf{loop}_\mu \\ \mathrm{proj}_\mu^{(2)}\mathbf{loop}_\mu \\ \vdots \\ \mathrm{proj}_\mu^{(8)}\mathbf{loop}_\mu \end{pmatrix} \right\}\ , \tag{A.16}$$

where we have suppressed the arguments for the sake of clarity. To solve for the dressing functions one has to invert the matrix M. Fortunately, the matrix inversion is easy enough to be performed beforehand, e.g. in *Mathematica* , and the result can then be included in the *C++* code. The inverted matrix occurs outside of the integral and has only to be evaluated at the external grid. Moreover, the result of the evaluation can even be stored in appropriate variables. In this way one prevents that certain terms are more often evaluated than necessary.

A further important point concerns the numerical integration. We found that the use of adaptive integration improved the results. We employed the adaptive integration routine *Cubature* [145]. Since it is difficult to parallelize an adaptive integration the parallelization was implemented with respect to the external grid.

For the interpolation we used standard linear interpolation. In principle, a non-linear interpolation like spline interpolation would be preferable, because it leads to smoother results. However, spline interpolation turned out to be extremely slow in three dimensions. Moreover, one has to take much care of unwanted effects due to a non-linear interpolation. Nevertheless, there are ways to deal with these effects in a proper way. This will be demonstrated in the next section. A good balance between speed and smoothness of the interpolation may therefore consist in a Chebyshev expansion.

For the coupled system of quark-gluon vertex equation and quark propagator DSE a fixed point iteration was employed. Here, we proceeded analogously to a micro-macro cycle. At first the quark-gluon vertex was iterated until convergence keeping the quark propagator fixed. The result was then plugged into the quark propagator DSE and the quark propagator was iterated until it convergenced. Then the result

for the quark propagator was again plugged into the equation for the quark-gluon vertex and so forth. These steps were repeated until convergence was found for the whole system of quark-gluon vertex and quark propagator.

A.5. Calculation of the quark-gluon vertex in the generalized Ball-Chiu basis

In this chapter we give a short outline of how a calculation of the quark-gluon vertex can be performed if one uses the "generalized Ball-Chiu" basis instead of the "naive basis" [2]. The reason is that in this basis new problems appear with which one has to cope. We start by recalling the "generalized Ball-Chiu" basis given in (4.5).

$$
\begin{aligned}
X_\mu^{(1)} &= \gamma_\mu^{(T)} \;, & X_\mu^{(2)} &= \not{l} l_\mu^{(T)} \;, \\
X_\mu^{(3)} &= i l_\mu^{(T)} \;, & X_\mu^{(4)} &= \frac{i}{2}(l\cdot k)\left[\gamma_\mu^{(T)}, \not{l}\right] \;, \\
X_\mu^{(5)} &= \frac{i}{2}\left[\gamma_\mu, \not{k}\right] \;, & X_\mu^{(6)} &= \frac{1}{6}\left(\left[\gamma_\mu, \not{l}\right]\not{k} + \left[\not{l}, \not{k}\right]\gamma_\mu + \left[\not{k}, \gamma_\mu\right]\not{l}\right) \;, \\
X_\mu^{(7)} &= (l\cdot k)\tau_{\mu\nu}\gamma_\nu \;, & X_\mu^{(8)} &= \frac{i}{2}\tau_{\mu\nu}\left[\gamma_\nu, \not{l}\right] \;,
\end{aligned}
$$

with $\tau_{\mu\nu} = (l\cdot k)\delta_{\mu\nu} - l_\mu k_\nu$, the relative momentum $l = (p+q)/2$ and the total momentum $k = p - q$. The arguments of the dressing functions in this basis can be parametrized as $h^{(i)}(s_0, a, s)$ with

$$
\begin{aligned}
s_0 &= \frac{l^2}{3} + \frac{k^2}{4} \;, \\
a &= \frac{l\cdot k}{\sqrt{3}s_0} \;, \\
s &= 1 - \frac{k^2}{2s_0} \;,
\end{aligned}
$$

These variables form a cylinder of height s_0 with a circle of unit radius as base (see figure A.4). It is therefore more convenient to use polar coordinates for a and s:

$$
\begin{aligned}
a &= r\cos(\phi) \;, \\
s &= r\sin(\phi) \;.
\end{aligned}
\tag{A.17}
$$

The complete basis has the form

$$
\Gamma_\mu^{(qgv)} = \sum_{i=1}^{8} h^{(i)}(s_0, r, \phi) X_\mu^{(i)} \;. \tag{A.18}
$$

One of the first things one encounters in the numerical integration is the appearance of a singularity at the boundary in one of the integration angles. A numerical integration routine that is suited for such issues is the *tanh-sinh quadrature* [146]. One detriment of this method is that one has to set the parameter for the step size h by hand and a bad choice for h may lead to a unfavourable distribution of integration points. We therefore found the following rule of thumb helpful which relates the number of integration points m_{int} to the step size h: $m_{int} = 2^n - 1$ and $h = 4/(m_{int}+1)$, where n is an integer.
Regarding the angular integration a further problem arises in form of a cancellation of terms that is numerically not well fulfilled. However, not all dressing functions

[2] We would like to thank Richard Williams who instructed us on the methods presented here.

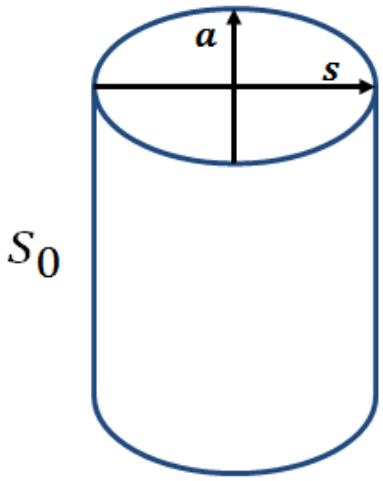

Figure A.4.: The geometric depiction of the variables used in the dressing functions $h^{(i)}$. The variables a and s form a circle of unit radius and are therefore better represented in polar coordinates.

are affected by this problem. The incomplete cancellation has the biggest impact on the dressing function $h^{(7)}$. Taking out $h^{(4)}$ and $h^{(7)}$ we found that an iteration of the remaining subset of dressing functions is possible. To also include $h^{(4)}$ and $h^{(7)}$ one has to perform a basis transformation to a basis where the cancellation problem is less severe, perform the calculation in this basis and rotate back to the old basis. For this purpose the following basis can be employed

$$\begin{aligned}
\hat{X}^{(1)} &= \gamma_\mu^{(T)} & \hat{X}^{(2)} &= \gamma_\mu^{(T)}[\not{l}^{(T)}, \not{k}] \,, \\
\hat{X}^{(3)} &= l_\mu^{(T)} \not{k} & \hat{X}^{(4)} &= l_\mu^{(T)} \not{l} \,, \\
\hat{X}^{(5)} &= i\gamma_\mu^{(T)} \not{k} & \hat{X}^{(6)} &= i(l \cdot k)[\gamma_\mu^{(T)}, \not{k}] \,, \\
\hat{X}^{(7)} &= i l_\mu^{(T)} & \hat{X}^{(8)} &= i l_\mu^{(T)} [\not{l}^{(T)}, \not{k}] \,.
\end{aligned} \tag{A.19}$$

The last point we would like to address concerns effects that are due to the use of non-linear interpolation. These effects are not limited to the calculation in this basis but can possibly affect also other basis systems whenever non-linear interpolation is used.
An advantage of the parametrization of the dressing functions in s_0, r and ϕ is that the dependence of $h^{(i)}$ on r and ϕ is extremely small. Hence, only the interpolation in s_0 needs a more careful treatment.
A direct implementation of spline interpolation leads to an oscillatory behaviour (see figure A.5). This behaviour is linked to the fast decline of the dressing function. In order to flatten out the dressing functions we multiply them with the highest dimension of the basis tensors (except for $h^{(1)}$):

$$h^{(i)} \longrightarrow h^{(i)}(1 + s_0)^3 \,. \tag{A.20}$$

However, in this way we overshoot the damping for the dressing functions with smaller dimension. Consequently, these dressing functions will rise at large s_0 due to the additional factor in terms of $(1+s_0)$. At first glance we have not gained much

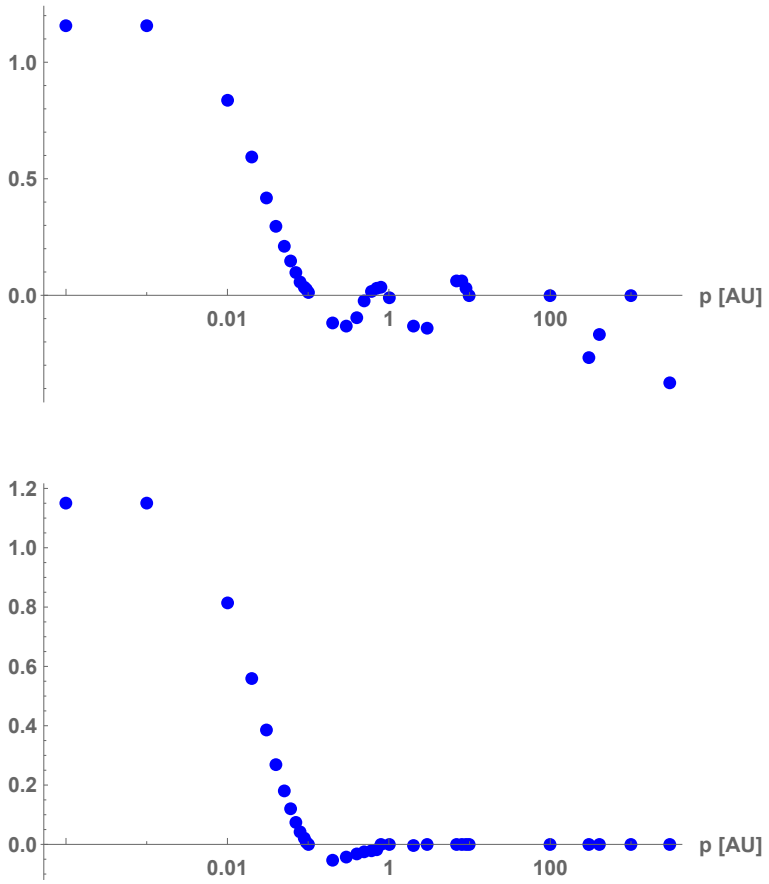

Figure A.5.: Example for problems due to non-linear interpolation. Top: On account of the steep decrease of the function a spline interpolation leads to an oscillatory behaviour. Bottom: carrying out the procedure explained in the text improves the result of the interpolation.

except that instead of a too fast decline we have now to deal with a too fast increase of some dressing functions. This problem can however be overcome in an elegant way by interpolating $\sinh^{-1}[h^{(i)}(1+s_0)^3]$ instead of $h^{(i)}(1+s_0)^3$. In this manner the following properties of $\sinh^{-1}(x)$ are exploited:

$$\sinh^{-1}(x) \approx \begin{cases} \log(x) & \text{for } |x| \gg 1 \,, \\ x & \text{for } x \leq 1 \,. \end{cases} \tag{A.21}$$

The logarithmic behaviour of $\sinh^{-1}$ then takes care of the fast increase of the dressing functions and the interpolation is performed on a logarithmic grid. After the interpolation the result has to be transformed back to the unaltered dressing functions. Hence, within each iteration step the following mapping has to be carried out:

$$h^{(i)} \rightleftarrows \sinh^{-1}[h^{(i)}(1+s_0)^3] + \text{interpolation on log. grid}\,. \tag{A.22}$$

A.6. Charge conjugation for non-Abelian Theories

In this chapter we will define charge conjugation for non-Abelian theories [147, 148, 43] which is a necessary prerequisite for the proofs given in the next section.
The difference between charge conjugation for Abelian and for non-Abelian theories is that in the latter case the gauge field is charged and hence the charge conjugation operator has to act on the gauge bosons as well. But since for fermions the behaviour under charge conjugation is the same for both theories we will start with QED and later amend it to derive the charge conjugation operator of non-Abelian theories.

Charge Conjugation in QED:
The charge conjugated field (anti-particle) has to fullfill the Dirac equation in the same form as for the particle but for opposite charge [75]:

$$[i\gamma_\mu\partial^\mu + e\gamma_\mu A^\mu - m]\,\psi^c = 0\,. \tag{A.23}$$

To get there we start with the Dirac equation

$$[i\gamma_\mu\partial^\mu - e\gamma_\mu A^\mu - m]\,\psi = 0\,. \tag{A.24}$$

We then take the adjoint of this equation

$$-i\partial^\mu\psi^\dagger\gamma_\mu^\dagger - e\psi^\dagger\gamma_\mu^\dagger A^\mu - m\psi^\dagger = 0\,, \tag{A.25}$$

where we have used that A_μ is hermitean. Next we use

$$(\gamma^\mu)^\dagger = \gamma^0\gamma^\mu\gamma^0\,, \tag{A.26}$$

and multiply A.25 from the right-hand side by γ_0:

$$-i\partial^\mu\psi^\dagger\gamma_0\gamma_\mu - e\psi^\dagger\gamma_0\gamma_\mu A^\mu - m\psi^\dagger\gamma_0 = 0\,. \tag{A.27}$$

Transposing this equation we get

$$-i\gamma_\mu^T\partial^\mu\bar{\psi}^T - e\gamma_\mu^T\bar{\psi}^T A^\mu - m\bar{\psi}^T = 0\,. \tag{A.28}$$

Since $(\gamma^\mu)^T$ also satisfies the Clifford algebra there must be a matrix C so that

$$C(\gamma^\mu)^T C^{-1} = -\gamma^\mu\,. \tag{A.29}$$

It can be shown that in the Dirac representation the matrix C has the form

$$C = i\gamma^2\gamma^0 \tag{A.30}$$

which fulfills the equations $C^{-1} = C^\dagger = C^T = -C$. Multiplying (A.28) from left with C and inserting $C^{-1}C = 1$ we arrive at

$$-iC\gamma_\mu^T C^{-1}\partial^\mu C\bar{\psi}^T - eC\gamma_\mu^T C^{-1}C\bar{\psi}^T A^\mu - mC\bar{\psi}^T = 0 \tag{A.31}$$

which leads with the help of (A.29) to

$$(i\gamma_\mu \partial^\mu + e\gamma_\mu A^\mu - m)\, C\bar{\psi}^T = 0\,. \tag{A.32}$$

This is the Dirac equation for opposite charge as requested in (A.23). We can therefore – up to a phase – identify:

$$\psi^c = C\bar{\psi}^T\,, \tag{A.33}$$

$$\bar{\psi}^c = -\psi^T C^{-1}\,. \tag{A.34}$$

Charge Conjugation in QCD:

To do the same for a non-abelian theory we have to have a closer look at how charge conjugation is defined. We can define charge conjugation by the complex conjugate of the gauge transformation [43]:

$$e^{-iT^a\theta^a} \to e^{-i(-\overline{T}^a)\theta^a} = e^{-i(-(T^a)^T)\theta^a}\,, \tag{A.35}$$

since T^a is hermitean $T^a = (T^a)^\dagger = (\bar{T}^a)^T$. Here, the overbar refers to complex conjugation.

One can then define the transformation of the gauge fields under charge conjugation in such a way that the Lagrangian remains invariant [148]. By using (A.33) and (A.34) we get for example for the gauge part of the covariant derivative

$$-iA^a_\mu \bar{\psi}\gamma^\mu T^a \psi = -iA^a_\mu \bar{\psi}_{i,\alpha}\gamma^\mu_{\alpha\beta} T^a_{ij}\psi_{j,\beta}\,, \tag{A.36}$$

$$= iA^a_\mu \psi^{cT}_{i,\alpha} C\gamma^\mu_{\alpha\beta} C^{-1} T^a_{ij}\bar{\psi}^{cT}_{j,\beta}\,, \tag{A.37}$$

$$= -iA^a_\mu \psi^{cT}_{i,\alpha} (\gamma^\mu_{\alpha\beta})^T T^a_{ij}\bar{\psi}^{cT}_{j,\beta}\,, \tag{A.38}$$

$$= iA^a_\mu \bar{\psi}^c_{j,\beta} (\gamma^\mu_{\beta\alpha}) T^a_{ij}\psi^c_{i,\alpha}\,. \tag{A.39}$$

In the third line (A.29) was used and the indices have been written out explicitly for the convenience of the reader. For this expression to be invariant under charge conjugation the gauge field has to transform in the following way:

$$A_\mu = A^a_\mu T^a \to -A^T_\mu = -A^a_\mu (T^a)^T\,. \tag{A.40}$$

We can easily fulfill this condition by introducing a matrix C^{ab} [147] that helps us to define the transformation of the gauge field A^a_μ,

$$A^{a\,c}_\mu = -C^{ab}A^b_\mu\,, \tag{A.41}$$

so that we can express the charge conjugated gluon in terms of the untransformed field times an operator. This matrix must then also act in the following way on the generator

$$C^{ab}T^b = (T^a)^T\,. \tag{A.42}$$

The matrix C^{ab} can be identified with a diagonal matrix with elements ± 1. Therefore it has moreover the properties

$$C^{ab} = C^{ba} \,, \tag{A.43}$$

$$C^{aa'} C^{a'b} = \delta^{ab} \,. \tag{A.44}$$

In a similar way one can show that the ghost fields transform according to

$$c^{a\,c} = C^{ab} c^b \quad \text{and} \quad \overline{c}^{\,a\,c} = C^{ab} \overline{c}^{\,b} \,. \tag{A.45}$$

With the above defined transformation behaviour of the various fields one can show that the gauge fixed Lagrangian of QCD is invariant under charge conjugation. Since we will work in momentum space we have to Fourier transform the expressions for the charge conjugated fields:

$$\begin{aligned} \psi^c(x) = \int \frac{d^4p}{(2\pi)^4} e^{-ipx} \psi^c(p) &= C \overline{\psi}(x)^T \,, \\ &= C \overline{\left(\int \frac{d^4p}{(2\pi)^4} e^{-ipx} \psi(p) \right)}^T \,, \\ &= C \int \frac{d^4p}{(2\pi)^4} e^{ipx} \overline{\psi}(p)^T \\ &= \int \frac{d^4p}{(2\pi)^4} e^{-ipx} C \overline{\psi}(-p)^T \end{aligned} \tag{A.46}$$

From comparison we get

$$\psi^c(p) = C \overline{\psi}(-p)^T \,. \tag{A.47}$$

In the same way the following relations are obtained

$$\overline{\psi}^c(p) = -\psi(-p)^T C^{-1} \,, \tag{A.48}$$

$$A_\mu^{a\,c}(p) = -C^{ab} A_\mu^b(p) \,. \tag{A.49}$$

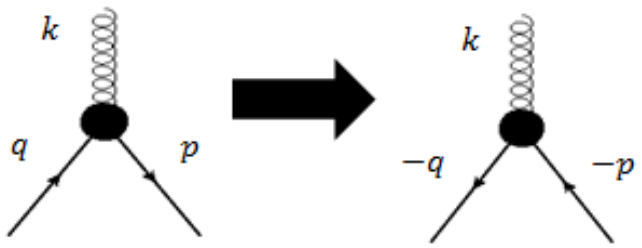

Figure A.6.: The quark-gluon vertex before and after charge conjugation.

A.7. Furry's theorem and the color structure of the three-gluon vertex

In QED it can be shown that all diagrams containing a fermion loop with an odd number of vertices may be omitted in the computation of a Green's function. This is known as Furry's Theorem. Roughly speaking the underlying idea is that there are always two fermion loops – one for particles and one for anti-particles – and that the diagram for anti-particles can be viewed as the one for particles with the loop going into the opposite direction. If the number of vertices is odd, reversing the loop direction leads to an additional minus sign due to the Grassmannian nature of fermions. Hence both diagrams cancel each other. In QED a proof can be given that is based on charge conjugation (see e.g. [149]). We will do the same in QCD using the charge conjugation for non-Abelian theories derived in the previous section.
Before we can start with the computation we have to know how the quark propagator and the quark-gluon vertex behave under charge conjugation. This is alleviated by the fact that the dressed vertex has to transform like the bare vertex [92]

$$C^{ab}C^{-1}\gamma_\mu T^b C = -\gamma_\mu^T (T^a)^T \ . \tag{A.50}$$

Thus, we get for the dressed vertex

$$C^{ab}C^{-1}\Gamma_\mu^b(p,q)C = -\Gamma_\mu^a(-q,-p)^T \ . \tag{A.51}$$

The interchange of the momenta and their sign flip are a direct consequence of the relations (A.47) and (A.48). This can be also seen in the diagramatic representation Fig. A.6 where after the transformation of particle into anti-particle the incoming momentum q (outgoing momentum p) becomes the outgoing momentum $-q$ (incoming momentum $-p$).
We can treat the quark propagator in the same manner[3]. The bare propagator

[3] Of course it is also possible to obtain the same transformation behaviour of the quark-gluon vertex and the quark propagator by starting directly from the expecation values (like $\langle\psi\overline{\psi}\rangle$) and using the relations (A.47) , (A.48) and (A.49).

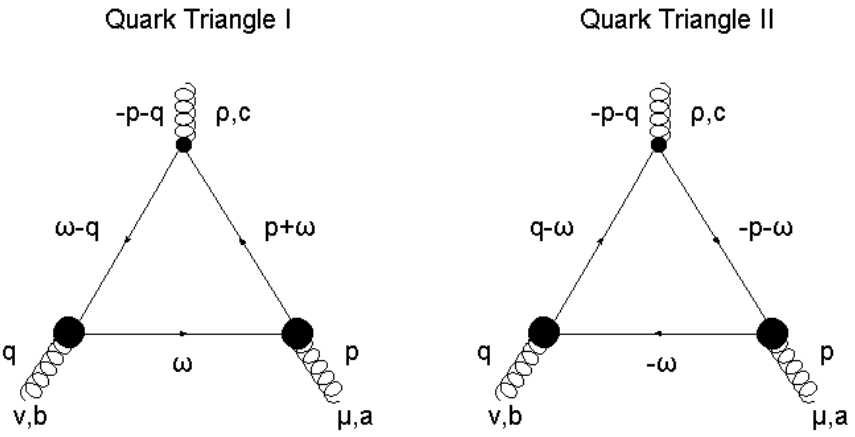

Figure A.7.: The momentum rooting of both quark triangle diagrams.

transforms as

$$\begin{aligned} C^{-1}S^{(0)}(p)C &= \frac{m + iC^{-1}\gamma_\mu C p_\mu}{m^2 + p^2} \\ &= \frac{m - i\gamma_\mu^T p_\mu}{m^2 + p^2} \\ &= S^{(0)}(-p)^T \end{aligned} \tag{A.52}$$

Accordingly the dressed propagator transforms as

$$C^{-1}S(p)C = S(-p)^T \tag{A.53}$$

We can now have a closer look at the two quark triangle diagrams and their momentum rooting, which is detailed in figure A.7. For the first diagram on the left-hand side of figure A.7 we finally have to calculate the trace

$$\mathrm{Tr}\left[S(\omega)\Gamma^a_\mu(p+\omega,\omega)S(p+\omega)\gamma_\rho T^c S(\omega-q)\Gamma^b_\nu(\omega,\omega-q)\right] , \tag{A.54}$$

where the trace acts on color as well as Dirac indices. By using $\Gamma^a_\mu(p,q) = T^a\Gamma_\mu(p,q)$ we can separate the color and Dirac part and obtain

$$\begin{aligned} &\mathrm{Tr}\left[T^aT^cT^b\right]\mathrm{Tr}\left[S(\omega)\Gamma_\mu(p+\omega,\omega)S(p+\omega)\gamma_\rho S(\omega-q)\Gamma_\nu(\omega,\omega-q)\right] = \\ &\frac{1}{4}(d^{acb}+if^{acb})\mathrm{Tr}\left[S(\omega)\Gamma_\mu(p+\omega,\omega)S(p+\omega)\gamma_\rho S(\omega-q)\Gamma_\nu(\omega,\omega-q)\right] = \\ &\frac{1}{4}(d^{abc}-if^{abc})\mathrm{Tr}\left[S(\omega)\Gamma_\mu(p+\omega,\omega)S(p+\omega)\gamma_\rho S(\omega-q)\Gamma_\nu(\omega,\omega-q)\right] . \end{aligned} \tag{A.55}$$

Here, we carried out the color trace to get from the first to the second line and reordered the indices in the third line.
The second quark triangle diagram reads

$$\mathrm{Tr}\left[S(-\omega)\Gamma^b_\nu(q-\omega,-\omega)S(q-\omega)\gamma_\rho T^c S(-p-\omega)\Gamma^a_\mu(-\omega,-p-\omega)\right] . \tag{A.56}$$

Next, we insert the identity CC^{-1} and $C^{aa'}C^{a'b} = \delta^{ab}$:

$$\begin{aligned}
&\mathrm{Tr}\left[S(-\omega)\delta^{bb'}\Gamma^{b'}_{\nu}(q-\omega,-\omega)S(q-\omega)\gamma_\rho\delta^{cc'}T^{c'}S(-p-\omega)\delta^{aa'}\Gamma^{a'}_{\mu}(-\omega,-p-\omega)\right] = \\
&\mathrm{Tr}\left[CC^{-1}S(-\omega)CC^{-1}C^{bb''}C^{b''b'}\Gamma^{b'}_{\nu}(q-\omega,-\omega)CC^{-1}S(q-\omega)CC^{-1}C^{cc''}C^{c''c'}\gamma_\rho T^{c'}\right. \\
&\left.CC^{-1}S(-p-\omega)CC^{-1}C^{aa''}C^{a''a'}\Gamma^{a'}_{\mu}(-\omega,-p-\omega)\right] = \\
&-\mathrm{Tr}\left[S(\omega)^T C^{bb''}\Gamma^{b''}_{\nu}(\omega,\omega-q)^T S(\omega-q)^T C^{cc''}\gamma^T_\rho\left(T^{c''}\right)^T S(p+\omega)^T C^{aa''}\Gamma^{a''}_{\mu}(p+\omega,\omega)^T\right]
\end{aligned}$$

Here, we exploited the cyclicicity of the trace in going from the second to the third line to bring the C operator to the right-hand side. We can now again separate the color and the Dirac part and use that the trace of a matrix is equal to the trace of the transposed matrix.

$$\begin{aligned}
&-\mathrm{Tr}\left[C^{bb''}\left(T^{b''}\right)^T C^{cc''}\left(T^{c''}\right)^T C^{aa''}\left(T^{a''}\right)^T\right]\mathrm{Tr}\left[S(\omega)^T\Gamma_\nu(\omega,\omega-q)^T S(\omega-q)^T\gamma^T_\rho\right. \\
&\left.S(p+\omega)^T\Gamma_\mu(p+\omega,\omega)^T\right] = \\
&-\mathrm{Tr}\left[T^bT^cT^a\right]\mathrm{Tr}\left[\Gamma_\mu(p+\omega,\omega)S(p+\omega)\gamma_\rho S(\omega-q)\Gamma_\nu(\omega,\omega-q)S(\omega)\right] = \\
&-\frac{1}{4}(d^{bca}+if^{bca})\mathrm{Tr}\left[S(\omega)\Gamma_\mu(p+\omega,\omega)S(p+\omega)\gamma_\rho S(\omega-q)\Gamma_\nu(\omega,\omega-q)\right] = \\
&\frac{1}{4}(-d^{abc}-if^{abc})\mathrm{Tr}\left[S(\omega)\Gamma_\mu(p+\omega,\omega)S(p+\omega)\gamma_\rho S(\omega-q)\Gamma_\nu(\omega,\omega-q)\right]
\end{aligned} \tag{A.57}$$

which is up to a different color part the same trace as for the first triangle. Adding the contribution from both quark triangle diagrams we see that the color symmetric part drops out and the color antisymmetric part adds up. If we abbreviate the diagrams on the left and on the right in figure A.7 with QTI and QTII, respectively, we can write

$$\begin{aligned}
&\mathrm{Tr}\left[\mathrm{QT\ I}\right] + \mathrm{Tr}\left[\mathrm{QT\ II}\right] = 2\left(\mathrm{Tr}\left[\mathrm{QT\ I}\right]\right)_{\text{color antisym}} = \\
&-\frac{1}{2}if^{abc}\mathrm{Tr}\left[S(\omega)\Gamma_\mu(p+\omega,\omega)S(p+\omega)\gamma_\rho S(\omega-q)\Gamma_\nu(\omega,\omega-q)\right]
\end{aligned} \tag{A.58}$$

With the help of the charge conjugation for non-Abelian theories we can now also prove that the full three-gluon vertex has to be proportional to the antisymmetric structure constant. This was already demonstrated in [112], but its result remained for some reason unrecognized[4]. However, the proof we will carry out differs slightly from [112].

The basic idea is to show that the assumption of a symmetric structure constant for the three-gluon vertex leads to a contradiction. For this we have at first to find out how the symmetric and antisymmetric structure constants behave under charge

[4] See however [5] for an argument concerning a perturbative calculation at four-loop order.

conjugation. We begin with the symmetric structure constant

$$\begin{aligned}
d^{abc} &= 2\mathrm{Tr}\left[\{T^a, T^b\}T^c\right] , \\
&= 2\mathrm{Tr}\left[T^aT^bT^c + T^bT^aT^c\right] , \\
&= 2\mathrm{Tr}\left[(T^aT^bT^c + T^bT^aT^c)^T\right] , \\
&= 2\mathrm{Tr}\left[(T^c)^T(T^b)^T(T^a)^T + (T^c)^T(T^a)^T(T^b)^T\right] , \\
&= 2C^{cc'}C^{bb'}C^{aa'}\mathrm{Tr}\left[T^{c'}T^{b'}T^{a'}\right] + 2C^{cc'}C^{bb'}C^{aa'}\mathrm{Tr}\left[T^{c'}T^{a'}T^{b'}\right] , \\
&= 2C^{cc'}C^{bb'}C^{aa'}\frac{1}{4}(d^{c'b'a'} + if^{c'b'a'}) + 2C^{cc'}C^{bb'}C^{aa'}\frac{1}{4}(d^{c'a'b'} + if^{c'a'b'}) \\
&= \frac{1}{2}C^{aa'}C^{bb'}C^{cc'}(2d^{a'b'c'} - if^{a'b'c'} + if^{a'b'c'}) \\
&= C^{aa'}C^{bb'}C^{cc'}d^{a'b'c'}
\end{aligned} \tag{A.59}$$

For the antisymmetric structure constant we consider the algebra

$$\begin{aligned}
\left[T^{a'}, T^{b'}\right] &= if^{a'b'c'}T^{c'} , \\
\left(\left[T^{a'}, T^{b'}\right]\right)^T &= if^{a'b'c'}(T^{c'})^T , \\
-\left[(T^{a'})^T, (T^{b'})^T\right] &= if^{a'b'c'}(T^{c'})^T .
\end{aligned} \tag{A.60}$$

This can be used to arrive at

$$\begin{aligned}
C^{aa'}C^{bb'}\left[T^{a'}, T^{b'}\right] &= iC^{aa'}C^{bb'}f^{a'b'c'}T^{c'} , \\
\left[(T^a)^T, (T^b)^T\right] &= iC^{aa'}C^{bb'}f^{a'b'c'}T^{c'} , \\
-if^{a'b'c'}(T^{c'})^T &= iC^{aa'}C^{bb'}f^{a'b'c''}\delta^{c''c'}T^{c'} , \\
-if^{a'b'c}C^{cc'}T^{c'} &= iC^{aa'}C^{bb'}f^{a'b'c''}C^{c''c}C^{cc'}T^{c'} .
\end{aligned} \tag{A.61}$$

Via comparison we get the transformation behaviour of the antisymmetric structure constant:

$$C^{aa'}C^{bb'}C^{cc'}f^{a'b'c'} = -f^{abc} . \tag{A.62}$$

Now, we have everything to examine the color structure of the three-gluon vertex. We start from the generating functional where we, for the sake of brevity, suppress all source terms except for the source term of the gluon. Moreover, we use that the QCD action is invariant under charge conjugation: $S(A, \psi, \overline{\psi}, c, \overline{c}) = S(A^c, \psi^c, \overline{\psi}^c, c^c, \overline{c}^c)$.

$$\begin{aligned}
Z[J] &= \int \mathcal{D}[A\psi\overline{\psi}c\overline{c}]e^{-S(A,\psi,\overline{\psi},c,\overline{c})}e^{\int J^a_\mu A^a_\mu} , \\
&= \int \mathcal{D}[A\psi\overline{\psi}c\overline{c}]e^{-S(A,\psi,\overline{\psi},c,\overline{c})}e^{\int J^a_\mu \delta^{ab} A^b_\mu} , \\
&= \int \mathcal{D}[A\psi\overline{\psi}c\overline{c}]e^{-S(A,\psi,\overline{\psi},c,\overline{c})}e^{\int J^a_\mu C^{aa'}C^{a'b}A^b_\mu} , \\
&= \int \mathcal{D}[A^c\psi^c\overline{\psi}^c c^c\overline{c}^c]e^{-S(A^c,\psi^c,\overline{\psi}^c,c^c,\overline{c}^c)}e^{\int J^{a',c}_\mu A^{a',c}_\mu} , \\
&= Z[J^c] = Z[-J^a_\mu C^{aa'}] .
\end{aligned} \tag{A.63}$$

Here, we have used (A.41) and introduced the new source $J^{a,c} = -J^{a'}_{\mu} C^{a'a}$. We can now derive the three-gluon vertex by using the above relation

$$\begin{aligned} K^{abc}_{\mu\nu\rho}(p,q,k) &= \frac{\partial^3 Z[J]}{\partial J^a \partial J^b \partial J^c} \\ &= \frac{\partial^3 Z[J^c]}{\partial J^a \partial J^b \partial J^c} \\ &= \frac{\partial J^{a',c} \partial J^{b',c} \partial J^{c',c}}{\partial J^a \partial J^b \partial J^c} \frac{\partial^3 Z[J^c]}{\partial J^{a',c} \partial J^{b',c} \partial J^{c',c}} \\ &= -C^{aa'} C^{bb'} C^{cc'} K^{a'b'c'}_{\mu\nu\rho}(p,q,k)\,. \end{aligned} \tag{A.64}$$

Here K denotes the three-gluon vertex derived from the generating functional Z. If we now parametrize the color part of the three-gluon vertex in terms of a symmetric and an antisymmetric structure constant and use the above found relations (A.59) and (A.62), we get

$$\begin{aligned} (d^{abc} + f^{abc}) K_{\mu\nu\rho}(p,q,k) &= -C^{aa'} C^{bb'} C^{cc'} (d^{a'b'c'} + f^{a'b'c'}) K_{\mu\nu\rho}(p,q,k) \\ &= (-d^{abc} + f^{abc}) K_{\mu\nu\rho}(p,q,k)\,. \end{aligned} \tag{A.65}$$

Consequently, the color symmetric term has to vanish.

B. Symmetry-broken phase of ϕ^4-theory from the FRG

B.1. Regulator shapes

In principle one is free to choose for the regulator whatever shape one likes as long as it obeys the three restrictions mentioned in subsection (3.3) (and as long as convergence is achieved). However, it turned out that some shapes are appropriate for a large number of problems and are thus frequently employed. In this subsection two of those regulator shapes shall be introduced. In the following we use that the regulator $R_k(p^2)$ can be written as[1]

$$R_k(p^2) = p^2 r(p^2/k^2)\,, \tag{B.1}$$

where the information about the shape is contained in the dimensionless function $r(p^2/k^2)$.

B.1.1. Exponential Regulator

The exponential regulator is of the following form

$$r^{exp,n}(p^2/k^2) = \frac{(p^2/k^2)^{n-1}}{e^{(p^2/k^2)^n} - 1}\,. \tag{B.2}$$

Here n is a free parameter by which the steepness of the regulator function can be controlled. In figure B.1 some examples are given for how the shape of the regulator changes with n. For small momenta $p^2/k^2 \ll 1$ the function $r^{exp,n}(p^2/k^2)$ goes as k^2/p^2 so that according to (B.1) the full regulator $R_k(p^2)$ is proportional to k^2. It thus serves as a mass term.
Due to the fact that one can modify the sharpness of the regulator by changing the parameter n one advantage of the exponential regulator is that it facilitates a regulator study.

B.1.2. Optimized Regulator

The optimized regulator, sometimes also referred to as Litim regulator, has the following form [150]:

$$\begin{aligned} r_k^{opt}(p^2/k^2) &= \frac{(k^2 - p^2)}{p^2}\Theta(k^2 - p^2)\,, \\ &= ((p^2/k^2)^{-1} - 1)\Theta(1 - p^2/k^2)\,. \end{aligned} \tag{B.3}$$

Special about the optimized regulator besides its simple form is that it fulfills a special condition known as optimization criterion. This criterion is derived from the

[1] In the strict sense this is only true for a scalar boson. However, we will use this form for the sake of clarity.

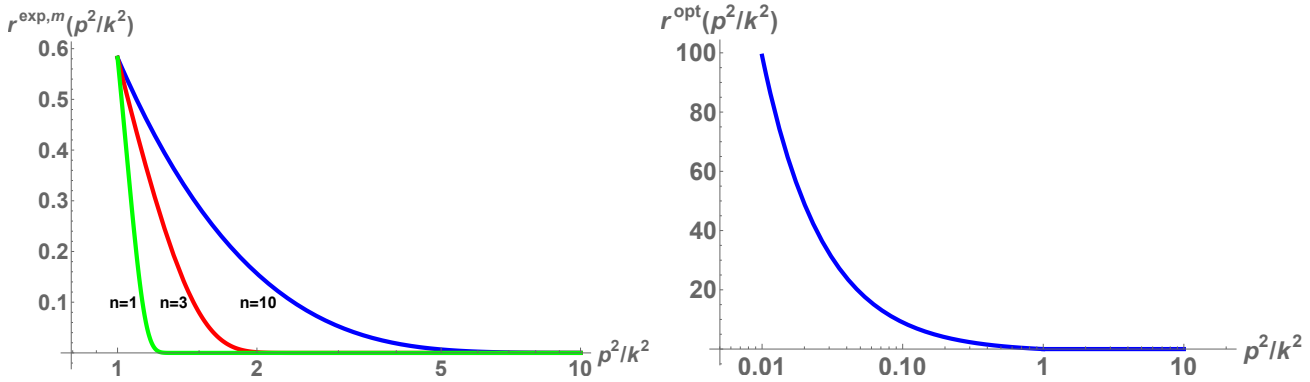

Figure B.1.: Left: The exponential regulator for different parameters n. The smaller n gets the steeper the regulator becomes in the infrared. Right: The optimized regulator.

observation that the inverse propagator shows a gap [151, 152, 150]

$$\min_{p^2\geq 0}\left[\left.\frac{\delta^2\Gamma_k[\Phi]}{\delta\Phi(p)\delta\Phi(-p)}\right|_{\Phi=0}+R_k(p^2)\right]=Ck^2>0\,. \tag{B.4}$$

The existence of this gap is necessary, because otherwise zero modes in the inverse propagator would give rise to singularities in the flow equation (3.40). Moreover, it is a consequence of (3.29), that is, a consequence of demanding the regulator to provide an infrared regularisation. However, it should be emphasized that the size of the gap C still depends on the theory under consideration. It is therefore more convenient to bring this equation into a theory independent form. To achieve this we assume a standard kinetic term and expand the full propagator around its tree-level $(p^2+R_k(p^2)+...)$ which gives us

$$\min_{p^2\geq 0}\left[p^2+R_k(p^2)\right]=Ck^2>0\,. \tag{B.5}$$

The value of C has no theory dependence anymore but it still dependends on the chosen regulator. It has been shown that the size of C is directly linked to the convergence of the derivative expansion, the radius of convergence for the amplitude expansion and the spurious scheme dependence that arises when truncations are employed [152, 150]. On account of this one finds that the regulator is chosen best if it maximizes the gap C:

$$C^{opt}=\max_{R_k}\left(\min_{p^2\geq 0}\frac{[p^2+R_k(p^2)]}{k^2}\right)\,. \tag{B.6}$$

Therefore, it is reasonable to impose on the regulator the constraints that it should satisfy the optimization condition (B.6) and that it should have a comparatively simple form. These conditions then lead to the optimized regulator (B.3). Though, it should be stressed that this is not the only possible solution since the space of regulator functions that respect the optimization condition is infinite-dimensional.

B.2. Propagator of the O(N)-Model

We start with the effective action in the LPA:

$$\Gamma_k[\Phi] = \int \frac{d^4q}{(2\pi)^4}\frac{1}{2}q^2\Phi^2 + \lambda_{0,k} + \frac{1}{2}\lambda_{1,k}(\Phi^2 - \Phi_0^2) + \frac{\lambda_{2,k}}{8}(\Phi^2 - \Phi_0^2)^2$$

where the momentum dependence of the field has been suppressed and Φ_0^2 denotes the minimum of the potential. We thus get for the (inverse) propagator including the regulator

$$(G_{ij}(p))^{(-1)} = \frac{\delta^2\Gamma_k[\Phi]}{\delta\Phi_i(p)\delta\Phi_j(-p)} + R_k\delta_{ij} = (p^2 + \lambda_{1,k} + R_k + \lambda_{2,k}(\rho - \rho_0))\delta_{ij} + \lambda_{2,k}\Phi_i\Phi_j \tag{B.7}$$

The potential and its first and second derivative are given by

$$V_k(\rho) = \lambda_{0,k} + \lambda_{1,k}(\rho - \rho_0) + \frac{\lambda_{2,k}}{2}(\rho - \rho_0)^2\,, \tag{B.8}$$

$$V_k'(\rho) = \lambda_{1,k} + \lambda_{2,k}(\rho - \rho_0)\,, \tag{B.9}$$

$$V_k''(\rho) = \lambda_{2,k} \tag{B.10}$$

with $\rho = \frac{1}{2}(\Phi)^2$. To separate the propagator into its transverse and longitudinal part, we project it with the corresponding tensors $P_{ij}^{trans}(\Phi)$ and $P_{ij}^{long}(\Phi)$. This leads for the transverse projection to

$$\begin{aligned}(G_{i\alpha}(p))^{(-1)}P_{\alpha j}^{trans}(\Phi) &= \Big((p^2 + \lambda_{1,k} + R_k + \lambda_{2,k}(\rho - \rho_0))\delta_{i\alpha} + \lambda_{2,k}\Phi_i\Phi_\alpha\Big)\left(\delta_{\alpha j} - \frac{\Phi_\alpha\Phi_j}{\Phi^2}\right)\\ &= (p^2 + \lambda_{1,k} + R_k + \lambda_{2,k}(\rho - \rho_0))\left(\delta_{ij} - \frac{\Phi_i\Phi_j}{\Phi^2}\right)\\ &= (p^2 + V_k'(\rho) + R_k)\left(\delta_{ij} - \frac{\Phi_i\Phi_j}{\Phi^2}\right)\end{aligned} \tag{B.11}$$

and for the longitudinal propagator to

$$\begin{aligned}(G_{i\alpha}(p))^{(-1)}P_{\alpha j}^{long}(\Phi) &= \Big((p^2 + \lambda_{1,k} + R_k + \lambda_{2,k}(\rho - \rho_0))\delta_{i\alpha} + \lambda_{2,k}\Phi_i\Phi_\alpha\Big)\left(\frac{\Phi_\alpha\Phi_j}{\Phi^2}\right)\\ &= \Big(p^2 + \lambda_{1,k} + R_k + \lambda_{2,k}(\rho - \rho_0) + 2\lambda_{2,k}\rho\Big)\left(\frac{\Phi_i\Phi_j}{\Phi^2}\right)\\ &= \Big(p^2 + V_k'(\rho) + R_k + 2\rho V_k''(\rho)\Big)\left(\frac{\Phi_i\Phi_j}{\Phi^2}\right)\end{aligned} \tag{B.12}$$

We thus obtain for the propagator

$$\begin{aligned}G_{ij}(p) &= \frac{1}{(p^2 + V_k'(\rho) + R_k)}\left(\delta_{ij} - \frac{\Phi_i\Phi_j}{\Phi^2}\right) + \frac{1}{(p^2 + V_k'(\rho) + R_k + 2\rho V_k''(\rho))}\left(\frac{\Phi_i\Phi_j}{\Phi^2}\right)\\ &= G_{trans}(p)\left(\delta_{ij} - \frac{\Phi_i\Phi_j}{\Phi^2}\right) + G_{long}(p)\left(\frac{\Phi_i\Phi_j}{\Phi^2}\right)\end{aligned} \tag{B.13}$$

Plugging the propagator into the flow equation for the potential and taking the trace we thus arrive at

$$\partial_t V_k(\rho) = \frac{1}{2} \int \frac{d^4q}{(2\pi)^4} \dot{R}_k(q) \left[G_{trans}(q)(N-1) + G_{long}(q) \right] . \tag{B.14}$$

Bibliography

[1] A. I. Davydychev, P. Osland, and L. Saks, *Quark gluon vertex in arbitrary gauge and dimension*, *Phys. Rev.* **D63** (2001) 014022, arXiv:hep-ph/0008171 [hep-ph].

[2] J. A. Gracey, *Two loop QCD vertices at the symmetric point*, *Phys. Rev.* **D84** (2011) 085011, arXiv:1108.4806 [hep-ph].

[3] J. A. Gracey, *Off-shell two-loop QCD vertices*, *Phys. Rev.* **D90** no. 2, (2014) 025014, arXiv:1406.0649 [hep-ph].

[4] R. Bermudez, L. Albino, L. X. Gutiérrez-Guerrero, M. E. Tejeda-Yeomans, and A. Bashir, *Quark-gluon Vertex: A Perturbation Theory Primer and Beyond*, *Phys. Rev.* **D95** no. 3, (2017) 034041, arXiv:1702.04437 [hep-ph].

[5] B. Ruijl, T. Ueda, J. A. M. Vermaseren, and A. Vogt, *Four-loop QCD propagators and vertices with one vanishing external momentum*, *JHEP* **06** (2017) 040, arXiv:1703.08532 [hep-ph].

[6] J. I. Skullerud, P. O. Bowman, A. Kizilersu, D. B. Leinweber, and A. G. Williams, *Nonperturbative structure of the quark gluon vertex*, *JHEP* **04** (2003) 047, arXiv:hep-ph/0303176.

[7] H.-W. Lin, *Quark-gluon vertex with an off-shell O(a)-improved chiral fermion action*, *Phys. Rev.* **D73** (2006) 094511, arXiv:hep-lat/0510110 [hep-lat].

[8] A. Kizilersu, D. B. Leinweber, J.-I. Skullerud, and A. G. Williams, *Quark-gluon vertex in general kinematics*, *Eur.Phys.J.* **C50** (2007) 871–875, arXiv:hep-lat/0610078 [hep-lat].

[9] A. Sternbeck, P.-H. Balduf, A. Kızılersu, O. Oliveira, P. J. Silva, J.-I. Skullerud, and A. G. Williams, *Triple-gluon and quark-gluon vertex from lattice QCD in Landau gauge*, *PoS* **LATTICE2016** (2017) 349, arXiv:1702.00612 [hep-lat].

[10] A. Windisch, Ph.D.Thesis, University of Graz, 2014.

[11] M. Hopfer, Ph.D.Thesis, University of Graz, 2014.

[12] R. Williams, *The quark-gluon vertex in Landau gauge bound-state studies*, *Eur. Phys. J.* **A51** no. 5, (2015) 57, arXiv:1404.2545 [hep-ph].

[13] R. Williams, C. S. Fischer, and W. Heupel, *Light mesons in QCD and unquenching effects from the 3PI effective action*, *Phys. Rev.* **D93** no. 3, (2016) 034026, arXiv:1512.00455 [hep-ph].

[14] R. Alkofer, C. S. Fischer, F. J. Llanes-Estrada, and K. Schwenzer, *The quark-gluon vertex in Landau gauge QCD: Its role in dynamical chiral*

symmetry breaking and quark confinement, *Annals Phys.* **324** (2009) 106–172, arXiv:0804.3042 [hep-ph].

[15] A. Aguilar, D. Binosi, D. Ibáñez, and J. Papavassiliou, *New method for determining the quark-gluon vertex*, *Phys.Rev.* **D90** no. 6, (2014) 065027, arXiv:1405.3506 [hep-ph].

[16] A. C. Aguilar, J. C. Cardona, M. N. Ferreira, and J. Papavassiliou, *Non-Abelian Ball-Chiu vertex for arbitrary Euclidean momenta*, *Phys. Rev.* **D96** no. 1, (2017) 014029, arXiv:1610.06158 [hep-ph].

[17] M. Mitter, J. M. Pawlowski, and N. Strodthoff, *Chiral symmetry breaking in continuum QCD*, *Phys.Rev.* **D91** (2015) 054035, arXiv:1411.7978 [hep-ph].

[18] A. K. Cyrol, M. Mitter, J. M. Pawlowski, and N. Strodthoff, *Non-perturbative quark, gluon and meson correlators of unquenched QCD*, arXiv:1706.06326 [hep-ph].

[19] M. Peláez, M. Tissier, and N. Wschebor, *Quark-gluon vertex from the Landau gauge Curci-Ferrari model*, arXiv:1504.05157 [hep-th].

[20] E. Rojas, J. de Melo, B. El-Bennich, O. Oliveira, and T. Frederico, *On the Quark-Gluon Vertex and Quark-Ghost Kernel: combining Lattice Simulations with Dyson-Schwinger equations*, *JHEP* **1310** (2013) 193, arXiv:1306.3022 [hep-ph].

[21] R. Williams, *Bethe-Salpeter studies of mesons beyond rainbow-ladder*, *EPJ Web Conf.* **3** (2010) 03005, arXiv:0912.3494 [hep-ph].

[22] H. Sanchis-Alepuz and R. Williams, *Probing the quark–gluon interaction with hadrons*, *Phys. Lett.* **B749** (2015) 592–596, arXiv:1504.07776 [hep-ph].

[23] A. I. Davydychev, P. Osland, and O. V. Tarasov, *Two loop three gluon vertex in zero momentum limit*, *Phys. Rev.* **D58** (1998) 036007, arXiv:hep-ph/9801380 [hep-ph].

[24] A. I. Davydychev and P. Osland, *On-shell two loop three gluon vertex*, *Phys. Rev.* **D59** (1999) 014006, arXiv:hep-ph/9806522 [hep-ph].

[25] M. Pelaez, M. Tissier, and N. Wschebor, *Three-point correlation functions in Yang-Mills theory*, *Phys.Rev.* **D88** (2013) 125003, arXiv:1310.2594 [hep-th].

[26] M. Binger and S. J. Brodsky, *The Form-factors of the gauge-invariant three-gluon vertex*, *Phys. Rev.* **D74** (2006) 054016, arXiv:hep-ph/0602199 [hep-ph].

[27] D. R. Campagnari and H. Reinhardt, *Non-Gaussian wave functionals in Coulomb gauge Yang–Mills theory*, *Phys.Rev.* **D82** (2010) 105021, arXiv:1009.4599 [hep-th].

[28] R. Alkofer, M. Q. Huber, and K. Schwenzer, *Infrared Behavior of Three-Point Functions in Landau Gauge Yang-Mills Theory*, *Eur. Phys. J.* **C62** (2009) 761–781, arXiv:0812.4045 [hep-ph].

[29] D. Binosi and J. Papavassiliou, *Gauge invariant Ansatz for a special three-gluon vertex*, *JHEP* **03** (2011) 121, arXiv:1102.5662 [hep-ph].

[30] A. Blum, M. Q. Huber, M. Mitter, and L. von Smekal, *Gluonic three-point correlations in pure Landau gauge QCD*, *Phys. Rev. D* **89** (2014) 061703(R), arXiv:1401.0713 [hep-ph].

[31] G. Eichmann, R. Williams, R. Alkofer, and M. Vujinovic, *The three-gluon vertex in Landau gauge*, *Phys.Rev.* **D89** (2014) 105014, arXiv:1402.1365 [hep-ph].

[32] M. Q. Huber, D. R. Campagnari, and H. Reinhardt, *Vertex functions of Coulomb gauge Yang–Mills theory*, *Phys.Rev.* **D91** no. 2, (2015) 025014, arXiv:1410.4766 [hep-ph].

[33] M. Q. Huber, *Correlation functions of three-dimensional Yang-Mills theory from Dyson-Schwinger equations*, *Phys. Rev.* **D93** no. 8, (2016) 085033, arXiv:1602.02038 [hep-th].

[34] M. Vujinovic, Ph.D.Thesis, University of Graz, 2015.

[35] A. K. Cyrol, L. Fister, M. Mitter, J. M. Pawlowski, and N. Strodthoff, *Landau gauge Yang-Mills correlation functions*, *Phys. Rev.* **D94** no. 5, (2016) 054005, arXiv:1605.01856 [hep-ph].

[36] A. Cucchieri, A. Maas, and T. Mendes, *Three-point vertices in Landau-gauge Yang-Mills theory*, *Phys. Rev.* **D77** (2008) 094510, arXiv:0803.1798 [hep-lat].

[37] P. Boucaud, F. De Soto, J. Rodríguez-Quintero, and S. Zafeiropoulos, *Refining the detection of the zero crossing for the three-gluon vertex in symmetric and asymmetric momentum subtraction schemes*, *Phys. Rev.* **D95** no. 11, (2017) 114503, arXiv:1701.07390 [hep-lat].

[38] A. Athenodorou, D. Binosi, P. Boucaud, F. De Soto, J. Papavassiliou, J. Rodriguez-Quintero, and S. Zafeiropoulos, *On the zero crossing of the three-gluon vertex*, *Phys. Lett.* **B761** (2016) 444–449, arXiv:1607.01278 [hep-ph].

[39] L. H. Ryder, *Quantum Field Theory*. Cambridge University Press, Cambridge, 1996.

[40] L. D. Faddeev and V. N. Popov, *Feynman diagrams for the Yang-Mills field*, *Phys. Lett.* **B25** (1967) 29–30.

[41] A. Haar, *Der Massbegriff in der Theorie der Kontinuierlichen Gruppen*, *Annals of Mathematics* **34** (1933) 147–169.

[42] T. Muta, *Foundations of quantum chromodynamics*. World Scientific, Singapore, 1998.

[43] S. Pokorski, *Gauge Field Theories*. Cambridge University Press, Cambridge, 1990.

[44] M. E. Peskin and D. V. Schroeder, *An introduction to quantum field theory*. Westview press, 1995.

[45] V. Gribov, *Quantization of Nonabelian Gauge Theories*, *Nucl.Phys.* **B139** (1978) 1.

[46] N. Vandersickel and D. Zwanziger, *The Gribov problem and QCD dynamics*, *Phys.Rept.* **520** (2012) 175–251, arXiv:1202.1491 [hep-th].

[47] A. D. Pereira, *Exploring new horizons of the Gribov problem in Yang-Mills theories*. PhD thesis, Niteroi, Fluminense U., 2016. arXiv:1607.00365 [hep-th].
http://inspirehep.net/record/1473345/files/arXiv:1607.00365.pdf.

[48] R. F. Sobreiro and S. P. Sorella, *Introduction to the Gribov ambiguities in Euclidean Yang-Mills theories* in *13th Jorge Andre Swieca Summer School on Particle and Fields Campos do Jordao, Brazil, January 9-22, 2005.* 2005. arXiv:hep-th/0504095 [hep-th].

[49] H. Lehmann, K. Symanzik, and W. Zimmermann, *On the formulation of quantized field theories*, *Nuovo Cim.* **1** (1955) 205–225.

[50] E. E. Salpeter and H. A. Bethe, *A Relativistic equation for bound state problems*, *Phys. Rev.* **84** (1951) 1232–1242.

[51] C. Becchi, A. Rouet, and R. Stora, *Renormalization of Gauge Theories*, *Annals Phys.* **98** (1976) 287–321.

[52] I. V. Tyutin, *Gauge Invariance in Field Theory and Statistical Physics in Operator Formalism*, *LEBEDEV-75-39* (1975) , arXiv:0812.0580 [hep-th].

[53] T. Kugo and I. Ojima, *Local Covariant Operator Formalism of Nonabelian Gauge Theories and Quark Confinement Problem*, *Prog. Theor. Phys. Suppl.* **66** (1979) 1.

[54] T. Kugo, *The universal renormalization factors Z(1) / Z(3) and color confinement condition in non-Abelian gauge theory*, arXiv:hep-th/9511033. Talk given at International Symposium on BRS Symmetry on the Occasion of Its 20th Anniversary, Kyoto, Japan, 18-22 Sep 1995. Published in *Kyoto 1995, BRS symmetry* 107-119,

[55] N. Nakanishi and I. Ojima, *Covariant operator formalism of gauge theories and quantum gravity*, *World Sci. Lect. Notes Phys.* **27** (1990) 1–434.

[56] L. Baulieu and J. Thierry-Mieg, *The Principle of BRS Symmetry: An Alternative Approach to Yang-Mills Theories*, *Nucl. Phys.* **B197** (1982) 477.

[57] A. A. Slavnov, *Ward Identities in Gauge Theories*, *Theor. Math. Phys.* **10** (1972) 99–107. [Teor. Mat. Fiz.10,153(1972)],

[58] J. C. Taylor, *Ward Identities and Charge Renormalization of the Yang-Mills Field*, *Nucl. Phys.* **B33** (1971) 436–444.

[59] B. W. Lee and J. Zinn-Justin, *Spontaneously Broken Gauge Symmetries. 1. Preliminaries*, *Phys. Rev.* **D5** (1972) 3121–3137.

[60] B. W. Lee and J. Zinn-Justin, *Spontaneously broken gauge symmetries. 2. Perturbation theory and renormalization*, *Phys. Rev.* **D5** (1972) 3137–3155. [Erratum: Phys. Rev.D8,4654(1973)],

[61] B. W. Lee and J. Zinn-Justin, *Spontaneously broken gauge symmetries. 3. Equivalence*, *Phys. Rev.* **D5** (1972) 3155–3160.

[62] E. Eichten and F. Feinberg, *DYNAMICAL SYMMETRY BREAKING OF NONABELIAN GAUGE SYMMETRIES*, *Phys. Rev.* **D10** (1974) 3254–3279.

[63] W. J. Marciano and H. Pagels, *Quantum Chromodynamics: A Review*, *Phys.Rept.* **36** (1978) 137.

[64] P. Pascual and R. Tarrach, *QCD: Renormalization for the practitioner*, vol. 194 of *Lecture Notes in Physics*. Springer, Heidelberg, 1984.

[65] K. Fujikawa, *Path Integral Measure for Gauge Invariant Fermion Theories*, *Phys. Rev. Lett.* **42** (1979) 1195–1198.

[66] V. A. Miransky, *ON DYNAMICAL CHIRAL SYMMETRY BREAKING*, *Phys. Lett.* **165B** (1985) 401–404.

[67] D. Binosi and J. Papavassiliou, *Pinch Technique: Theory and Applications*, *Phys. Rept.* **479** (2009) 1–152, `arXiv:0909.2536 [hep-ph]`.

[68] H. Reinhardt, G. Burgio, D. Campagnari, E. Ebadati, J. Heffner, M. Quandt, P. Vastag, and H. Vogt, *Hamiltonian approach to QCD in Coulomb gauge - a survey of recent results* in *5th Winter Workshop on Non-Perturbative Quantum Field Theory (WWNPQFT) Sophia-Antipolis, France, March 22-24, 2017*. 2017. `arXiv:1706.02702 [hep-th]`. `http://inspirehep.net/record/1604030/files/arXiv:1706.02702.pdf`.

[69] H. Reinhardt, D. R. Campagnari, J. Heffner, and M. Pak, *Hamilton approach to QCD in Coulomb gauge*, *Prog. Part. Nucl. Phys.* **67** (2012) 173–179.

[70] M. Tissier and N. Wschebor, *An Infrared Safe perturbative approach to Yang-Mills correlators*, *Phys. Rev.* **D84** (2011) 045018, `arXiv:1105.2475 [hep-th]`.

[71] F. J. Dyson, *The S matrix in quantum electrodynamics*, *Phys. Rev.* **75** (1949) 1736–1755.

[72] J. S. Schwinger, *On the Green's functions of quantized fields. 1*, *Proc. Nat. Acad. Sci.* **37** (1951) 452–455.

[73] J. S. Schwinger, *On the Green's functions of quantized fields. 2*, *Proc. Nat. Acad. Sci.* **37** (1951) 455–459.

[74] R. Alkofer and L. von Smekal, *The infrared behavior of QCD Green's functions: Confinement, dynamical symmetry breaking, and hadrons as relativistic bound states*, *Phys. Rept.* **353** (2001) 281, `arXiv:hep-ph/0007355`.

[75] C. Itzykson and J.-B. Zuber, *Quantum Field Theory*. Dover Publications, Mineola, New York, 1980.

[76] R. Alkofer, M. Q. Huber, and K. Schwenzer, *Algorithmic derivation of Dyson-Schwinger Equations*, *Comput. Phys. Commun.* **180** (2009) 965–976, `arXiv:0808.2939 [hep-th]`.

[77] D. Binosi and L. Theussl, *JaxoDraw: A Graphical user interface for drawing Feynman diagrams*, *Comput.Phys.Commun.* **161** (2004) 76–86, arXiv:hep-ph/0309015.

[78] J. M. Cornwall, R. Jackiw, and E. Tomboulis, *Effective Action for Composite Operators*, *Phys. Rev.* **D10** (1974) 2428–2445.

[79] M. Carrington and Y. Guo, *Techniques for n-Particle Irreducible Effective Theories*, *Phys.Rev.* **D83** (2011) 016006, arXiv:1010.2978 [hep-ph].

[80] R. Jackiw, *Functional evaluation of the effective potential*, *Phys. Rev.* **D9** (1974) 1686.

[81] G. Aarts, D. Ahrensmeier, R. Baier, J. Berges, and J. Serreau, *Far from equilibrium dynamics with broken symmetries from the 2PI - 1/N expansion*, *Phys. Rev.* **D66** (2002) 045008, arXiv:hep-ph/0201308 [hep-ph].

[82] J. Berges, *Controlled nonperturbative dynamics of quantum fields out-of-equilibrium*, *Nucl. Phys.* **A699** (2002) 847–886, arXiv:hep-ph/0105311 [hep-ph].

[83] J. Berges, *n-PI effective action techniques for gauge theories*, *Phys. Rev.* **D70** (2004) 105010, arXiv:hep-ph/0401172.

[84] C. de Dominicis and P. C. Martin, *Stationary Entropy Principle and Renormalization in Normal and Superfluid Systems. I. Algebraic Formulation*, *J. Math. Phys.* **5** (1964) 14–30.

[85] M. E. Carrington, *The 4 PI effective action for phi**4 theory*, *Eur. Phys. J.* **C35** (2004) 383–392, arXiv:hep-ph/0401123 [hep-ph].

[86] J. Alexandre, *BUSSTEPP 2015 lecture notes: Exact Wilsonian Renormalization*, arXiv:1508.07763 [hep-th].

[87] H. Gies, *Introduction to the functional RG and applications to gauge theories*, *Lect.Notes Phys.* **852** (2012) 287–348, arXiv:hep-ph/0611146 [hep-ph].

[88] J. Berges, N. Tetradis, and C. Wetterich, *Non-perturbative renormalization flow in quantum field theory and statistical physics*, *Phys. Rept.* **363** (2002) 223–386, arXiv:hep-ph/0005122.

[89] C. Wetterich, *Exact evolution equation for the effective potential*, *Phys. Lett.* **B301** (1993) 90–94.

[90] C. S. Fischer, A. Maas, and J. M. Pawlowski, *On the infrared behavior of Landau gauge Yang-Mills theory*, *Annals Phys.* **324** (2009) 2408–2437, arXiv:0810.1987 [hep-ph].

[91] J. S. Ball and T.-W. Chiu, *ANALYTIC PROPERTIES OF THE VERTEX FUNCTION IN GAUGE THEORIES. 1*, *Phys. Rev.* **D22** (1980) 2542.

[92] A. Kizilersu, M. Reenders, and M. R. Pennington, *One loop QED vertex in any covariant gauge: Its complete analytic form*, *Phys. Rev.* **D52** (1995) 1242–1259, arXiv:hep-ph/9503238 [hep-ph].

[93] J. Skullerud and A. Kizilersu, *Quark-gluon vertex from lattice QCD*, *JHEP* **09** (2002) 013, arXiv:hep-ph/0205318.

[94] G. Eichmann and C. S. Fischer, *Nucleon Compton scattering in the Dyson-Schwinger approach*, *Phys. Rev.* **D87** no. 3, (2013) 036006, arXiv:1212.1761 [hep-ph].

[95] G. Eichmann, C. S. Fischer, and W. Heupel, *Four-point functions and the permutation group S4*, *Phys. Rev.* **D92** no. 5, (2015) 056006, arXiv:1505.06336 [hep-ph].

[96] G. Eichmann, C. S. Fischer, and W. Heupel, *The light scalar mesons as tetraquarks*, *Phys. Lett.* **B753** (2016) 282–287, arXiv:1508.07178 [hep-ph].

[97] L. von Smekal, A. Hauck, and R. Alkofer, *A Solution to Coupled Dyson–Schwinger Equations for Gluons and Ghosts in Landau Gauge*, *Annals Phys.* **267** (1998) 1–60, arXiv:hep-ph/9707327 [hep-ph]. [Erratum: Annals Phys.269,182(1998)],

[98] L. von Smekal, R. Alkofer, and A. Hauck, *The infrared behavior of gluon and ghost propagators in Landau gauge QCD*, *Phys. Rev. Lett.* **79** (1997) 3591–3594, arXiv:hep-ph/9705242.

[99] D. Atkinson and J. C. R. Bloch, *Running coupling in non-perturbative QCD. I: Bare vertices and y-max approximation*, *Phys. Rev.* **D58** (1998) 094036, arXiv:hep-ph/9712459.

[100] C. S. Fischer, arXiv:hep-ph/0304233, PhD thesis, Eberhard-Karls-Universität zu Tübingen, 2003.

[101] M. Q. Huber and L. von Smekal, *On the influence of three-point functions on the propagators of Landau gauge Yang-Mills theory*, *JHEP* **1304** (2013) 149, arXiv:1211.6092 [hep-th].

[102] J. C. Taylor, *WARD IDENTITIES AND CHARGE RENORMALIZATION OF THE YANG- MILLS FIELD*, *Nucl. Phys.* **B33** (1971) 436–444.

[103] P. Boucaud, J. P. Leroy, A. Le Yaouanc, A. Y. Lokhov, J. Micheli, O. Pene, J. Rodriguez-Quintero, and C. Roiesnel, *The infrared behaviour of the pure Yang-Mills Green functions*, arXiv:hep-ph/0507104.

[104] L. von Smekal, K. Maltman, and A. Sternbeck, *The Strong coupling and its running to four loops in a minimal MOM scheme*, *Phys.Lett.* **B681** (2009) 336–342, arXiv:0903.1696 [hep-ph].

[105] P. Boucaud *et al.*, *IR finiteness of the ghost dressing function from numerical resolution of the ghost SD equation*, *JHEP* **06** (2008) 012, arXiv:0801.2721 [hep-ph].

[106] A. Aguilar, D. Binosi, and J. Papavassiliou, *Gluon and ghost propagators in the Landau gauge: Deriving lattice results from Schwinger-Dyson equations*, *Phys.Rev.* **D78** (2008) 025010, arXiv:0802.1870 [hep-ph].

[107] A. Sternbeck, arXiv:hep-lat/0609016, PhD thesis, Humboldt-Universität zu Berlin, 2006.

[108] M. Hopfer, A. Windisch, and R. Alkofer, *The Quark-Gluon Vertex in Landau gauge QCD*, *PoS* **ConfinementX** (2012) 073, arXiv:1301.3672 [hep-ph].

[109] J. Braun, *Fermion Interactions and Universal Behavior in Strongly Interacting Theories*, *J. Phys.* **G39** (2012) 033001, arXiv:1108.4449 [hep-ph].

[110] A. L. Blum, R. Alkofer, M. Q. Huber, and A. Windisch, *Three-point vertex functions in Yang-Mills Theory and QCD in Landau gauge*, *EPJ Web Conf.* **137** (2017) 03001, arXiv:1611.04827 [hep-ph].

[111] J. A. Gracey, *Symmetric point four-point functions at one loop in QCD*, *Phys. Rev.* **D95** no. 6, (2017) 065013, arXiv:1703.01094 [hep-ph].

[112] N. Smolyakov, *Furry Theorem for Nonabelian Gauge Lagrangians*, *Theor.Math.Phys.* **50** (1982) 225–228.

[113] A. L. Blum, master thesis, Technische Universität Darmstadt, 2014.

[114] W. Schleifenbaum, diploma thesis, Eberhard-Karls-Universität zu Tübingen, 2004.

[115] W. Schleifenbaum, A. Maas, J. Wambach, and R. Alkofer, *Infrared behaviour of the ghost-gluon vertex in Landau gauge Yang-Mills theory*, *Phys.Rev.* **D72** (2005) 014017, arXiv:hep-ph/0411052 [hep-ph].

[116] A. Cucchieri, T. Mendes, and A. Mihara, *Numerical study of the ghost-gluon vertex in Landau gauge*, *JHEP* **12** (2004) 012, arXiv:hep-lat/0408034.

[117] A. Aguilar, D. Ibáñez, and J. Papavassiliou, *Ghost propagator and ghost-gluon vertex from Schwinger-Dyson equations*, *Phys.Rev.* **D87** (2013) 114020, arXiv:1303.3609 [hep-ph].

[118] A. K. Cyrol, M. Q. Huber, and L. von Smekal, *A Dyson–Schwinger study of the four-gluon vertex*, *Eur.Phys.J.* **C75** no. 3, (2015) 102, arXiv:1408.5409 [hep-ph].

[119] A. Maas, *Two- and three-point Green's functions in two-dimensional Landau-gauge Yang-Mills theory*, *Phys. Rev.* **D75** (2007) 116004, arXiv:0704.0722 [hep-lat].

[120] M. Q. Huber, A. Maas, and L. von Smekal, *Two- and three-point functions in two-dimensional Landau-gauge Yang-Mills theory: Continuum results*, *JHEP* **1211** (2012) 035, arXiv:1207.0222 [hep-th].

[121] A. Aguilar, D. Binosi, D. Ibáñez, and J. Papavassiliou, *Effects of divergent ghost loops on the Green's functions of QCD*, *Phys.Rev.* **D89** (2014) 085008, arXiv:1312.1212 [hep-ph].

[122] W. H. Furry, *A Symmetry Theorem in the Positron Theory*, *Phys. Rev.* **51** (1937) 125–129.

[123] A. L. Blum, R. Alkofer, M. Q. Huber, and A. Windisch, *Unquenching the three-gluon vertex: A status report*, *Acta Phys. Polon. Supp.* **8** no. 2, (2015) 321, arXiv:1506.04275 [hep-ph].

[124] W. Kamleh, P. O. Bowman, D. B. Leinweber, A. G. Williams, and J. Zhang, *Unquenching effects in the quark and gluon propagator*, *Phys. Rev.* **D76** (2007) 094501, arXiv:0705.4129 [hep-lat].

[125] P. O. Bowman, U. M. Heller, D. B. Leinweber, M. B. Parappilly, and A. G. Williams, *Unquenched gluon propagator in Landau gauge*, *Phys. Rev.* **D70** (2004) 034509, arXiv:hep-lat/0402032 [hep-lat].

[126] A. C. Aguilar, D. Binosi, and J. Papavassiliou, *Unquenching the gluon propagator with Schwinger-Dyson equations*, *Phys. Rev.* **D86** (2012) 014032, arXiv:1204.3868 [hep-ph].

[127] P. O. Bowman, U. M. Heller, D. B. Leinweber, M. B. Parappilly, A. G. Williams, and J.-b. Zhang, *Unquenched quark propagator in Landau gauge*, *Phys. Rev.* **D71** (2005) 054507, arXiv:hep-lat/0501019 [hep-lat].

[128] M. Hopfer, C. S. Fischer, and R. Alkofer, *Running coupling in the conformal window of large-Nf QCD*, *JHEP* **11** (2014) 035, arXiv:1405.7031 [hep-ph].

[129] J. M. Pawlowski and F. Rennecke, *Higher order quark-mesonic scattering processes and the phase structure of QCD*, *Phys. Rev.* **D90** no. 7, (2014) 076002, arXiv:1403.1179 [hep-ph].

[130] L. Fister and J. M. Pawlowski, *Functional renormalization group in a finite volume*, *Phys. Rev.* **D92** no. 7, (2015) 076009, arXiv:1504.05166 [hep-ph].

[131] J. P. Blaizot, R. Mendez Galain, and N. Wschebor, *A New method to solve the non perturbative renormalization group equations*, *Phys. Lett.* **B632** (2006) 571–578, arXiv:hep-th/0503103 [hep-th].

[132] P. Kopietz, L. Bartosch, and F. Schütz, *Introduction to the Functional Renormalization Group*, vol. 798 of *Lecture Notes in Physics*. Springer, Berlin Heidelberg, 2010.

[133] J.-P. Blaizot, A. Ipp, R. Mendez-Galain, and N. Wschebor, *Perturbation theory and non-perturbative renormalization flow in scalar field theory at finite temperature*, *Nucl. Phys.* **A784** (2007) 376–406, arXiv:hep-ph/0610004 [hep-ph].

[134] N. Tetradis and C. Wetterich, *The high temperature phase transition for phi**4 theories*, *Nucl. Phys.* **B398** (1993) 659–696.

[135] J.-P. Blaizot, A. Ipp, and N. Wschebor, *Calculation of the pressure of a hot scalar theory within the Non-Perturbative Renormalization Group*, *Nucl. Phys.* **A849** (2011) 165–181, arXiv:1007.0991 [hep-ph].

[136] E. Braaten and A. Nieto, *Effective field theory approach to high temperature thermodynamics*, *Phys. Rev.* **D51** (1995) 6990–7006, arXiv:hep-ph/9501375 [hep-ph].

[137] M. Q. Huber and L. von Smekal, *Spurious divergences in Dyson-Schwinger equations*, *JHEP* **1406** (2014) 015, arXiv:1404.3642 [hep-ph].

[138] M. Huber, private communication.

[139] J. Meyers and E. S. Swanson, *The Gluon Propagator with Two-loop Schwinger-Dyson Equations*, *Phys.Rev.* **D90** (2014) 045037, arXiv:1403.4350 [hep-ph].

[140] V. Mader and R. Alkofer, *Including 4-gluon interactions into*

Dyson-Schwinger studies, *PoS* **ConfinementX** (2012) 063, arXiv:1301.7498 [hep-th].

[141] M. Q. Huber and J. Braun, *Algorithmic derivation of functional renormalization group equations and Dyson-Schwinger equations*, *Comput.Phys.Commun.* **183** (2012) 1290–1320, arXiv:1102.5307 [hep-th].

[142] J. Kuipers, T. Ueda, J. A. M. Vermaseren, and J. Vollinga, *FORM version 4.0*, *Comput. Phys. Commun.* **184** (2013) 1453–1467, arXiv:1203.6543 [cs.SC].

[143] M. Tentyukov, D. Fliegner, M. Frank, A. Onischenko, A. Retey, H. M. Staudenmaier, and J. A. M. Vermaseren, *ParFORM: Parallel version of the symbolic manipulation program FORM* in *7th International Workshop on Computer Algebra in Scientific Computing (CASC 2004) St. Petersburg, Russia, July 12-19, 2004*. 2004. arXiv:cs/0407066 [cs-sc].

[144] M. Q. Huber and M. Mitter, *CrasyDSE: A Framework for solving Dyson-Schwinger equations*, *Comput.Phys.Commun.* **183** (2012) 2441–2457, arXiv:1112.5622 [hep-th].

[145] S. Johnson, "Cubature (Multi-dimensional integration)." http://ab-initio.mit.edu/wiki/index.php/Cubature. [Last access; 08-June-2017].

[146] H. Takahasi and M. Mori, *Double exponential formulas for numerical integration*, *Publ. RIMS Kyoto Univ.* **9** (1974) 721–741.

[147] I. v. Tyutin and B. b. Lokhvitsky, *CHARGE CONJUGATION OF NONABELIAN GAUGE FIELDS*, *Sov. Phys. J.* **25** (1982) 346–348.

[148] V. P. Nair, *Quantum Field Theory:A Modern Perspective*. Springer, New York, NY, 2005.

[149] W. Greiner and J. Reinhardt, *Quantum electrodynamics*. Springer, Berlin, 2003.

[150] D. F. Litim, *Optimised renormalisation group flows*, *Phys. Rev.* **D64** (2001) 105007, arXiv:hep-th/0103195.

[151] D. F. Litim, *Mind the gap*, *Int. J. Mod. Phys.* **A16** (2001) 2081–2088, arXiv:hep-th/0104221 [hep-th].

[152] D. F. Litim, *Optimisation of the exact renormalisation group*, *Phys. Lett.* **B486** (2000) 92–99, arXiv:hep-th/0005245.